TISSUE ENGINEERING SITES FOR PANCREATIC ISLET TRANSPLANTATION

A Thesis Presented to

the faculty of the School of Engineering and Applied Science

University of Virginia

In Partial Fulfillment

of the requirements for the Degree

Master of Science in Biomedical Engineering

by

DANIEL THORN BOWERS

July, 2013

APPROVAL SHEET

The thesis is submitted in partial fulfillment of the

requirements for the degree of

Master of Science in Biomedical Engineering

Daniel T. Bowers

AUTHOR

The thesis has been read and approved by the examining Committee:

Dr. Edward Botchwey, Advisor, Biomedical Engineering

Dr. Shayn Peirce-Cottler, Chair, Biomedical Engineering

Dr. Kenneth Brayman, Co-Advisor, Surgery

Dr. Cassandra Fraser, Chemistry

Dr. Robin Felder, Pathology

Accepted for the School of Engineering and Applied Science:

_____

Dean, School of Engineering and Applied Science

July, 2013

ABSTRACT

Pancreatic islet transplantation, a curative treatment for Type 1 Diabetes, is restricted from broad application due to hypoxia as well as innate and specific immunity. Encapsulation technology offers the ability to exclude cellular immunity, however clinical success has not yet been achieved. This thesis aims to prepare a transplantation site for islets using a novel encapsulation device through three approaches. Firstly, Aim 1 was to investigate the pre-seeding of accessory cells to the biomimetic nanofibers and evaluate the dimensional stability of these fibers. Cell pre-seeding did not have a significant effect on nanofiber implant volume however porcine decellularized dermis was much more dimensionally stable. Secondly, Aim 2 sought to equip the encapsulation device with boron dye based hypoxia sensors. Using a novel polymer conjugated form of the dye, nanofibers were electrospun that displayed reduced signal decay in a hydrated environment for 3 weeks. Hypoxia, due to a 5X cell density increase *in vitro* (13.9 vs 6.7 PPM) and after islets are infused *in vivo*, is evident with spatiotemporal resolution. Thirdly, Aim 3 is to evaluate the ability of the device to precondition a space for islet transplant by neovascularization and immunomodulation. Vessel length density in dorsal skinfold window chambers is increased by FTY720 loaded fibers over the unloaded fibers in healthy mice and moderately diabetic animals (Day 0 - 3.37%, Day 7 - 4.22%, $p<0.05$). Local release of FTY720 decreases the proportion of inflammatory macrophages in surrounding subcutaneous tissue (ratio of inflammatory to non-inflammatory: 14:1 vs 8:1). The nanofiber morphology and local release of FTY720 has been shown to improve islet health *in vitro*. Using the dimensionally stable ECM from Aim 1 an *in vivo* void is maintained (confirmed by ultrasound) in order to ensure that the 2nd procedure to deliver islets can be done without disturbing the tissue implant interface. Therefore, a FTY720 releasing nanofiber membrane could address both innate and specific immunity while also increasing vasculature even in the diabetic environment. These findings improve major challenges, including the need to monitor oxygenation, facing islet transplant as well as other tissue engineering applications.

ACKNOWLEDGEMENTS

Rebekah Neal, PhD for techniques and previous data
Marc Seaman for Rapid Analysis of Vessel Elements (RAVE) image analysis software
Parker Merrill for image analysis and RAVE modification programming, assistance with mouse islet isolation
Dan Lin from the Hossack Lab at UVA for assistance with ultrasound imaging
Ritu Linhart for assistance in electrospinning parameter optimization in new polymers
Anthony Bruce from the Peirce-Cottler lab for many mice I have used for pilot studies
Anthony Awojoodu, MS for being in the trenches of grad school in the Botchwey Lab
Anusuya Das, PhD for mentorship in science
Steven Lenz for being the only grad student left at UVA from the Botchwey Lab
Botchwey Lab members: Richard Murry, Shaun Tanner, PhD, Molly Tinius, Cythnia Huang, MS
Kevin Klembczyk, Carter Shields and Danqing Zhu for assistance with data collection
Nicole Keane, Michael Tanes and Yong Lin for much hard work as the only Capstone team I mentored
Songpan Xu, Alexander Zestos and Jelena Samonina-Kosicka, PhD from the Fraser lab for expertise in boron dyes
Preeti Chhabra, PhD and Linda Langman, MT(ASCP) for much scientific discussion and methods
Farah Mukheef for assistance with perifusion assays

This thesis is dedicated to the memory of my cousin Jason

who taught me that diabetes should not limit your dreams.

To my mother and father who never stop encouraging, listening and loving.

And to my brother who is a constant encouragement and who is always ready to have some fun when

I have a couple days away from the lab.

To my running group and fellow grad students.

ABBREVIATIONS USED

SI: Stimulation Index – A measure of islet function – Insulin Secreted in 28mM glucose divided by insulin secreted in 2.8 mM glucose
ECM: Extracellular matrix
NF: Nanofibers
PTFE: polytetrafluoroethylene
PLG: poly (lactide-co-glycolide)
PEG: Polyethylene glycol
CITR: Clinical Islet Transplant Registry
FDA: Food and Drug Administration
NGF: nerve growth factor
NOD: Non-obese diabetic mouse
PDMS: Polydimethylsiloxane
PET: polyethylene terephthalate
2-HEMA: 2-hydroxyethyl methacrylate
MMP: matrix metalloproteinases
VEGF: vascular endothelial growth factor
PVA: polyvinyl alcohol
HGF: hepatocyte growth factor
STZ: streptozotocin
Tregs: T-regulatory cells
IBMIR: Instant Blood Mediated Immune Reaction
ROS: Reactive Oxygen Species
PLGA or PLAGA: poly(lactic-co-glycolic acid)
PCL: polycaprolactone
MicroCT: microcomputed tomography
SEM: Scanning Electron Microscopy
eGFP: enhanced Green Fluorescent Protein
PFA: Paraformaldehyde
H&E: Hematoxylin and Eosin
TCPS: tissue culture polystyrene
FBGC: foreign body giant cell
PHBV: Poly(3-hydroxybutyrate-co-3-hydroxyvalerate)
FBS: fetal bovine serum
PPM: Parts per million
FDA: fluorescein diacetate
PI: propidium iodide
EC: endothelial cell
SMC: smooth muscle cell
S1P: sphingosine-1-phosphate
DMSO: dimethyl sulfoxide
PBS: phosphate buffered saline
HBSS: Hank’s Balanced Salt Solution
IP: intraperitoneal
KRB: krebs ringer buffer
ELISA: Enzyme-linked immunosorbent assay
HEPES: 2-[4-(2-hydroxyethyl)piperazin-1-yl]ethanesulfonic acid
HBSS: Hank's Balanced Salt Solution
GSIS: Glucose Stimulated Insulin Secretion
ADSC: adipose derived stem cell

TABLE OF CONTENTS

LIST OF FIGURES

INTRODUCTION

Literature Review: Abstract

Islet transplant will be a curative treatment for insulin dependent diabetes, not only increasing quality of life through reduced complications, but also decreasing the burden of self-management. Since the discovery that insulin is produced by the pancreas, many advances have been made in self-management systems and the closed-loop artificial pancreas is on the brink of clinical application, an effort led by a small team of researchers including world renowned experts here at UVA. In order for islet transplant to reach more patients, a number of challenges must be overcome. Encapsulation technology is rapidly developing, promising to be a part of the solution. From open porous scaffolds to diffusion barrier hydrogels, scaffolding and encapsulation materials can provide many desirable properties, including acting as a vehicle for therapeutic agents. The combination of multiple factors delivered in a temporally controlled fashion is likely to improve the long-term function of transplanted islets, defining a path toward greater future clinical success.

Literature Review: Pancreatic Islet Macro - and Micro - Encapsulation Devices

The Diabetes Control and Complications Trial (DCCT) established glucose control as an important factor in the progression of diabetic complications. Advances in insulin formulations and delivery methods since the discovery of insulin have made diabetes a chronic disease which can be managed instead of one with a particularly short life expectancy. Some patients have lived with the disease free of major complications for more than 50 years [1–3]. However the number of patients that can achieve this level of control is limited. The correlation between control and staying complication free is still being defined, but may be also be related to residual endogenous insulin production [4]. The promise of tighter control by allowing pancreatic islets to perform their function has been the focus of intense research ever since the discovery that a transplant can cure a diabetic animal or human. Since the vast majority of patients

with Type 1 Diabetes will have complications despite using the best insulin self management techniques and equipment available [5], pancreas and islet transplant is expected to be the major advance in clinical diabetes care to follow the closed loop artificial pancreas.

In clinical trials, short term success, as measured by the ability of patients to have near normal blood glucoses without exogenous insulin, has been somewhat accomplished. The results from the Edmonton group were truly exciting[6], however the testing of the protocol in multiple centers gave a more measured perspective[7]. More recently, the results of the Clinical Islet Transplant Registry (CITR) Trials are being examined[8]. As Phase III trials are coming to a close the hope for achieving FDA approval for islet transplant is solidifying.

Despite these exciting results, much work remains to be done. There are challenges in the choice of immune suppression regimen and the fact that islets from multiple donors are required. Long term, beyond one year, the results from the international trial of the Edmonton protocol were noticeably worse and the long term results of the CITR (although not a primary endpoint) are not yet known. The long term survival of a critical mass of functional islets that can prevent a patient from requiring insulin therapy has not yet been achieved in a significant number of patients.

One of the distinct advantages of islet transplant as compared to pancreas transplant is the reduced volume of tissue that must be transplanted. This reduced tissue volume is transplanted clinically by infusion into the portal vein allowing for delivery of insulin at a primary site of action. However there are numerous factors which are known or hypothesized to contribute to the poor survival rate of islets in the portal circulation. Thus alternative site transplants (outside liver) may be of interest.

The immune reaction to the transplanted islets is likely the single overarching adverse factor that affects both short and long term survival of transplanted islets. Islet encapsulation provides an alternative to immune suppression drugs. Semi-permeable membranes of many shapes, characteristics and sizes have

been investigated. In extrahepatic sites the volume of tissue is not as restricted, allowing for multiple types of encapsulation systems[9].

Knowing that the short term survival of islets is at hand clinically, the long term survival of islets inside encapsulation devices is of particular interest and has been reported in pre-clinical models[10–12]. The combination of immune suppression drugs or agents and encapsulation is also useful [13], [14]. Local release is a method to deliver agents at therapeutic levels in a spatially controlled manner. The local release of agents from scaffolds or encapsulation devices may prove to allow the use of certain agents whose application has been avoided due to adverse effects arising from systemic delivery. To the extent that an environment can be created that has similarity to the pancreatic microenvironment it is likely to aid in the islet function[15], [16]. Below examples of local release in islet transplant are explored, considering different encapsulation constructions and examples of locally delivered factors.

ENCAPSULATION TECHIQUES

Diffusion Chambers

Diffusion chambers have been used for the macroencapsulation of islets. This type of device usually provides a protected space that many if not all the islets in a transplant occupy. Considerations of shape and size as well as the ability to vascularize the outside surface of the device are important to achieving success. This type of device is particularly well suited for xenogenic and engineered cell sources where the ability to retrieve the transplanted tissue is highly valued.

The pore size of semipermeable membranes is a key design parameter for any device configuration. In diffusion devices the membrane is usually a sheet which has characteristics allowing diffusion of essential nutrients, waste, and importantly insulin. Consideration of the ability of immune related molecules such as chemokines and immunoglobulin to diffuse as well as cells to migrate is also important. Although cellular infiltration might be a negative when considering inflammatory cells, a pore size which can allow

cellular infiltration does not disqualify the membrane from being useful. Brauker et al showed that larger pore sizes (~5 micron) in polytetrafluoroethylene(PTFE) membranes were superior in facilitating blood vessel investment in the membrane tissue boundary as compared to a membrane with a 0.02 micron pore size[17]. This was followed by the discovery that a 0.4 micron membrane, although it can prevent cellular infiltration and protect allogenic tissue, does not prevent xenogenic tissue from being destroyed through a molecular mechanism or perhaps by a strong inflammatory infiltrate around the implant that weakens blood supply[18]. Loudovaris et al demonstrated that insulinoma cells, both from a NOD and allogenic source, can be protected from attack in an NOD mouse within a cell impermeable device[19], [20].

Rods / hollow fiber diffusion chambers

Hollow fibers can be used to culture cells provided the diffusion characteristics are appropriate [21]. A cylinder of poly(acrylonitrile/vinyl chloride) has protected cells that secrete nerve growth factor (NGF) in vivo[22]. Injection of hydrogels into prevascularized spaces has proven effective in improving islet function. Transplantation of islets embedded within an agarose/poly (styrene sulfonic acid) hydrogel of cylindrical shape into a subcutaneous space preconditioned by basic fibroblast growth factor releasing gelatin beads could cure an animal in a xenotransplant setting for as long as 101 days[23]. This has also been shown to protect porcine pancreatic endocrine cells in a mouse host [24]. Hollow fibers have been shown to create an environment for improved cell aggregate culture[25]. Thus hollow fibers may play a role in the clinical application of diffusion membranes[26], although more work is required.

Spherical capsules

Alginate microcapsules are arguably the first microencapsulation technique employed for pancreatic islets. Microencapsulation techniques provide a semi-permeable membrane around one larger or sometimes up to three smaller islets. The first description of microcapsules was published in 1980 by Lim and Sun [27]. Since that time microcapsules of various materials have been continually investigated.

Alginate, naturally occurring in seaweed, has been used extensively in islet encapsulation studies. Various forms of alginate exist, including high-M alginates, high-G alginates and clinical grade alginates that are commercially available, as well as custom isolated forms by individual investigators. Success in pre-clinical models has been widespread with constant improvements. High-M alginate crosslinked with barium can protect neonatal porcine islets from attack in diabetic animals with intact immune systems giving better cure rates than without encapsulation [28]. Also, single and double capsules of high-M alginate can protect adult porcine islets from immediate destruction as is seen with bare islets despite some kind of humoral immune response, but it appears that a slow attrition of beta cell mass still occurs inside the capsules[29]. Transplants in non-human primates and some exploratory clinical studies have extended the interest in this encapsulation technique. Agarose microcapsules can protect NOD islets, isolated from pre-diabetic mice, from immune destruction in a diabetic NOD mouse, demonstrating the usefulness of an agarose membrane as a barrier to autoimmune destruction when transplanted intraperitoneally or in an omental pouch[10]. Improvements on this technique continue to come. For instance combining microencapsulated islets into a larger connected device in some fashion would address the concern of irretrievability[30], [31], which would have otherwise limited this promising approach.

Porous bulk scaffolds

Several bulk porous scaffolds exist. These scaffolds do not provide a strict immune barrier, but rather a physical support for the islets and in many cases for vascularization, producing exciting results. Gibly et al report the use of a microsphere poly (lactide-co-glycolide) (PLG) scaffold implanted in an intraperitoneal fat pad can cure diabetes both in murine and porcine models [32]. They noted that scaffold pore size can affect the depth of host tissue penetration. A gelatin sponge inside a silicone chamber placed around a vascular pedicle showed the ability to cure a diabetic mouse[33]. Porous scaffolds have also been tested in islet transplant being made from PDMS[34], [35], lactide and glycolide copolymers[32], [36–38], Polyglactin and poly-P-Dioxanon[39], polyvinyl alcohol[40], and polyglycolic acid[40].

Collagen generating devices

Collagen generating devices have produced exciting results in small animals[41], large animals and human clinical trials[42], [43]. A stainless steel mesh tube enshethes a PTFE rod which is removed after a period of up to several months allowing time for the host to produce a natural vascularized collagenous capsule around the PTFE rod. This collagenous membrane grows into the steel mesh which provides support for the cylindrical void into which the islets are infused once the PTFE rod is removed. These native matrix capsules have been shown to provide some protection and support of function for porcine xenotransplants into humans [42]. Recent evidence suggests that the matrix surrounding these devices may be able to create an immunoprivileged site [44].

A chamber surrounding a vascular pedicle in the groin of a mouse made of a surgical grade tube filled with matrigel can be used as a method to create a prevasclarized space where islets can be placed in a second procedure within the collagenous capsule that formed around the tube in the 3 week period after the original implant[45]. Some new techniques are being explored, such as encapsulation within chondrocyte sheets which creates another type of ECM capsule which may have immune privilege

qualities[46–48]. Despite the fact that excess build up of ECM is often viewed as detrimental to implant function these approaches are working well.

Conformal coatings

One primary concern with many encapsulation techniques is the excess volume within the device. This increases the distance for diffusion to and from the islet as well as the volume of the material that must be implanted, hence these very thin coatings are a newer very interesting approach. Several methods exist to create coatings or encapsulation membranes that closely fit the surface of the islet including PEG based layers[49–54] often applied using layer-by-layer techniques. Jeong et al report the use of 6 arm PEG catechol. The coating alone is not found to have an effect on xenotransplant islet survival, however when FK506 is administered the uncoated islets survive only half as long as the coated ones[55]. Layer-by-layer addition of a conformal coating has been investigated with phosphorycholine-modified poly-L-lysine/heparin[56], demonstrating the ability to use the PEG coating as a place to anchor other agents which will be explored later in this review.

Combination devices

Advantageous properties of different encapsulation or scaffolding designs can be captured by combining them into a composite device. Physical support for the spherical shape of islets using microcapsules can be combined with the ability to retrieve the islets from the peritoneal cavity by using a macroencapsulation approach such as an agarose rod[57]. A polyethylene terephthalate (PET) mesh bag containing a collagen sponge and gelatin microspheres loaded with basic fibroblast factor has been shown by Balamurugan et. al. to successfully aid in the survival and function of allogenic islets when implanted at the intramuscular space[58]. A macroencpasulation approach can be combined with a method to generate oxygen in the implant as well as local release of an agent showing promise of these techniques[59]. Due to the complexity of the challenges in islet transplant, combinations of approaches are likely to be part of the eventual solution.

Other device configurations of interest

Acrylic selectively permeable membranes can protect xenogenic transplants into diabetic rats[60], [61]. Membranes made of 2-hydroxyethyl methacrylate (2-HEMA) [62] and regenerated cellulose [63] have also been investigated. Polyethylene film has been used for its oxygen permeability characteristics (3,000 cm3/m2 atm) as a new material for islet culture bags[64], and may show promise as a selectively permeable membrane in a transplant setting. Many other device designs have been investigated including AV shunt devices and bulk hydrogels, however the reader is directed to other expert reviews that cover these and other device types[65].

LOCAL RELEASE OF AGENTS

Localized release of compounds offers advantages over systemic delivery. Side effects arising from systemic delivery can be avoided. Furthermore the timing and dose in the area of interest can be controlled, allowing specific therapeutic targets to be reached. Depending on the delivery system local release can be limited to the space where the biomaterial is. This works well for many clinical situations where the target tissue, perhaps an implant or transplanted cells, are stationary as is the case for islet transplant. Thus local release of drugs may be an effective strategy to combat common problems with implants going forward such as fibrosis, non-specific inflammation, specific immunity against the material or encapsulated cells, and regeneration of the target tissue.

Combating Fibrosis

Fibrosis is regularly cited as a histologically quantifiable negative factor in many biomaterial implant situations. Stratifin is a protein (also known as 14-3-3 sigma protein), which has been shown to be released from keratinocytes. Fibroblasts upregulate expression of MMP1 upon stimulation with Stratifin through a p38 MAPK cFos pathway[66]. While expression of MMP-3, collagenase 1, neutrophil collagenase, and membrane type 5 MMP also goes up in fibroblasts, type 1 collagen and fibronectin

expression are reduced[67]. Fibroblasts also upregulate hyaluronan upon exposure to stratifin which might suppress scar formation[68]. Of particular interest for the application of islet transplant, the presence of insulin in the culture medium completely blocks the upregulation of collagenase mRNA induced by stratifin suggesting that local release of stratifin from islet encapsulating materials may not be an effective strategy. Conversely it may be useful to consider at least in the broader context of diabetes. Recent proteomic analysis revealed that stratifin 14-3-3 are abnormally expressed in T1D patients and T1D patients who also have end stage renal disease. This abnormal expression was found to be reversed however with a simultaneous pancreas kidney transplant[69], indicating that stratifin may be a key possible target for correcting diabetes related abnormalities. Human pancreatic islets expression of stratifin is affected by the cAMP agonist forskolin[i]. The 14-3-3 proteins have also been recently implicated in the survival of beta cells[70]. Experiments should be done to determine if local delivery of Stratifin from an islet encapsulation device would be an effective strategy. Other possible agents to reduce fibrosis in islet transplant include conophylline[71], TAK-779[72], as well as many of the other anti-inflammatory agents discussed in the next section.

[i] http://natural.salk.edu/cgi-bin/creb?DB=human&TABLE=Pancreatic_Islet_Expression&FIELD=LocusLink&QUERY=2810 Accessed 3/22/13

Combating the immune system

Inflammation in the context of transplanted tissue or tissue engineering constructs is generally regarded as detrimental to the function of the implant. However there are positive aspects of inflammatory processes which help to promote the integration of implants or transplanted cells. Thus a balance must be struck to harness the power of inflammation to start a regenerative process. Many classic immune suppression drugs are not suitable for islet transplant such as cyclosporine, FK506, and steroids, because of diabetogenic effects [73] or antiangiogenic effects[74]. Alternatives have been examined including leflunomide[75], which has been examined in combination with tacrolimus[76], cyclosporine and mycophenolate mofetil plus cyclosporine A to promote xenograft survival[77], [78].

Many agents have garnered success by having known and unknown effects on many cell types. Some clinically applied agents in organ and islet transplant fall into this category. For instance, steroids are known to have effects on a wide range of cell types. The list of agents investigated with islet transplant as the goal includes: deoxyspergualin[79–86], dexamethasone [87], soft steroids (designated as soft due to their fast deactivation in the body)[88], [89]. It is interesting to note here that for local release dexamethasone may be a good candidate as it is known to stimulate islet insulin secretion, likely due to decreased insulin responsiveness in peripheral tissues[90–92]. Although corticosteroids are found to be detrimental in islet transplant recipients[93] the direct islet effects may be reversible[94–96].

Factors that are associated with the immune privilege of certain cell types may be a source for new candidate drugs. Clusterin, Fas ligand, and transforming growth factor-beta1 are thought to be associated with the success of Sertoli cells to protect islet allo- and xenografts[97]. Other possible factors include lipoxins, resolvins, and protectins[98], lisofylline[99], adenosine and agonists of adenosine[100], [101], and purines such as inosine[102].

Combating a lack of vascularization

A lack of efficient vascularization of the transplanted islets is a key challenge[103–105]. Not only are there many studies which show improvement by induction of angiogenesis, but the blocking of angiogenesis also has been studied. In a loss of function study, one group of animals received a daily dose of a potent anti-angiogenic factor (C-statin) for 14 days following transplant preventing the graft from vascularizing and functioning as well as the untreated controls[106]. Thus providing evidence that vascularization is key.

The most widely investigated molecule to induce vascularization is vascular endothelial growth factor (VEGF). It is not surprising that this is an effective strategy considering that VEGF is made in large quantities by islets following isolation. Indeed local release of VEGF from scaffolds has been investigated[107–109]. One approach has been to encapsulate VEGF in alginate macrospheres. These VEGF releasing macrospheres are included in a bioengineered implant constructed of a polyvinyl alcohol (PVA) sponge which is infused with a Type 1 collagen gel carrying the islets. The scaffolds with VEGF releasing alginate macrospheres implanted into the mesenteric fat of STZ diabetic mice cured 8 of 8 animals while only 5 of 8 were cured when the implant did not contain VEGF[110].

Attaching the VEGF to the bulk scaffold using a protease labile peptide could provide local release of VEGF when micro-environmental factors demand it. Using this approach VEGF has been released from hydrogels with improvements in islet vascularization and glucose control compared to the hydrogel without VEGF incorporated when syngeneic islets were transplanted into the mesentery[111]. The combination of locally delivered VEGF and HGF from growth factor reduced matrigel greatly improved the vascularity of the graft as well as the ability of a suboptimal number of islets to cure an STZ diabetic animal in a subcutaneous location[112]. Similar results were found for islets transplanted in a VEGF supplemented collagen gel[113].

A different approach to increase local supply of VEGF at the islet graft site is to transfect cells with VEGF, giving more insight into how local release from materials may be useful. This can be done in the islet cells themselves or in a support cell that is co-transplanted. Even without transfection production of VEGF can be raised from the graft by co-transplantation of endothelial progenitor cells[114]. Endothelial cells that over express VEGF 165 lead to a greater vessel density and greater insulin staining in kidney capsule transplants compared to islets alone or islets with non-transfected endothelial cells[115]. When the islets themselves were transfected with VEGF greater cure rates, as well as increased insulin and endothelial cell staining were found in comparison to islets transfected with a control vector[116].

Angiopoietin-1 has been transfected directly into islets as well with the added benefit of being anti-apoptotic as well as pro-angiogenic. When compared to control vector transfected islets in a marginal mass syngeneic kidney capsule transplant only the islet expressing angiopoietin-1 were able to cure the animal[117]. As the authors point out, the process of lymphangiogenesis may also be affected by Angiopoietin-1. If normal wound healing typically couples blood and lymph vessel development, this would seem to be a positive effect, however this is not completely clear. For instance, Yin et al blocked lymphangiogenesis following islet transplant and showed that the allograft survived significantly longer, suggesting that the presence of lymphatics in the graft allows more rapid and efficient immune recognition, as this is a primary lymphatic function[118]. Similar results were found in corneal allotransplant[119]. Yin et al also showed in a separate study that inhibition of lymphangiogensis can prevent the onset of multiple low dose streptozotocin diabetes in mice correlating to a decreased T-cell infiltration and preserved islets[120]. Thus it is useful to examine therapeutic agents being tested for islet transplant for their functionality in lymphangiogenesis.

Beta cell health or replication agents

A facet of local release that is not always harnessed effectively is the control of release rate or order in the case of multiple agent delivery. One way to effectively apply this to islet transplant would be to release an agent that can reduce the responsiveness of the islets to glucose or protect them from the elevated

glucose toxicity for a short time while they become established. Extendin-4 can protect beta cells from apoptosis induced by IL-1 beta[121], [122] and can reduce the number of cells required for transplant[123–126]. When delivered in combination with CXCL12 it can protect betaTC-tet cells in hypoxic environments[127]. Osteopontin[128], as well as flavonoids[129], and genistein[130] may also be candidates. Depending on the polymer system used to deliver the cells, protein delivery may not be possible, so molecules such as scoparone (6,7-dimethoxycoumarin), shown to decrease the production of nitric oxide[131], may be required. Another method to protect the beta cells from damage is to block apoptosis pathways[132–136].

The opposite hypothesis is that delivery of certain agents may increase the responsiveness of islets to glucose challenge[137]. Drugs typically applied to those with Type 2 Diabetes Mellitus have been tested in islet transplant without much success[138], although rosiglitazone may aid in islet engraftment, perhaps due to anti inflammatory effects rather than insulin sensitizing[139]. Maintenance of functional beta cell mass can instead be aided by maintenance of normoglycemia using exogenous insulin[140–145].

Local, but conjugated, presentation of molecules

Some molecules are functional, or perhaps more functional[146], when conjugated to a surface for presentation to cells as compared to release into the local space. Fas-ligand has been tethered to the surface of islets by creating a streptavidin conjugated Fas-L which then attached to the biotinylated islet surface. This islet surface modification resulted in a localized immunosuppression confirmed by survival of the islets Tregs were attached to as well as by adoptive transfer of Tregs from a graft draining lymph node[147]. Thrombomodulin has been attached also through biotinylation of islet surface, useful due to its ability to catalyze the production of activated protein C[148], as had been shown with preferential delivery of thrombomodulin to the liver at the time of intraportal transplant[149].

Heparin, due to its anti-coagulating properties, has also been conjugated to the surface of islets. In an interesting extension of this idea, Cabric et al showed that VEGF-A will bind to the heparinized islet

surface causing increased endothelial cell proliferation[150]. Other molecules such as urokinase[151], which can promote fibrin clot degradation, soluable compliment receptor 1[152], [153], which has anti-coagulant properties, and glucogon-like peptide 1[50], [154] have been attached to materials surrounding the islet. Soluable compliment receptor 1 has been attached to the surface of alginate coated islets as well as directly to the islet[155]. Using the direct surface conjugation technique, survival of islets in the intraportal transplant site was shown to be markedly improved in a syngenic model related to reduction of IBMIR with soluable compliment receptor 1 presentation[156]. Thus, molecules can be tethered to the encapsulation material, providing another route to improve transplant outcomes.

Provision of oxygen during the engraftment period to reduce apoptosis

Increasing the oxygen tension in the islet graft has been shown to improve islet survival[157–163] and monitoring the graft oxygen tension is desirable[164–166]. Strategies to increase local oxygen tension include: incorporation of hemoglobin[167–169], calcium peroxide-based oxygen generating particles[170], [171], perfluorocarbons[172], or a nearby gas phase oxygen reservoir[59], [173]. Hypoxia in islets often leads to intracellular generation of reactive oxygen species. These reactive oxygen species are known to lead to apoptosis of beta cells. Substances exist that can reduce the load of reactive oxygen species which when delivered to islet recipients/cultures[174–176] or overexpressed[177–180] can bring the pathologically high levels of ROS to near normal. A combination of strategies to increase oxygen and decrease ROS may be effective in reducing the effects of islet graft hypoxia.

LITERATURE REVIEW DISCUSSION

Class of molecule in local drug release

Because islet transplant faces many challenges the range of potentially useful agents to locally release is large. Small molecules are typically better suited for material encapsulation due to their broader solvent compatibility, however methods to encapsulate proteins exist if the appropriate material choice is made[30], [181–187]. Investigations on the delivery of insulin are particularly pertinent to islet encapsulation goals[188–194].

Temporal control of agent release

Knowledge of the temporal relationship between adverse events in the days and weeks following an islet transplant is growing[142], [195–197]. At the same time methods to temporally control the delivery of agents are being developed. Thus, an exciting method to improve encapsulated islet survival and function would be to deliver a combination of agents in phases designed to coincide in time with peaks of negative aspects of the host response to transplanted islets[82], [198], [199]. This is no doubt a complex solution, however the islet transplant microenvironment is extremely complex. The temporal control of release of agents is classified into two categories here, those which are "preprogrammed" and those which are "released on command".

The preprogrammed agent encapsulation methods are commonly made by placing agents in different layers of a construct so that release rates and times can be controlled by diffusional release from or degradation of sequential layers, or differential binding affinity of the species to the implant[200], [201]. Many adverse events are known to affect transplanted islets in the early stages post transplant[196], so the initial burst release often seen in typical matrix diffusional release can be an advantage. The released on command agent encapsulation methods can be accomplished by attaching agents to a material with linkers that are specific to an enzymatic reaction that might allow the release of the agent under certain conditions, or a linker that is reactive to some external stimuli intentionally applied such as electromagnetic energy.

Volume and shape of device

It is clear from many studies that 3D structure improves the survival and function of islets. Maintenance of the 3D spheroid shape of a pancreatic islet is in and of itself useful. A 3D support can take on many forms such as the porous scaffolds or microcapsules and hydrogels. Microcapsules provide a relatively constant islet volume to empty space volume on an individual islet basis. Macroencapsulation devices provide a mean ratio of islet volume to empty space, but usually result in individual islet variability based on the islet location in the device. While some will have nearest neighbor islets on all sides that reduce

local empty space, others will have either a device wall or some ‘empty’ space on their border. Thus it is important not only to think about the islet cell volume to empty volume ratio as a mean, but also as a distribution. Where some encapsulation methods may have a tight distribution about the mean and others will have a distribution with two populations.

Closely related to the volume ratio (cell to empty space) is the shape of the device. The shape of the device can assert effects via these volume ratios or via the simple distance from the islet core to the edge of the device. The edge of the device in cases where an immune barrier is maintained indicates the most proximal point where nutrients can be delivered and waste can be removed. Because this parameter can be difficult to assess in devices that differ in multiple characteristics studies that create different shape devices from the same material are important. Agarose was studied by Yang et al.[202] in the shape of microbeads, rods and disks in vitro and in vivo finding that the microbead was the best approach. Further head to head comparisons of device shape would be very useful in moving the islet encapsulation field forward.

Immune response to the material

The immune response to the encapsulation or scaffolding material itself could play as important a role as the barrier function it provides if it stimulates a strong foreign body reaction, acts as an antigen itself, or acts as a strong adjuvant. The M and G components of alginate affect the physical material properties of the gel or capsule, but it is also been found that high M capsules are more antigenic[203]. However other studies have shown that high-M capsules are better for curing animals and may not even need a poly-L-lycine permselective layer[204]. Some polymers such as PLGA have been associated with adjuvant activity[205], [206].

Modulation of the response to subcutaneous implants with 16 locally released compounds was recently compared. Having identified dexamethasone as one of the most efficacious, it was shown to improve the glycemic control of chemically induced diabetic mice when transplanted with xenogenic islets[207].

Careful consideration of the immune response to the material with its cellular payload and the locally released agent is required.

Exciting approaches

Many other exciting advances in cell encapsulation and monitoring were not addressed in detail here due to scope limitations, such as the inclusion of cell adhesive peptides in artificial hydrogels[111], [208], non-invasive imaging of the graft to monitor different aspects of function[209–220], and use of neurotrophic factors[221]. The commercially pursued devices are summarized in Table 1. The codelivery of specific cells with the islets can improve the function and survival of the islets. Co-encapsulation of cells with the islets provides a method to ensure that the cells are at least initially located at the site of the transplant. Aside from effects on angiogenesis as were discussed above, anti-inflammatory effects have also been noted with the use of several cell types. Graham JG et al recently reported the delivery of regulatory T lymphocytes in a microporous poly (lactide-co-glycolide) scaffold protects islets transplanted into NOD mice much more effectively than intravenous delivery of regulatory T-cells[222]. Presentation of natural ECM proteins is an exciting area of research as well that can take advantage of the cost effectiveness and reproducibility of synthetic polymers with the benefits of ECM ligands[38].

Table 1: Current Commercial Macroencapsulation Devices

Device	Description	Company
Encaptra	Diffusion barrier device	Viacyte
Cell Pouch	Natural ECM Membrane	Sernova
Islet Sheet	Alginate slab	Hanuman Medical

LITERATURE REVIEW CONCLUSION

Knowing that a population of Type 1 Diabetic patients have residual endogenous insulin production even with long standing diabetes but have few complications confirms the idea that reinstating the natural glucose regulatory system is a goal worthy of pursuit. Many islet transplants in preclinical models and in clinical trials have demonstrated the ability of an islet transplant to normalize blood glucose levels and reduce hypoglycemic events. Many challenges remain however that prevent widespread application of this curative treatment beyond the segment of patients whose diabetes is particularly uncontrolled.

RESULTS

INTRODUCTION

As discussed above anti-inflammatory and pro-angiogenic compounds should be given particular attention considering the evidence that an immune system attack and a lack of a functional intra- or peri-islet vasculature reduce the survival of transplanted islets. Recent publications in islet transplant and a growing body of evidence in regenerative medicine as a whole support local release of agent's ability to positively affect outcomes without the same risk of side effects seen with systemic delivery. Aim 3 of this thesis shows the advantages of locally released FTY720 including the ability to reduce the inflammatory profile of tissue macrophages and in contrast to systemically delivered FTY720 it is proangiogenic[223], even in the challenging diabetic environment. Aim 1 is centered around development of the device with dimensionally stable components. Aim 2 equips the device with oxygen sensors in the form of novel polymer conjugated boron dye nanofibers. Thus a new prototype device is constructed to address three major challenges in islet transplant.

CHAPTER 1: ACCESSORY CELLS ON BIOMIMETIC NANOFIBERS

ABSTRACT

Importance: Cell seeding throughout the thickness of a nanofiber construct is explored as a means to provide biomaterial implant alternatives in facial soft tissue augmentation and dermal replacement.

Objective: Utilize a novel cell pre-seeded nanofiber tissue engineering technique to create a 3D biocompatible implant alternative to decellularized extracellular matrix.

Setting: Academic research laboratory

Participants: Sprague-Dawley rats

Interventions: Enrofloxacin in the drinking water for 4 days prophylactically and buprenorphine (0.2-0.5mg/kg SC BIDx24 hrs) post operatively for pain for 48 hours.

Main Outcomes and Measures: Evaluated viability of NIH3T3 fibroblasts cultured on polycaprolactone (PCL) electrospun nanofibers using fluorescence microscopy. Examined soft tissue remodeling histologically and using novel ex vivo volume determinations of implants using MicroCT of cell-seeded implants relative to nanofibers without cells and commonly used dermal grafts of porcine and human origin (Enduragen and Alloderm respectively). Assessed fate and distribution of eGFP positive seeded donor fibroblasts using immunohistochemistry.

Results: Fibroblasts migrated across nanofiber layers within 12 hours and remained viable on a single layer up to 14 days. Scanning Electron Microscopy confirmed a nanoscale structure with diameters of 158+/-72 nm. Low extrusion rates demonstrated the excellent biocompatibility in vivo. Histological examination of the scaffolds demonstrated minimal inflammation. Cell seeding encouraged rapid vascularization of the nanofiber implants. Cells of donor origin (eGFP+) declined with duration of implant. Volume of implants was not significantly affected for as long as 8 weeks by the pre-seeding of cells ($p>0.05$).

Conclusions and Relevance: Polymer nanofiber based scaffolds mimic natural extracellular matrix. Cell pre-seeding the nanofiber construct improved vascularization without notable effects on volume. An effect of cell pre-seeding on scaffold vascularization was evident beyond the presence of pre-seeded cells. This 3D multilayer method of cell seeding throughout a 1mm thick construct is simple and feasible for clinical application. Further development of this technique may impact the clinical practice of facial plastic and reconstructive surgeons.

Key Words: nanofibers (NFs), polycaprolactone (PCL), collagen, NIH3T3, fibroblasts, primary, dermal, cells, facial, soft tissue, electrospinning

INTRODUCTION

Craniofacial soft tissue deficits often require use of implantable materials for reconstruction. Current solutions to this problem include autografts, and acellular dermis from either allogenic and xenogenic sources. Tissue engineering constructs provide hope of an alternative to the costs of acellular dermis and the morbidity of autograft tissue sources. Being made under consistent conditions allows the tissue substitute to perform more predictably and tissue engineering constructs can be shelf ready. Additionally a tissue engineering scaffold can be tailored to replace the missing tissue. Construct design choices include: material, material processing, addition of signaling factors to be released locally[224–227], addition of natural ECM polymers[228–232], cell seeding[233], [234], and conjugation of peptides or proteins for cell attachment[235]. Patient-specific autologous cells can be seeded onto a biocompatible polymeric scaffold, reducing the risk of immune rejection of the construct.

The study presented below focuses on the addition of cells throughout a nanofiber scaffold. These nanofiber scaffolds are composed of the synthetic polymer polycaprolactone (PCL) and the natural polymer collagen. Other studies have demonstrated that the addition of collagen to polymer nanofibers increases viability and adhesion of cells[236]. Seil et al. conducted a pertinent study in which cells were sprayed between electrospun layers of nanofibers resulting in a three dimensional construct with viable cells throughout[237]. The objective of the study presented herein is to make a nanofiber scaffold that would not need the intensive process of cell spraying between layers. To reach the desired implant thickness, the method of Seil et al. would require electrospinning and cell seeding longer than is feasible for cell viability. Therefore, a novel method of cell pre-seeding on each layer of a multilayered construct is investigated below. This method of cell distribution in the fibers may be easily integrated into industrial design and would require little preparation in the clinical setting.

METHODS

Electrospinning

Nanofibers are electrospun (Figure 1A) from polymer solutions of polycaprolactone (PCL, Mn = 80,000) (Sigma, Ref#440744) with Rat Tail Collagen (Becton-Dickinson) which is solvated in 1,1,1,3,3,3-Hexafluoro-2-propanol (Sigma). The polymer solution has an overall weight ratio of 2000:1 PCL to Collagen and is ejected at a 1mL/hour flow rate by syringe pump (World Precision Instruments, Sarasota, FL, USA) using an 18G blunt tipped needle. A tip to collector distance of 10cm with an applied voltage of 12kV was utilized.

Cell Culture

NIH3T3 fibroblasts were purchased from ATCC (Manassas,VA). All cell culture was done with high glucose Dulbecco's modified Eagle's medium (DMEM) supplemented with 10% FBS and 1% penicillin and streptomycin, 1% pyruvate, and 1% Non-Essential Amino Acids.

Primary Dermal Fibroblast Isolation

A section of skin between the scapulae was shaved and depilated (Nair) on the previously euthanized rat. Triplicate washes of Betadine followed by EtOH was used to remove loose hair and sterilize the skin. A 2cm x 2cm section of skin was then removed and cut into pieces that were distributed among the media filled wells of a six well plate followed by abrading with a scalpel. The tissue was placed in an incubator until the first media change. This occurred 2-4 days after tissue harvest depending on the condition of the media (indicator color change) or cell outgrowth. Seven to ten days following the initial seeding the plates were washed once to remove the bulk of the floating cellular material. Cells were then trypsinized and passed through a 70uM filter to remove any large particles. Cell proliferation was then followed in T75 tissue culture treated flasks (Figure 1C). Cells up to passage 5 were used for studies. Cell passaging was performed when the monolayer reached 70–80% confluence.

Multilayered Cell Seeded Construct Construction

Constructs consisted of ten layers of nanofibers with cells seeded on each layer. Ten centimeter by ten centimeter sections of nanofibers were lifted from the aluminum foil onto which they were collected by soaking in 70% ethanol for approximately 3 minutes. The nanofibers were spread out evenly in a petri dish. They were dried by removing as much ethanol as possible using a pipet at the edges and then allowed to dry inside a cell culture hood for 4 hours (Figure 1B). The scaffolds were placed in a desiccator overnight or until the day of seeding. On the day of seeding, the scaffold was sterilized in the cell culture hood using the UV lamp for 1-2 hours.

Trypsinized cells were washed and re-suspended to a concentration of approximately 3-5 x 10^5 cells per mL. 10µL of this cell suspension was added as a droplet to each 1cm square quadrant, resulting in approximately 3-5x10^4 cells per scaffold. Cells were allowed to settle in each droplet of media for 1-2 hours in the cell incubator. The plate was then flooded with prewarmed media, followed by culture overnight as a single layer.

The following day, the single layer of nanofibers (10cm x 10cm) was folded to build the 10 layers resulting in a group of 10 scaffolds measuring 10cm x 1cm x 1mm overall. A scalpel was then used to cut the group into 10 scaffolds ready for implant (1cm x 1cm x 1mm each) (Figure 1D). The thickness of a single nanofiber layer was measured to be approximately 0.15561mm on dry fibers, which would result in a scaffold of approximately 1 to 1.5 mm in thickness. Non-cell seeded scaffolds were prepared in the same way omitting the cell seeding step.

Preparation of Decellularized Dermis Implants

The decellularized dermis implants, Alloderm (LifeCell Corporation, Branchburg, NJ, USA) and Enduragen (Stryker Craniomaxillofacial, Kalamazoo, MI, USA), were prepared according to the product insert. Both were cut into 1cm x 1cm scaffolds, one for every animal.

Animal Implant Procedure

Each of 36 Sprague-Dawley rats were implanted, with the 4 implant types, and then post-operatively monitored according to a University of Virginia ACUC approved protocol. The study was taken to 3 time points with 12 animals for each timepoint. Grafts (1cm x 1cm in size) included: 1) rat primary (eGFP+) fibroblast-seeded PCL/collagen nanofiber scaffold; 2) PCL/collagen cell-free nanofiber scaffold; 3) acellular human cadaveric dermis (AlloDerm); and 4) acellular porcine dermis (ENDURAGen) (Figure 1E). After appropriate isoflurane anesthesia was attained, the rats were placed prone on a sterile operating table, their dorsal hair was clipped, and the skin was then sterilized with Betadine and 70% ethanol washes in triplicate. Incisions 1.5 cm in length were made in four paraspinal sites on the dorsum of the animal, one distinct site for each of the four implants compared. Subcutaneous pockets were created by blunt dissection between the panniculus carnosus and the deep fascia investing the dorsal musculature. The 4 grafts were sutured to the dorsum using 5-0 polypropylene sutures (Prolene; Ethicon Inc), and the skin incisions were closed using 4-0 prolene (Ethicon Inc) and skin glue. The animals were given an antibiotic (Enrofloxacin, Baytril, Bayer Animal Health Care) in the drinking water for 4 days prophylactically. The animals were given Buprenorphine (0.2-0.5mg/kg SC BIDx24 hrs) post operatively for pain for at least 48 hours or longer if the animal exhibited signs of pain. All animals maintained a healthy weight and overall appearance during the study.

Histological processing and staining

Explanted tissue was fixed in 4%PFA for 48 hours at room temperature and subsequently kept in 70% ethanol at 4 deg C before embedding in paraffin. Tissue specimens were embedded at the University of Virginia Research Histology Core (Figure 1E). Sections of the paraffin blocks were cut at 5 micron thickness. Hematoxylin and Eosin (H&E) and Masson's Trichrome stains were completed at the Research Histology Core.

Immunostaining was completed at the University of Virginia Biorepository and Tissue Research Facility. Anti-GFP antibody (AB3080, Millipore (Chemicon), Billerica, MA, USA) was used to trace the identity of cells in and around the construct to those seeded on the implant. Prolyl 4-hydroxylase subunit beta (P4HB, Acris, San Diego, CA, USA) was used to identify fibroblasts (Figure 1F-G). Antigen retrieval and deparaffinization were performed in PT Link (Dako, Glostrup, Denmark) using low pH (EnVision FLEX Target Retrieval Solution, Dako) for 20 min at 97°C. Immunohistochemistry was performed on a robotic platform (Autostainer, Dako). Endogenous peroxidases were blocked with peroxidase and alkaline Phosphatase blocking reagent (Dako) before incubating the sections antibodies for GFP at 1:200 for 60 min at room temperature. Antigen–antibody complex was detected using EnvisionTM Rabbit Link (Dako) followed by incubation with 3,3'-diaminobenzidine tetrahydrochloride (DAB+) chromogen (Dako). All the slides were counterstained with hematoxylin subsequently; they were dehydrated, cleared and mounted for assessment and imaging.

Staining for CD8 (clone OX-8, cat. #CBL1507, Chemicon, Chandlers Ford, UK) was done with these modifications to the above protocol. Antigen retrieval was conducted at high pH. Incubation at 1:100 for 30 min. Antigen–antibody complex was detected using biotinylated link and strepavidin-HRP (LSAB-HRP system,K0609, Dako).

Measurement of the fibrotic capsule thickness

A sample of slides was stained with Masson's Trichrome. The fibrotic capsule was defined as the blue stained collagen layer around the implant. NFs and NFs + Cells slides were examined under a 40X objective. Measurements were made on the electronic images in ImageJ.

GFP+ Cell and CD8 T-cell Quantification

40X objective images were quantified. eGFP cells were quantified by region in the scaffold, as depicted in Figure 4B for macrophage and fibroblast morphology cells as shown in Figure 5A. CD8 cells in the types of regions used for the eGFP cell quantification were quantified as well, with example positive staining cells shown in Figure 4D.

Hematoxylin and Eosin Section Examination

Hematoxylin and Eosin stained slides were randomly assigned a numerical code prior to the scoring examination. Individual slides were scored on the following scale: Both the depth of blood vessels and the depth of nucleated cells were scored as: 0 = Sparse, 1 = On Periphery, 2 = Scattered, 3 = Well Distributed, 4 = Very Dense. Ratings were then associated with their true identity and averaged by implant and time point to produce the presented analysis.

Vascularization was also quantified by measuring the area of blood vessels divided by the area of tissue qualified in each high power field of the periphery of the implant on electronic images in ImageJ. The thickness of tissue was measured in a similar way with ImageJ through the depth of constructs. Foreign Body Giant Cell (FBGC) presence was quantified by measuring the area of FBGCs defined as cells with 3 or more nuclei and quantifying the number of FBGC per tissue area.

MicroCT Scanning of Scaffolds

The scaffolds were scanned (Figure 1E) to obtain the percent change in volume of each implant calculated as the volume prior to implant minus the volume following explant divided by the volume prior to implant. The number of post-explant specimens available for scanning was not 12 due to two factors: 1) a few explants extruded and were lost, 2) the reserving of the implants from two rats at each timepoint for histological analysis of the tissue immediately surrounding the implant. Keeping the surrounding tissue

was not feasible for all implants, due to insufficient radiographic density differential at post explant timepoints.

After the cell seeding the implants were cultured in the folded form for no longer than 3 days prior to being implanted. The scan procedure required that an implant be outside the cell incubator for no more than 140 minutes. All implants were carefully curved to fit into a sterile 0.9mL conical centrifuge tube which was then placed into a custom holder mounted in the specimen scanner apparatus for the vivaCT40 MicroCT (Scanco, Brüttisellen, Switzerland). Evaluations post scan were done with a low threshold of -35 mg of hydroxyapatite, selected to exclude the plastic tube which the sample was in. All implants were sterilely hydrated in media (nanofiber constructs) or normal saline (decellularized dermis implants) before being scanned.

In vitro cell studies

For inter-layer migration studies, NIH3T3 cells were seeded only on certain quadrants of the 10x10cm grid and the constructs were folded as described for in vivo studies. For viability studies, cells were seeded onto single layer scaffolds. In either case a single layer (having been unfolded in the case of a folded scaffold) was stained using Propidium Iodide (Sigma) or Hoechst (Invitrogen), and Calcein AM (Invitrogen).

Statistics

Microsoft Excel was used to calculate the Student's T-test statistic reported as a p-value. MINITAB (State College, PA) was used to calculate standard deviation. Where appropriate, the Mann-Whitney test was used to determine statistical significance in MINITAB.

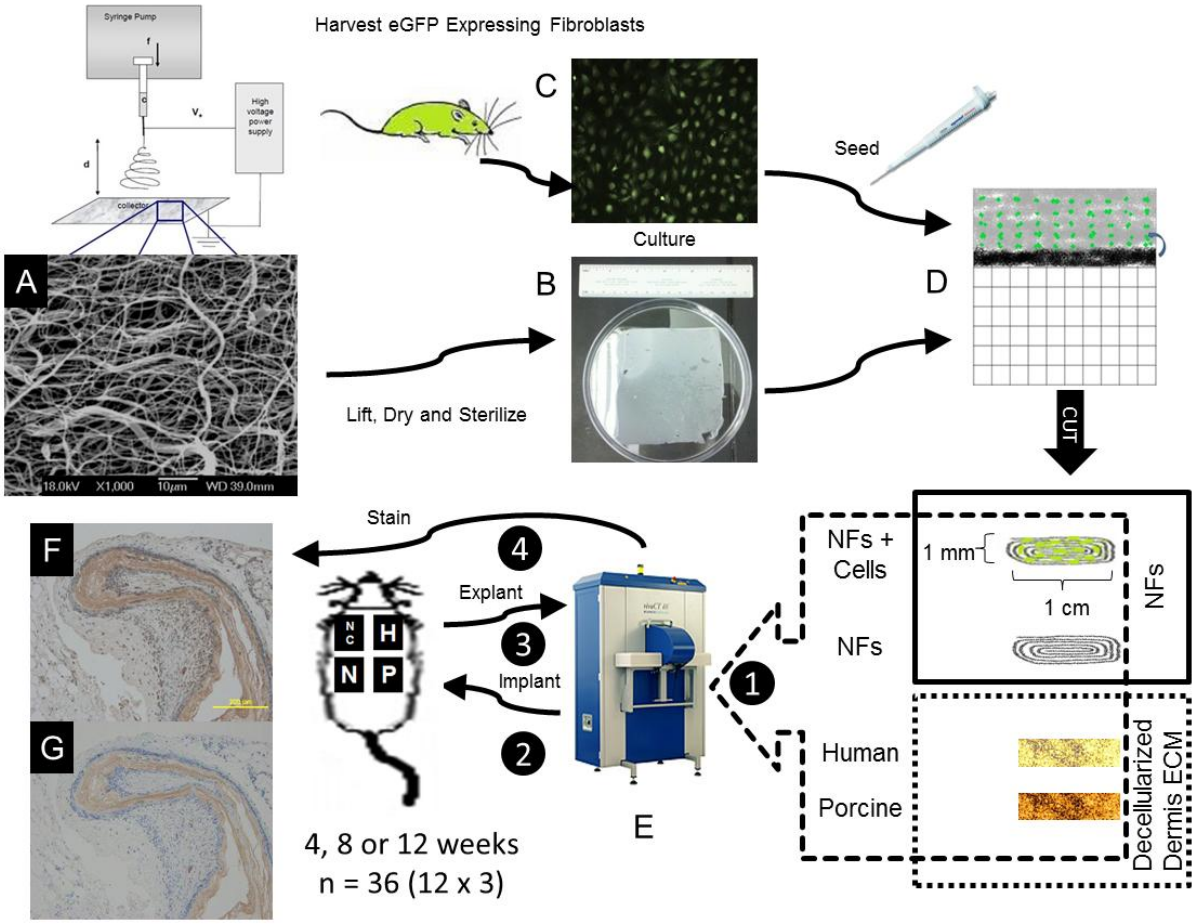

Figure 1: Experimental methods

Electrospun nanofibers made of PCL/collagen **(A)** were imaged under a Scanning Electron Microscope (SEM). The constructs were lifted from the collector and sterilized. An example 10 x 10 cm prepared construct is pictured next to a ruler measuring about 16 cm in length **(B)**. Primary fibroblasts were harvested **(C)** and seeded on the scaffold in monolayer. After cells were allowed to attach and culture on the fibers it was folded and cut **(D)**. Cross section of a scaffold shown. The cell pre-seeded scaffolds were compared to un-seeded scaffolds and decellularized dermis as controls in a single rat **(E)**. Before and after a duration of 4, 8, or 12 weeks in a rat. Each animal received one of each of the four implant types in distinct subcutaneous pockets on the dorsum. Implants were scanned **(1)**, implanted **(2)**, explanted, scanned a final time **(3)**, and processed for histology **(4)**. Post explant scanning **(3)** was completed following fixation in paraformaldehyde, therefore the samples were soaked in 70% EtOH at the second time of scanning, while implants for the first scan were in aqueous media. **(F,G)** Fibroblast antibody staining. Identification of fibroblasts using P4HB antibody **(F)** with antibody and **(G)** without antibody. Scale Bar 200um.

RESULTS

PCL/Collagen Fibers Support Fibroblast Viability and Migration

To characterize the interaction of fibroblasts with the PCL/collagen nanofibers, cells were seeded on a nanofiber sheet such that after folding cells were on the outer 2 layers (top and bottom) of a 10 layer construct. Within 12 hours of culture in vitro, the cells were present in the middle layers. Since no cells were seeded here, this suggests migration between layers. After 7 days of culture all 10 layers were found to contain cells (data not shown), suggesting that once folded the construct may function as a single scaffold rather than one made of 10 distinct layers. The viability of the cells was verified to remain high in comparison to tissue culture polystyrene (TCPS) for up to two weeks in vitro (**Figure 2A**) on a single layer of nanofibers. Furthermore, the morphology of the cells was more spindle-like on the nanofiber scaffolds (**Figure 2B**).

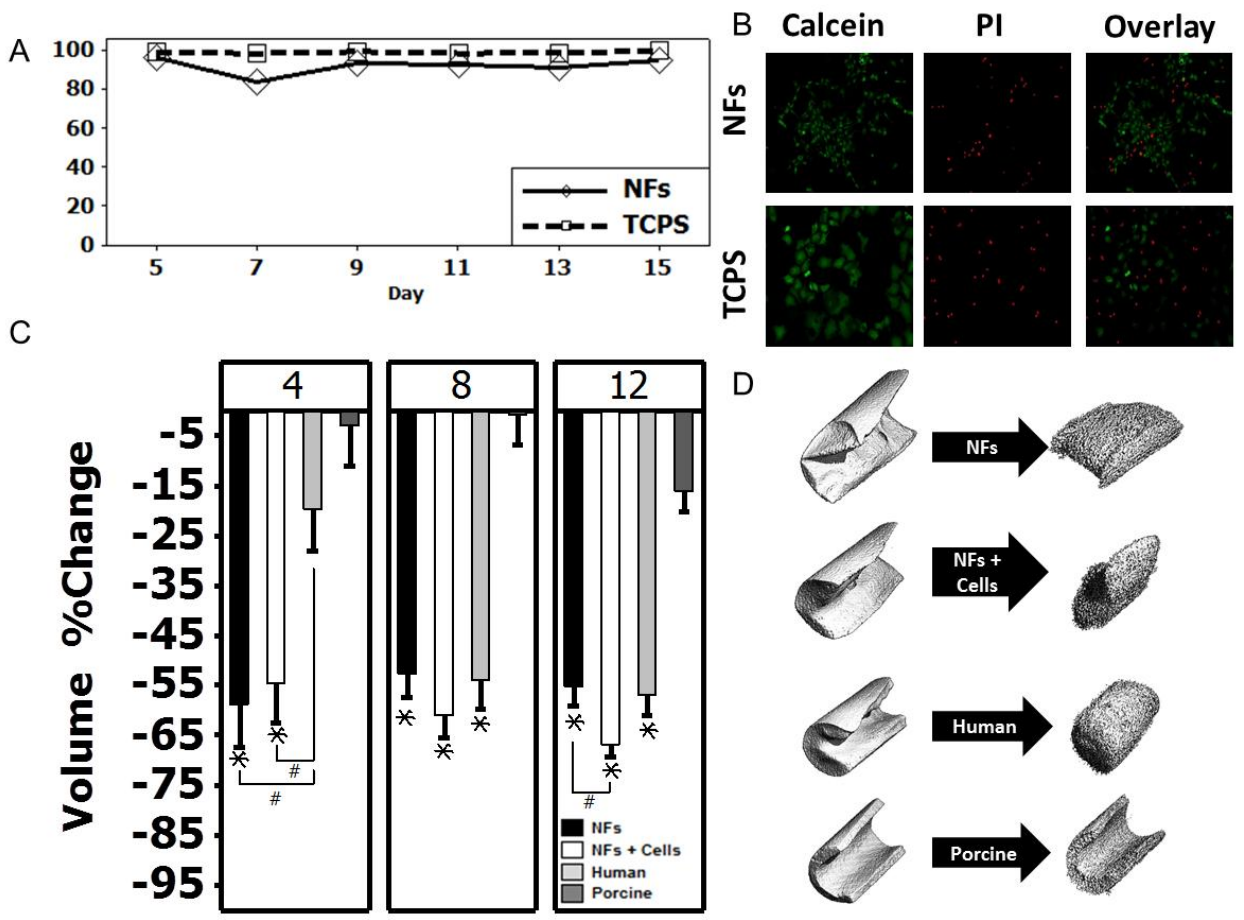

Figure 2: Viability of NIH3T3 fibroblasts on a single layer of nanofibers and volume changes

(A) Quantification of nanofibers (solid line, diamonds) verses TCPS (dashed line, squares). Mean of at least 3 samples in each group at each time point. (B) Representative images of cell viability. CalceinAM is converted to the fluorescent calcein in the cytoplasm of viable cells, while propidium iodide (PI) stains the nuclear material in cells that do not have a patent cell membrane. Notice in the overlay that calcein stained cells were not stained by PI, showing the accuracy of the stain. Calcien also reveals a spindle like cell footprint on the nanofiber substrate compared to the Tissue Culture Polystyrene (TCPS). (C) Percent change in volume at 4, 8 and 12 weeks of implantation based on MicroCT scan numerical evaluation. Each implant was referenced to that individual implant prior to surgery. The porcine ECM was significantly more stable. The seeding of cells did not have a significant effect until 12 weeks of implant. At 4 weeks n=10 for all implants, at 8 weeks n=8,9,9,8 for NFs, NFs+Cells, Human ECM, Porcine ECM respectively, and at 12 weeks n=10 for all implants. Standard Error Shown, * $p<0.05$ compared to Porcine, or # $p<0.05$ with connecting line showing indicated comparison. (D) Renderings of thresholded reconstruction of scanned implants from MicroCT scans before and after weeks in a subcutaneous pocket. Radiographic density became more punctate following implant.

Cell Seeding Resulted in Small Implant Volume Changes

Computed Tomography (CT) scans are capable of hard and soft tissue imaging. Based on the assumption that to a migrating cell the 10 layer construct is comparable to a single layer construct, the folding method needed to be validated in vivo. The 10 layers of the construct had cells seeded to each layer prior to folding (**Figure 1D**). One cell seeded scaffold and 1 of each of the 3 control implants were placed subcutaneously in each rat (**Figure 1E**). MicroCT scan evaluations revealed that all scaffolds except decellularized porcine dermis lost volume at all time points (**Figure 2C**). Regardless of cell seeding there was a large volume decrease at 4, 8, and 12 weeks in the nanofiber groups. The cell seeded and nanofibers alone implants were only statistically significant from each other at 12 weeks of implant ($p<0.05$). Human decellularized dermis in contrast lost the greatest volume between weeks 4 and 8, but was stable thereafter. Decellularized porcine dermis, essentially lost no volume until 12 weeks, and was still the most similar to pre-implant volume of all implant types. Renderings of the microCT scans demonstrate a decrease in radiographic density (**Figure 2D**).

Cell Seeding Promotes Host-Incorporation in-vivo

After 4, 8 and 12 weeks of implantation cell seeded nanofibers were compared against nanofibers alone, as well as the human and porcine decellularized ECM. Tissue deposition between nanofiber layers was observed in both cell seeded and nanofibers alone scaffolds indicating that the nanofibers provided a good substrate for de novo extracellular matrix secretion at 4 weeks post implant (**Figure 3A,C-H**), which was not necessarily dependent on cell pre-seeding. The thickness of new tissue was more varied on a layer verses layer basis within a single scaffold in the cell seeded constructs (**Figure 3F-H**), indicating that the pre-seeded cells were participating in this process.

Ratings and vessel area measurements of H&E stained sections of implants demonstrated that cell pre-seeding produced a significantly greater degree of vascularization at the 4 week time point (**Figure 3B**), which then decreased slightly through 12 weeks. The non-cell seeded scaffold group saw an increase in

vascularity between weeks 4 and 8. Human and porcine ECM were generally at a low level of vascularization throughout the study.

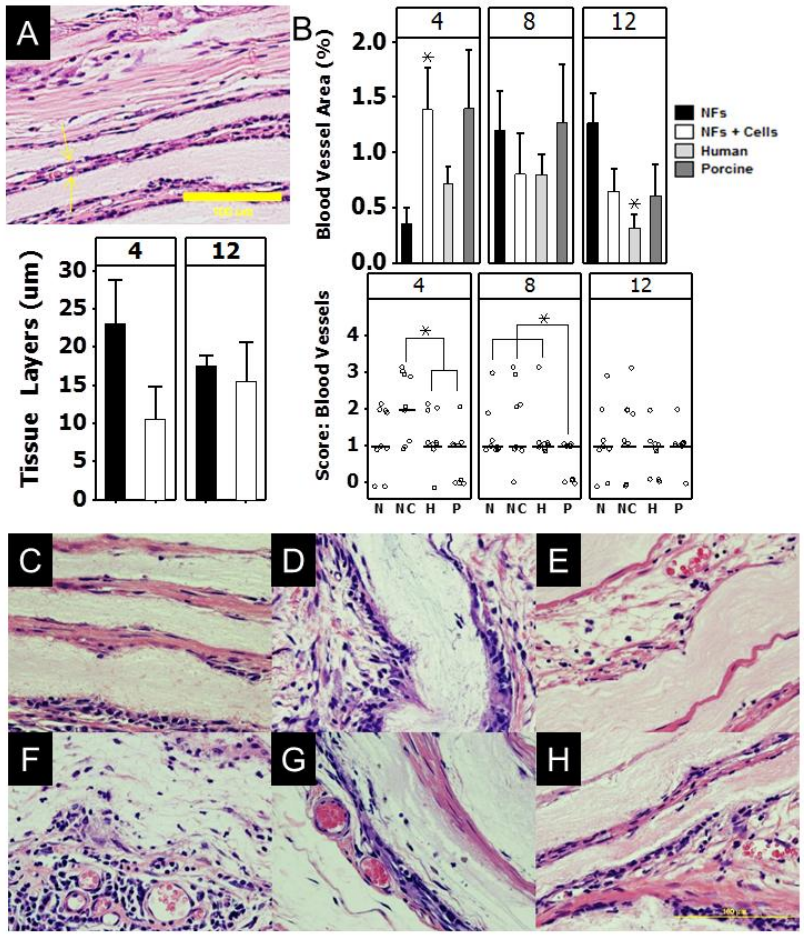

Figure 3: Histological analysis of tissue layers and blood vessel investment

(A) Thickness of host tissue (yellow arrows) was measured on 40x images of the cross-section of implants. Vertical bars indicate the standard deviation of the means of all the layers in 6 implants (Black bars NFs, empty bars NFs + cells). Host tissue deposited between nanofiber layers was variable but not statistically significant ($p>0.1$ for all comparisons of NFs vs. NFs+Cells). (B) Percent area of blood vessels outside the implant border. Cell seeding increases blood vessels early, but nanofibers without cells sustain blood vessels at longer time points. Standard error of n=30, * $p<0.05$ compared to NFs. Histological score of blood vessel penetration (see text for score key). Median shown as bar with individual data points shown by open circles, which all are integer numbers, slight offset used to allow individual data points to be resolved. n=9, *$p<0.05$ by Mann-Whitney test. Hematoxylin and Eosin stained slides show little inflammation and cellular residence as well as host ECM. NFs at 4,8,12 weeks (C,D,E respectively), NFs+Cells 4,8,12 weeks (F,G,H respectively). 40X objective. Scale Bar 100um.

Pre-seeded Fibroblasts do not Persist in the Construct

H&E staining established that the implants were highly cellular. Staining with P4HB antibody, specific for fibroblasts, suggests that cells in the implants were fibroblasts (**Figure 1F,G**). Since all dermal fibroblasts seeded onto the fibers expressed eGFP, the origin of the cells could be determined using immunohistochemistry. Two morphologies of the stained cells were quantified, either a fibroblastic or rounded macrophage type morphology (**Figure 4A**). The counted cells were also classified based on the region from which the 40X image was taken, either outside the implant, at the implant interface, or inside the implant (**Figure 4B**). Fibroblast morphology cells were found almost exclusively at the interface and the greatest number of cells per field were on the cell seeded implants at 4 weeks (**Figure 4C**).

The macrophage morphology cells were found primarily at the interface and outside the implant (**Figure 4D**). These cells likely engulfed seeded cells and therefore were still harboring eGFP or they arose by differentiation from the seeded cells. They were highly migratory showing up on the decellularized dermis implants at 4 weeks. There was only one implant still showing significant numbers of cells at 12 weeks, the human decellularized dermis. While the cause of this is not known, the human decellularized dermis was physically located closest to the cell seeded scaffolds. Thus the seeded fibroblasts did not persist over the course of this experiment however eGFP+ cells were actively participating in the response to the subcutaneous implants.

Immune Reaction to the Implants

The presence of cells promoted a thicker capsule (**Figure 5A-C**) and greater numbers as well as larger foreign body giant cells (**Figure 5F,G**). However, CD8+ cytotoxic lymphocytes (CD8 Tcells) while increased early, were significantly decreased at 12 weeks both at the interface and outside the implants with the seeding of cells (**Figure 5D,E**). This suggests that the pre-seeded cells affected the type of inflammatory response, characterized by FBGCs and reduced specific immunity.

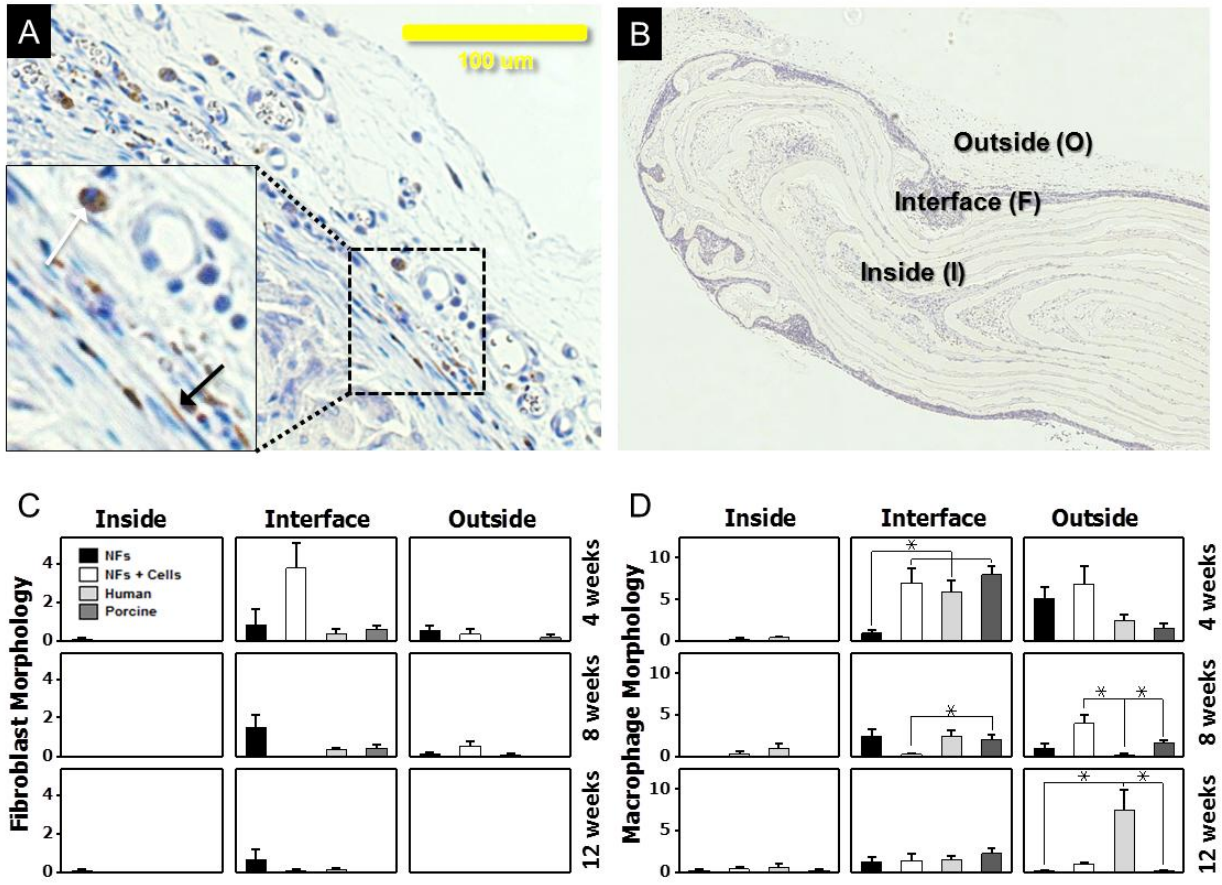

Figure 4: Fate of seeded (GFP+) donor cells

(A) Images of sections showing GFP positive cells. Arrows: Fibroblast Morphology (Filled), Macrophage Morphology (Open), 40X, scale bar 100um. Inset electronic enlargement of area indicated. (B) Large area of an implant shown to mark the regions referred to as Inside(I), Interface (F), and Outside (O). GFP positive cells in histological sections by immunohistochemistry. GFP+ cells were absent within the implants. (C) Fibroblasts were apparent at the interface of the implants they were originally seeded on and to some extent at other implants. (D) Macrophages that took up GFP+ donor cells migrated to other implants, but did not tend to infiltrate the implant, remaining outside or at the interface instead. Standard error of n=20 HP fields, * $p<0.01$ (40x objective).

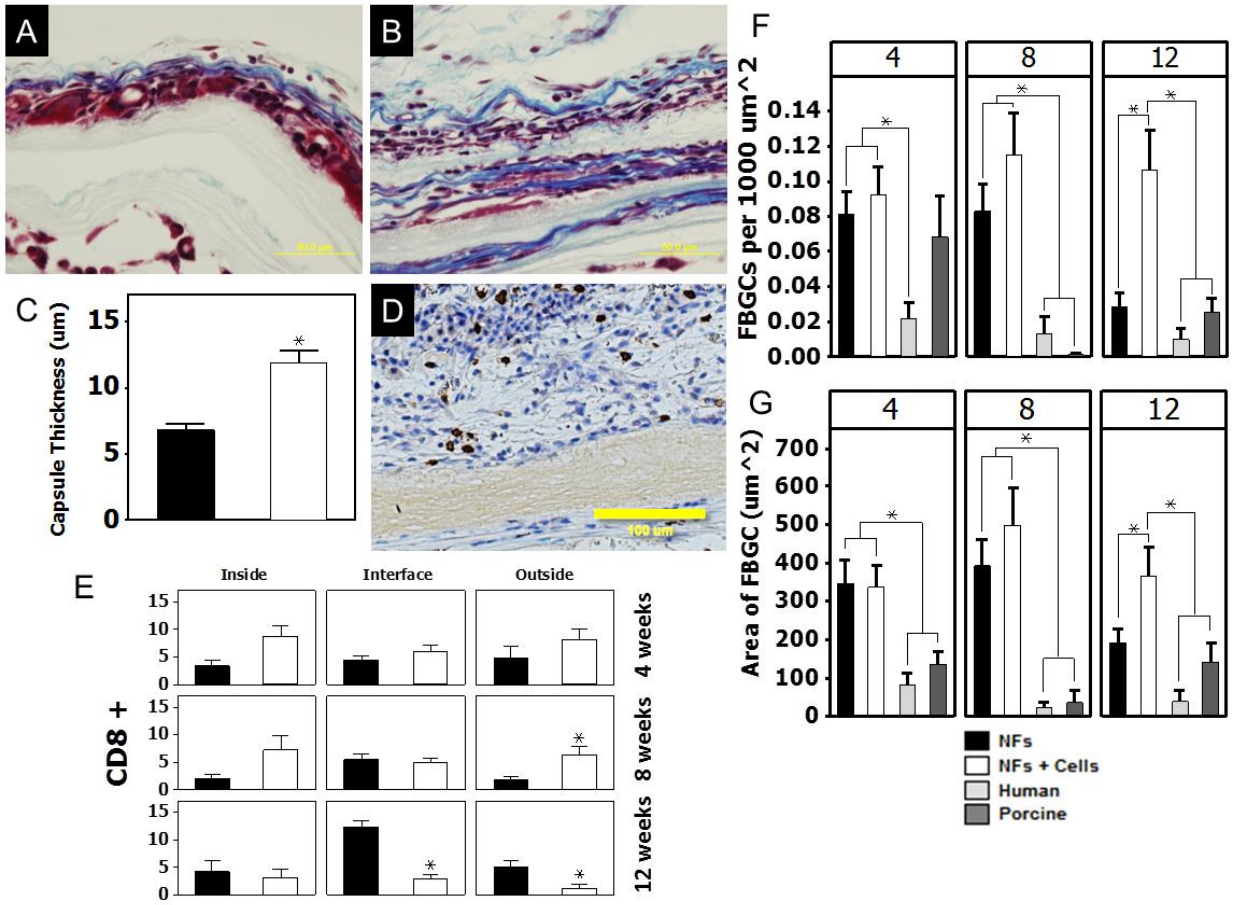

Figure 5: Immune reaction to nanofiber based implants

The thickness of the capsule was visualized using Masson's Trichrome stained sections on NFs (A) and NFs + Cells (B). The capsule thickness was measured (C), with *$p<0.05$. 40x Objective, scale bar 50um. n=25 minimum for each group. (D) CD8 immunostaining, scale bar 100um. CD8 positive cells were quantified (E) showing significant reductions in the NFs + Cells group at 12 weeks. Standard error of n=20 for each bar with *$p<0.02$ compared to NFs. Foreign Body Giant Cell (FBGC) number per slide area was greatest at the nanofibers implants with few exceptions (F). At 12 weeks there were fewer FBGCs on the NFs than there were on the NFs with cells. The area of the individual FBGCs followed almost the same trend with the nanofibers groups having larger FBGCs than the decellularized dermis groups at both 4 and 8 weeks (G). However by 12 weeks the cell seeded nanofibers implants were surrounded by larger FBGC than the nanofibers alone. Standard error shown with n=30 for each bar and * $p<0.05$.

DISCUSSION

Cell seeding has been shown to decrease inflammation[238] and increase acceptance despite the fact that the seeded cells are replaced by the host cells. The benefits of cell seeding would be difficult to bring to clinical practice with currently published methods. The construction method presented here allows for fast cell seeding and implant buildup that does not require special equipment.

Cells seeded onto the PCL/collagen matrix promoted incorporation of the implanted scaffold even though they were eventually replaced by host cells. The seeding density of cells within the implant was relatively low compared to published results (**Table 2**). This may support a hypothesis that cell presence is more important for integration with host tissue than the cultivation of cells on the constructs long enough for proliferation and laying down of ECM proteins[239]. The multi-layer constructs can be folded immediately prior to implant. This allows the clinician to tailor the implant at the time of implantation.

In the cell migration experiment, cell presence on all 10 layers indicates migration of individual cells across at least 4 layers of nanofibers from each side. The cell migration observed within the scaffolds is greater than the depth of penetration in a modified gelatin based scaffold where a maximum of 250 micrometers was noted[240]. Gee et al. reported the use of a natural cross linking agent[241], which was used to demonstrate that a greater proportion of collagen inhibited migration of mesenchymal stem cells. The collagen containing electrospun scaffolds used here were not crosslinked and supported fibroblast migration. The migration experiment suggests that although the implant begins as 10 distinct layers, once folded it acts as a single implant.

The volume of the implants was slightly reduced by the addition of cells. Change of implant volume, especially a reduction, may be seen as a negative result in terms of maintenance of appearance in a reconstructive surgical setting. The study design did not evaluate the effect of these volume changes on outward appearance at the implant site. However, as long as the implant does not decrease in volume

faster than the new tissue is formed, implant volume decrease does not indicate that there would be a visible surface deficit.

Observations from this study demonstrate that cell seeding can be accomplished on multi-layered PCL/collagen nanofiber constructs and this improves vascularization and modifies the inflammatory response. Cell migration over a 7 day timeframe, in combination with the single layer viability, suggests that diffusion limited nutrient delivery is not a limiting factor within these multi-layer scaffolds. The PCL/collagen fibers were well tolerated by the recipients. When eGFP expressing cells were used to differentiate between host and donor cells, many donor derived cells were found in close proximity to the nanofiber surface of individual layers. eGFP positive cells became less numerous throughout the study duration being replaced by host cells and participating in the remodeling process.

Table 2: Cell seeding density literature values

Density	***Medium***	***Cell Type***	***Reference***
30 or 60 million cells/mL	Injectable Hydrogel	Chondrocytes	[242]
2×106 cells/mL	10×10×0.5 mm PLGA nanofibers	hMSCs, hMSC-derived chondrocytes and osteoblasts	[243]
1–5×105 cells/cm2	P(LLA-CL) (75:25) electrospun nanofibers	ECs and SMCs	[244]
As many of 4.0×10^6 cells in a pellet as would stick over several days	1cm x 1cm x 1mm thick PCL nanofiber scaffold	Primary MSCs	[245]
0.2-5.7 x 10^6 cells per scaffold	Freeze dried Alginate scaffold (cm^3)	Primary Hepatocytes	[246]
15 × 10^6 cells/ml	agarose gel	Primary Chondrocytes	[247]

CHAPTER 2: EQUIP THE DEVICE WITH OXYGEN SENSORS

RESULTS AND DISCUSSION

Oxygen gradients drive cell migration and differentiation while both extremely high and low oxygen tensions cause cell death. Measuring the oxygen concentration within 3-dimensional cell migration permissive scaffolds would enable understanding of the dynamic aspects of oxygen gradient responses. Established methods to measure oxygen concentration, using electrodes, require mechanical disturbance of the tissue structure. However, imaging has allowed non-invasive oxygen monitoring using paramagnetic resonance, and fluorescence or phosphorescent quenching[248]. Iodine-substituted boron dyes, the oxygen sensor used here, emit a local oxygen concentration dependent signal. The ratio of the oxygen quenched phosphorescent emission to the oxygen independent fluorescent emission produces an internally standardized ratiometric molecular oxygen sensor. This negates the need for the commonly used separate photobleaching correction fluorophore component.

Nanofibers offer extracellular matrix (ECM) mimetic morphology that is beneficial for the culture of many cell types such as schwann cells[249], oligodendrocytes[250], cardiomyocytes[251], osteoblasts[252], smooth muscle and endothelial cells[253]. Electrospinning enables controlled morphology scaffolds to be made by tuning the process parameters making it an ideal method for synthetic tissue engineering scaffold production. The small diameter and large surface to volume ratio of nanofibers reduces the distance oxygen needs to diffuse within the polymer matrix to reach an embedded molecular sensor. Different types of oxygen sensors have been blended with polyurethane[254], polystyrene[255–258], and polycaprolactone (PCL)[259], to make nanofibers. We blended the oxygen sensitive boron dye with poly(lactic-co-glycolic acid) (PLAGA), an FDA approved biodegradeable polymer.

The faster degrading PLAGA co-polymer (50:50, lactic:glycolic subunits) blended with an unconjugated dye resulted in reduced oxygen sensing capabilities after time in aqueous buffer[260]. The slower degrading 85:15 co-polymer ratio of PLAGA was tested here in an attempt to increase the emission. Analysis by gel-permeation chromatography, at weekly timepoints up to 3 weeks, showed that in comparison to the 50:50 ratio the 85:15 ratio was degrading slower, and the addition of the dye had little effect (**Supplementary Table 1**). After a 14-day aqueous media degradation study, the room temperature phosphorescent peak blue shifted twice as much when the 50:50 co-polymer ratio was used as when the 85:15 co-polymer ratio was used (**Supplementary Table 2, Supplementary Figure 1c**), indicating preservation of dye microenvironment with the slower degrading polymer. However the phosphorescent peak was found to be weak in comparison to the fluorescent peak after *in vitro* aqueous degradation (**Figure 6i**), which reduces the utility of the scaffold for tissue engineering applications.

A new chemically conjugated form of the dye, attached to a polylactic acid (PLA) polymer, could replace the physical mixture of dye and polymer (PLAGA) blend for scaffold fabrication. Furthermore, we hypothesized that the chemical conjugation would reduce leaching of the dye in aqueous media and therefore preserve sensor function. A low molecular weight conjugated PLA produced good optical properties in the raw material[261], however electrospinning low molecular weight polymers requires careful modification to the electrospinning solutions and parameters. After some exploration (Figure 6**a-c**), we arrived at final parameters of 30% (w/v) dye-polymer in 10% (v/v) pyridinium formate, 20% (v/v) ethanol, in dichloromethane at a 25 kV applied voltage, 14.5 cm working distance, and 1 mL/hr solution flow rate applied to the polymer alone (**Figure 6d**) and then to the boron dye-polymer conjugate (**Figure 6e**).

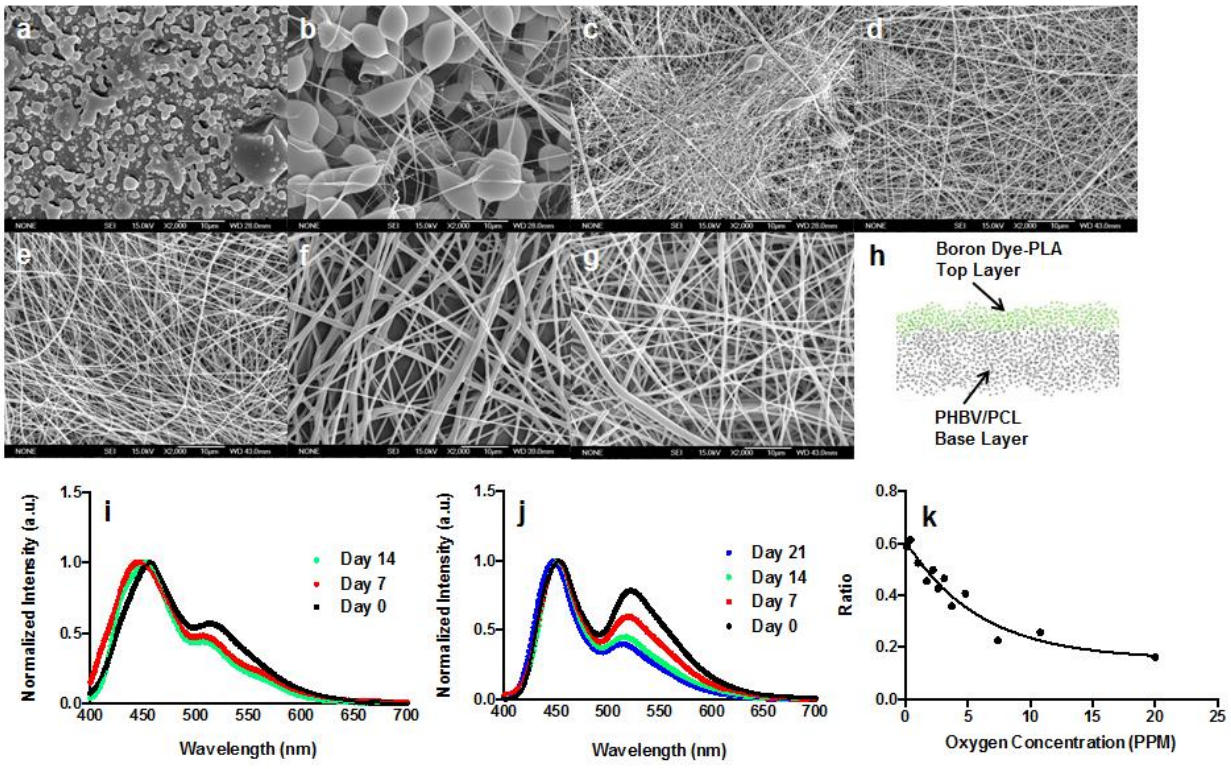

Figure 6: Optimized electrospinning parameters of dye-polymer conjugate nanofibers and performance after *in vitro* degradation

(a) The THF to DMF ratio was varied (30%w/v DMF:THF (3:1) shown) followed by (b) exploration of dichloromethane as a solvent (45% (w/v) PLA at 15 kV, at 14.5 cm at 1 mL/hr shown). (c) The addition of pyridinium formate improved the size and shape of the fibers dramatically, while (d) the addition of ethanol reduced beading and dripping. (e) The final parameters (see methods) were then applied to the boron dye conjugated PLA. The boron dye fibers were electrospun on a base of PHBV & PCL fibers (f) shown in the final form under SEM (g) and diagrammatically in cross sectional view (h). Nitrogen environment emission for dye polymer blend nanofibers(i) and dye-polymer conjugate nanofibers(j) (n=6 per time point). (k) Aqueous oxygen concentration calibration. PPM: Parts Per Million

Due to the brittle nature of electrospun low molecular weight polymer nanofiber mats, a support layer of Poly(3-hydroxybutyrate-co-3-hydroxyvalerate) and polycaprolactone (PHBV & PCL) nanofibers was employed (**Figure 6f**). The boron dye nanofibers were electrospun onto the dry PHBV & PCL nanofibers attached to the grounded collector plate (**Figure 6g-h**), allowing for the simultaneous removal of the nanofiber layers. The dual layer scaffold has a greater Young's modulus and maximum tensile strength than the PHBV & PCL layer alone **(Supplementary Figure 2a,b)**. The intermediate values of water

contact angle and nanofiber diameter (**Supplementary Table 3**) validate the thin nature of the boron dye layer (**Supplementary Figure 2c-h**).

Imaging through the support layer should be quantitatively equivalent to imaging the oxygen sensor layer directly to allow more freedom in applications. Ratiometric imaging confirmed that the signal is similar when imaged directly (**Supplementary Figure 3a**) or through the support layer (**Supplementary Figure 3b**). We also found similar ratios when the scaffold was submersed in phosphate buffered saline (**Supplementary Figure 3c**) demonstrating compatibility with a hydrated environment.

In order to further understand the effects of exposure to aqueous media, the spectral response was measured after 0, 7, 14 and 21 days of incubation at 37degC with rotational movement in phosphate buffered saline. The phosphorescent peak declined with increasing duration of incubation when compared to a normalized fluorescence peak (**Figure 6j**), but was distinct compared to the dye polymer blend nanofibers after degradation. A slight blue-shift in both phosphorescence and fluorescence peaks was also observed, indicating a change in the dye microenvironment, such as degradation of the polymer matrix. The scanning electron microscopy imaging showed that the slowly degrading support layer remained constant over the 3 weeks and that the dye layer fibers swelled with time in aqueous media (**Supplementary Figure 4**). Unlike the blended fibers, the material characteristics of the conjugated dye supported further validation.

Stem cells may maintain stemness longer[262], [263] and differentiation protocols may be more effective[264], [265] in low oxygen conditions although fine tuning of this oxygen tension is needed to prevent detrimental hypoxia. With those and general tissue engineering applications in mind, calibration curves were constructed. Similar curves were found regardless of data collection directly at sensor layer or through the support layer (**Supplementary Figure 5a**). In aqueous solutions of phosphate buffered saline (**Supplementary Figure 5b**), Dulbecco's Modified Eagle Medium (DMEM) (**Supplementary**

Figure 5c) and DMEM supplemented with fetal bovine serum (FBS) (**Figure 6k**), responsiveness was found for values less than 15 parts per million (PPM) dissolved oxygen.

It was now possible that the scaffold could quantify extracellular oxygen depletion around cells or tissues. To ensure that the response would be fast enough for living systems, a moving stream of nitrogen was passed over the fibers. The fibers in the low oxygen stream both activated (increased ratio) and returned to baseline very quickly. To further prepare for validation in living systems, the biocompatibility of the nanofiber constructs was tested. This was deemed necessary since a mixture of organic solvents was used to obtain desired fiber morphology. D1 cells (adherent mouse bone marrow stem cell line) were cultured on the dye nanofiber layer showing no concerns with the biocompatibility as most cells stained viable by fluorescein diacetate (FDA) (**Figure 7a**) and were not stained by propidium iodide (PI) (**Figure 7b**).

In vitro validation was conducted by seeding D1 cells onto the scaffold, this time fluorescently stained with a membrane stain to define a cell area mask (**Figure 7c**). The nanofiber scaffold was mounted on a glass slide with cover slip immediately prior to imaging to achieve a hypoxic environment. As time increased from 0 to 15 minutes the edge of the spatial oxygen gradient moved as shown in **Figure 7d** by the white area. The oxygen tension decreased in the regions with and without cells when the initial seeding density was increased by a factor of 5 (**Figure 7e**). The difference between the cell covered and non-covered region decreased with time and the rate of change was dependent on the initial cell density (**Figure 7f**). Next we wanted to validate the nanofiber mesh in the more challenging *in vivo* environment.

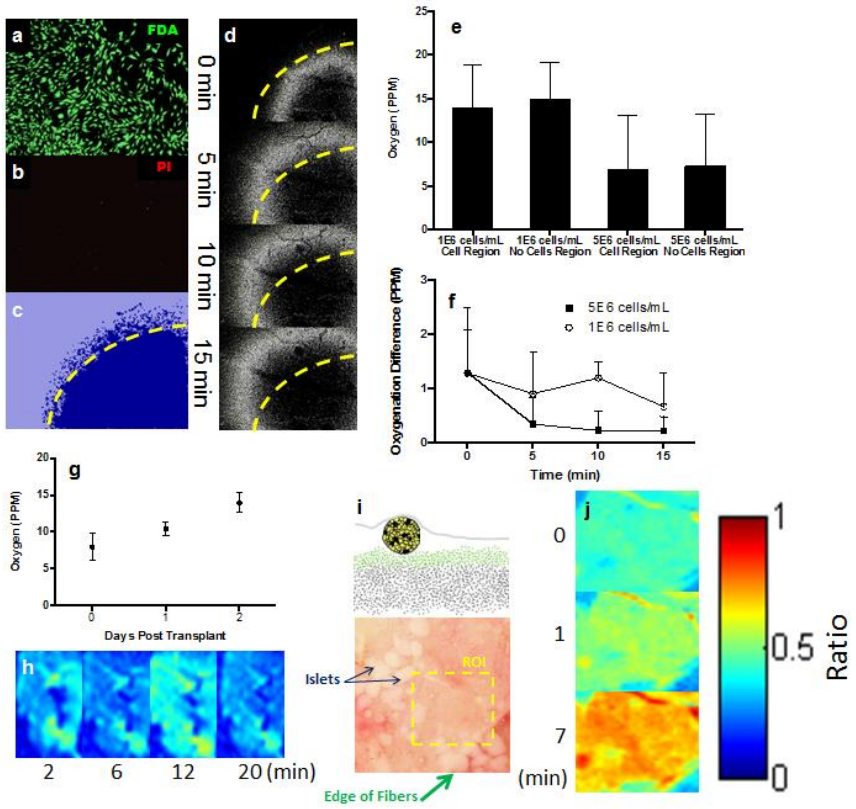

Figure 7: Nanofibers display oxygen gradients in vivo in response to ischemia and cell transplant as well as oxygen poor regions in vitro due to scaffold adherent cells

Cells were viable on the boron dye fibers (a, viable (FDA); b, non-viable (PI)). Oxygenation around cells could be imaged longitudinally, referenced to a cell mask (c), with lower oxygen corresponding to the area covered with cells (c, dark blue) advancing with time (d). Higher cell concentration resulted in lower sensed oxygen (e, n=3 each bar) and differential rate of change (f, n=3 for each seeding density). (g) Oxygenation increased with time following implant. (h) Nanofibers show variation in oxygen tension in ischemia. Hypoxia following implantation of pancreatic islets on top of the nanofibers (i-j). Color bar shows ratio for pseudocolored images.

The dorsal skinfold window chamber was selected for *in vivo* validation as it provides a planar tissue surface that lends itself to fluorescence and brightfield imaging. Over the course of 48 hours following surgery and sensor implantation, the oxygen tension increased as the tissue recovered from the insult (**Figure 7g**). It was observed that oxygen gradients could be sensed in proximity to blood vessels as well (**Supplementary Figure 6**). Tissue oxygenation following ischemia initiated at t=0 min varied with time and space (**Figure 7h**), showing the scaffold is tuned to a relevant range of dissolved oxygen. Pancreatic

islets are known to suffer from hypoxia due to their multicellular spheroid shape. We transplanted recently isolated syngeneic pancreatic islets in a type 1 collagen gel onto the nanofibers (**Figure 7i**), finding that hypoxia was strikingly evident by 7 minutes following the delivery of the islets (**Figure 7j**).

Thus, nanofibers with controlled morphology can be made entirely of a polymer conjugated oxygen sensitive dye. The ratiometric method used here self corrects for the photobleaching usually requiring a separate component, increasing the complexity of electrospinning. Shelf stability was shown as the fibers used for the *in vivo* studies were stored dry at 4degC for a year. Function of the dye after 21 days in saline solution at 37degC indicates that the nanofibers could work as an oxygen-sensing scaffold for *in vitro* cell culture or as a cell transplant scaffold *in vivo*. Although we have validated this new nanofiber oxygen sensor as a hypoxia sensor, it is calibrated to a range of oxygen concentrations. Therefore, these fibers could also be used to map hyperbaric oxygen used as a therapy[266] for chronic wounds. In conclusion, we have confirmed that this novel oxygen sensing scaffold can be a platform for scientific investigation with clinical potential.

	50:50 PLGA				85:15 PLGA			
	unloaded		dye-loaded		unloaded		dye-loaded	
Day	M_n	PDI	M_n	PDI	M_n	PDI	M_n	PDI
0	25000	1.85	25000	1.80	32000	1.86	37000	1.54
7	21000	1.96	24000	1.83	37000	1.95	38000	1.84
14	15000	2.29	16000	2.09	32000	1.93	41000	1.87
21	14000	1.85	15000	1.77	34000	1.73	33000	1.60

Supplementary Table 1: 85:15 PLGA degraded slower without an observed effect of the addition of dye

	50:50 PLGA		85:15 PLGA	
	I_{RTP}	$t_{RTP/x2}$	I_{RTP}	$t_{RTP/x2}$
Day	(nm)	(ms)	(nm)	(ms)
0	531	4.68 ms/1.32	525	4.16ms/1.25
7	522	5.12 ms/1.08	520	3.24ms/1.04
14	520	5.13 ms/1.10	520	3.11ms/1.11

Supplementary Table 2: 85:15 PLGA reduced the blue shift of the phosphorescent peak

	Boron Dye-PLA	PHBV/PCL	PHBV/PCL+ Boron Dye-PLA
Diameter (nm)	258+/-81	712+/-254	543+/-199
Contact Angle (deg)	106 +/- 5.9	118.7 +/- 3.2	113.5 +/- 5.7

Supplementary Table 3: Nanofiber diameter and nanofiber mat liquid contact angle

METHODS

Electrospinning of dye-blend nanofibers

The luminescent difluoroboroniodo-dibenzoylmethane dye (BF_2dbm(I)OH) was synthesized by the Fraser laboratory following previously published protocols[261]. Nanofiber meshes containing the BF_2dbm(I)(OH) (hereafter referred to as dye) were fabricated by blending with polylactide-coglycolide (PLGA, Lakeshore Biomaterials in two formulations: 50:50 PLGA (Mw = 65 kDa, PDI = 1.6) and 85:15 PLGA (Mw = 109 kDa, PDI = 1.5)) and electrospinning. 20 % (w/v) PLGA with the addition of 5% (w/w) of the dye were dissolved in equal parts tetrahydrofuran (THF) and dimethylformamide (DMF) (Fisher Scientific). This solution was loaded into a syringe, mounted into a programmable syringe pump (Aladdin-1000, World Precision Instruments, Sarasota, FL), and dispensed at a flow rate of 1mL/hr. A driving voltage of 15 kV was supplied to an 18G needle by a high voltage power source (Gamma High Voltage Research, Ormond Beach, FL) across a 15 cm collecting distance to a grounded aluminum collector plate. For imaging purposes, some fibers were collected on plasma-treated glass coverslips. Control PLGA fibers were fabricated by the same methods, with an additional 5% (w/w) PLGA to take the place of the dye in solution.

Electrospinning PHBV/PCL Fibers

Poly(hydroxylbutyrate-co-valerate) (PHBV; Carbomer) and poly(caprolactone) (PCL; Sigma) were dissolved in equivalent amounts in 1:3 methanol:chloroform (Fisher Scientific) to yield an 18% weight-to-volume solution. The solution was loaded into a syringe mounted in a syringe pump (1 mL/hr) suspended above an aluminum foil collecting plate in a sealed case. The metal blunt ended syringe tip was charged to 19 kV relative to ground and placed 14 cm above the collecting plate. The fibers were dried in a lyophilizer (Labconco, Kansas City, MO).

Electrospinning BF2dbm(I)PLA Fibers

BF_2dbm(I)PLA (synthesized according to a previously published technique[261]) was dissolved in a solution of 10% pyridinium formate (PF; equimolar amounts of formic acid and pyridine), 20% ethanol, and 70% methylene chloride (Fisher Scientific, Waltham, MA) to yield a 30% weight-to-volume solution. The aluminum foil with dried PHBV/PCL fibers was used as the collecting plate for fabricating the dual-layer fibers while a clean aluminum foil sheet was used to collect only BF_2dbm(I)PLA fibers. The BF_2dbm(I)PLA polymer solution was loaded into a syringe as described above and displaced at 1mL/hr. The metal syringe tip was charged to 25 kV relative to ground and placed 14.5 cm above the collecting plate. The fibers were dried in a lyophilizer.

Diameter Characterization

To image fibers, samples were mounted on ½ cm-diameter aluminum mounts. Mounted samples were gold-coated with a BAL-TEC SCD 005 Sputter Coater (BAL-TEC AG, Liechtenstein) for 210 seconds and observed under a scanning electron microscope (JEOL JSM-6400 SEM; Advanced Microscopy Facility, University of Virginia) at an accelerating voltage of 15 kV and magnification of 2000x. SEM images were acquired using ORION software to assess nanofiber morphology.

The diameters of the fibers were measured using ImageJ software. SEM images from each group were opened in ImageJ and a line was drawn across the center of the image. 50 diameter measurements were taken from nanofibers intercepting the line.

Hydrophobicity Characterization

Hydrophobicity of each nanofiber condition was quantified through contact angle measurements. A drop of deionized water was placed on top of the nanofibers for each condition. A goniometer (Rame-Hart Standard Contact Angle Goniometer, Model 200; Rame-Hart Instrument Co., Succasunna, NJ) and

DROPimage Standard software were used to measure the contact angle between the fiber and the liquid. Contact angle measurements were repeated three times for each type of nanofiber.

Strength Characterization

To characterize nanofiber strength, three samples from each nanofiber condition (except BF_2dbm(I)PLA) were subjected to tensile strength testing using an Instron materials testing instrument (Instron Model 5543; Instron Worldwide Headquarters, Norwood, MA). The BlueHill2 Program Software (version 2.14) was used to obtain force-displacement graphs for each sample. Dimensions of each sample (length, width, thickness) were measured prior to testing. The force-displacement curve data was used to calculate engineering stress and strain; stress (MPa) was calculated by dividing load (N) by cross-sectional area (width x thickness; mm^2) of the sample at each time point. Strain was calculated by evaluating the percent extension, or extension (mm) divided by length (mm), at each time point. Stress-strain curves were plotted for each sample. Ultimate Tensile Strength (UTS) was determined by the highest point on the stress-strain curve. Young's Modulus (E) was determined by regression fitting the linear region on the stress-strain curve and evaluating the slope. Values for E and UTS were averaged across samples for each condition. An independent means t-test was conducted to assess the strength differences between the two conditions. BF_2dbm(I)PLA fibers were not subjected to strength testing due to the inability to remove fibers from collecting foil.

Ratiometric Imaging

To test the oxygen-sensing capabilities of the dual-layer fibers (BF_2dbm(I)PLA fibers on PHBV/PCL fibers), a section of the fibers was cut from collecting foil. The dual-layer fibers were then peeled from the foil after soaking in EtOH and air-dried. Then the dual-layer section was taped to the bottom of a plastic, non-tissue-culture petri dish. To image the BF_2dbm(I)PLA fiber layer, the dual-layer fibers were exposed to UV light (395-415 nm) from a fluorescent lamp (X-Cite 120Q; Lumen Dynamics Group, Inc., Ontario, Canada). Then the fluorescent and phosphorescent modes of emission were collected with a

Beta-Lactamase Filter 1 (440-480 nm) and Beta-Lactamase Filter 2 (485-515 nm) (Chroma Technology Corp; Bellows Falls, VT), respectively, for the same area at a constant exposure time (4.5 ms or 25 ms for boron dye side facing objective or support layer facing objective respectively) and lamp intensity level (lowest setting). Images were taken at 10x magnification on an inverted microscope (Microscope Axio Observer.A1; Carl Zeiss, Bulgaria) with an AxioCam HSM camera (Carl Zeiss). Once an area was imaged while air-exposed, nitrogen was blown into the petri dish through a pipette tip for five minutes before imaging the same area. Then, a new area was chosen and the petri dish was exposed to only air for five minutes before being imaged. This was repeated for five different areas.

To generate the ratiometric images, the separate fluorescent and phosphorescent intensity images for a single area were loaded into MATLAB. The phosphorescent-to-fluorescent intensity ratio was calculated at each pixel (pixels with zero fluorescent intensity were skipped in all calculations). To quantify the phosphorescent-to-fluorescent ratio for an entire condition (air-exposed vs. nitrogen-exposed), all five sets of fluorescent and phosphorescent images were loaded into MATLAB. The average intensity was calculated for each image, and then the phosphorescent-to-fluorescent ratio was calculated by dividing average phosphorescent by average fluorescent intensities for each field of view imaged. Finally, the five phosphorescent-to-fluorescent ratios were averaged and compared between conditions.

Standard Curves

A section of the dual-layer fibers were cut, removed from the foil, and taped to the bottom of a petri dish. Two holes were cut into opposite sides of the dish and one hole was cut into the cover. The petri dish was placed onto the stage of an inverted microscope and gas inlet and outlet hoses were attached to the holes on the side of the dish. The probe of an oxygen sensor (Oxygen Analyzer Model 600; Engineered Systems & Designs, Inc, Newark, DE) was placed over the hole in the top of the petri dish. The gas inlet hose was connected to a mixing chamber, which was connected to an oxygen tank and a nitrogen tank. The gas outlet was connected to a flask open to the atmosphere. The entire setup is depicted in

Supplementary Figure 7. The outputs of the oxygen and nitrogen tanks were adjusted such that the reading on the oxygen sensor was stable at the following oxygen concentrations: 1.0%, 2.0%, 4.0%, 8.0%, 12.0%, 16.0%, 20.0%, 25.0%, 30.0%, 40.0%, 50.0%, 60.0%, 70.0%, 80.0%, 90.0%. When the oxygen concentration was stable, fluorescent and phosphorescent images were taken for five different spots. The imaging procedure was the same for the various conditions except that the exposure time for direct imaging of the BF_2dbm(I)PLA side was 31.8 milliseconds and for indirect imaging was 68.8 milliseconds. The images were then loaded into MATLAB. For each oxygen concentration and spot imaged, the average phosphorescent intensity was divided by the average fluorescent intensity to obtain the phosphorescent-to-fluorescent ratio. Then the five ratios were averaged for each oxygen concentration.

Oxygen Tension of Adherent Cells

D1 cells (obtained from a colleague at UVA, are also deposited at ATCC, CRL-12424) were cultured in DMEM (Invitrogen, Grand Island, NY) supplemented with fetal bovine serum, penicillin, and streptomycin. Sections (1 cm x 1 cm) of dual-layer fibers were cut and removed from the collecting foil and placed in multi-well non-tissue culture plates (BD, Franklin Lakes, NJ). Cells were stained with DiO and were placed on the center of the fiber section in a 10-uL droplet. The well-plates were placed in the incubator for 1 hour to allow the cells to adhere to the fibers, followed by flooding with media and being placed back in the incubator. Next fiber sections were placed on glass slides and covered and sealed with a glass coverslip, which not only accelerated the time required for the cells to consume a significant amount of the oxygen available to them, but also flattened the nanofibers so that reasonably focused images could be obtained. One spot was chosen for each section and imaged at 0, 5, 10, and 15 minutes after sealing. DiO, oxygen sensor fluorescent, and oxygen sensor phosphorescent images were captured at 4x magnification with a Cy5 filter, Beta-Lactamase Filter 1, and Beta-Lactamase Filter 2, respectively.

Analysis was completed in MATLAB using code which is available upon request. A set of images (cells, fluorescent, and phosphorescent) for a given time point were loaded into MATLAB. The cells in the cell image were identified with a segmentation algorithm giving a mask of each image to define the cell-occupied and cell-devoid areas. The phosphorescent-to-fluorescent ratio was calculated for each pixel and then averaged for the image areas and averaged appropriately to create the time and/or cell density data reported.

Degradation Study

Sections (1 cm x 1 cm) of dual-layer fibers were cut and removed from the collecting foil and placed in PBS in polycarbonate vials. The vials were incubated at 37°C in a water bath with circular agitation for 0, 7, 14 or 21 days. After being removed from the water bath and PBS, the fibers were dried in a lyophilizer. Then, 6 samples from each time point were placed and sealed in glass scintillation vials with Teflon lids under nitrogen in a glove box. The emission spectrum (400-700 nm) of each sample was obtained using a UV-Vis spectrophotometer (Hewlett Packard 8452A diode-array). All emission spectra were normalized to the fluorescent peak and the 6 spectra from each time point were averaged together.

Gel Permeation Chromatography

Samples were dissolved in HPLC-grade tetrahydrofuran (THF), filtered through 0.2um filter, and loaded into vials with a septum for gel permeation chromatography analysis (GPC). Molecular weight was measured by GPC (THF, 20°C, 1.0ml/min) against polystyrene standards on a Hewlett-Packard instrument (series 1100 HPLC) equipped with Polymer Laboratories 5 μm mixed-C columns and connected to refractive index (Viscotek LR 40) detector. Data were processed with the OmniSEC software (version 4.2, Viscotek Corp).

Pancreatic Islet Isolation

Pancreatic islets were isolated from C57BL/6 mice (Jackson Laboratories, Bar Harbor, ME) that were sacrificed immediately prior to the procedure. After confirmation of euthanasia, a lateral incision exposed the peritoneal cavity and two lobes of the liver were placed onto sterile gauze over the animal's ribcage. The common bile duct was occluded by tying off with suture at the entrance to the intestine and was cannulated with a 30G needle for injection of 2-3mL of 1.4mg/mL collagenase P (Roche) dissolved in Hank's Balanced Salt Solution (HBSS, Thermo Scientific) supplemented with 10mg/L heat treated bovine serum albumin and 0.35g/L sodium bicarbonate (supplemented HBSS). The pancreas was carefully removed from the animal after distension and placed in 1mL of supplemented HBSS on ice to which 4 mL of enzyme solution was added in individual 15mL centrifuge tubes for each mouse. Incubation in a 37degC water bath (15 minutes was selected with this batch of enzyme) was followed by vigorous shaking by hand to disrupt tissue structure. Next the tubes were placed immediately on ice and the balance of the 15 mL was filled with supplemented HBSS. Two washes in supplemented HBSS were followed by a filtering through a steel mesh and density separation with Histopaque 1077(Sigma #10771). Two more washes and a wash in fully supplemented culture media (RPMI1640 + 10% FBS, 2% Penicillin Streptomycin + 2.5% 1X HEPES) completed the isolation. The islets were placed onto ice in 50mL tubes containing 10mL of media and transported to another building for the *in vivo* experiment 4 hours after isolation completion.

Dorsal Skinfold Window Chamber Experiments

All surgeries were performed according to a protocol approved by the Institutional Animal Care Committee at the University of Virginia. Three C57BL/6 background mice (bred in house under an approved protocol) were used. Anesthesia was induced with isoflurane gas (2-3%) and the surgical plane was maintained throughout the procedure with a nose cone (1-2%) equipped with a scavenging apparatus. Briefly, dorsal skin was attached to a corkboard with 26 gauge needles and the top layer of skin

corresponding with the window portion of the chamber (10mm diameter) was removed to expose the cutaneous microcirculation of the panniculus carnosus. Ringers solution was added throughout the process to keep the area hydrated. The top titanium chamber was secured with sutures and the screws were tightened to hold the chamber together. Ringers solution was used to fill the cavity before implanting two 6 mm diameter nanofiber scaffold hemispheres and applying the glass coverslip. Post-operative bupronex was administered to the animals every 12 hours for 48 hours.

Microscopy color CCD images (Nikon, Melville, NY) were taken on Days 0, 1, and 2 after surgery using unfiltered brightfield light or UV excitation with the two beta-lactamase filters and a 10X objective to capture the images used for the time course shown in Figure 7**g**. The same color CCD camera was mounted on a stereomicroscope for the ischemia and islet transplant experiments to obtain a larger field of view. Excitation was from a handheld UV lamp.

For the 48 hours following implants, the same 4 randomly selected regions were imaged each day to produce a mean value for each of 3 mice, bars show deviation of three mice. Recently isolated pancreatic islets were placed in the chamber of a mouse on Day 3. The islets were reconstituted in cold type 1 rat tail collagen (Becton-Dickinson) immediately prior to placement on the exposed tissue and nanofibers at t=0. On Day 4 a transient ischemia in a different mouse was created by placing bulldog clamps on the skin which is tented up outside the two pieces of the dorsal skinfold window chamber at t=0 min. Exposure time was 1ms for the florescence and phosphorescence images.

In vivo Image Analysis

Because no filters were used during the ischemia and islet transplant experiments, the two sensor emissions were distinguished solely on the basis of the green (phosphorescence) and blue (fluorescence) channels of the color images. These two channels were also used for the images when the filters were used during the 48 hour observation period. The basic image reading and ratio calculations that were used for the *in vitro* experiments were used for the *in vivo* experiments, with the exception being that it

was channels of a single color image rather than two separate grayscale images as the inputs. For quantification, areas of the images that did not include sensor nanofibers were excluded for the analysis.

Statistics

The student's t-test are used for determining significance at a $p<0.05$.

FURTHER DISCUSSION

A cell within an *in vivo* implanted construct will not be able to perform its desired functions unless nutrients including proteins, glucose, and molecular oxygen (O_2) are able to diffuse in sufficient quantity to support cell viability before a construct is vascularized. While any species diffusional flux is directly proportional to the gradient, hence driving a greater flux of oxygen to more hypoxic areas, the solubility of oxygen is low in extracellular fluid, making the effective diffusional distance of oxygen low. Thus understanding oxygen gradients not only has a significant direct effect on cells, but also is likely to be the most limiting cell nutrient as depth in the construct increases.

In addition to the implantation of tissue engineered constructs hypoxia occurs in vivo in a number of pathological conditions including tumor growth and tissue ischemia. Tumors that have a hypoxic core are resistant to therapy[267]. Tissue ischemia arises in situations such as peripheral arterial disease, trauma and non-healing wounds. The normal response to ischemia that would drive angiogenesis is altered in non-healing wounds due to a condition such as diabetes.

In physiological conditions the concentration of oxygen, not just hypoxia or normoxia, is known to exist as a cellular environmental factor. All tissues have complex oxygen gradients, derived from the structure of arterioles, venules, and capillaries in addition to the density of cells and extracellular matrix composition[268–270]. Variation in these gradients further depends on the type of tissue and its state, exercising muscle verses resting muscle, and not oxygen permeability rules that can be applied to arterioles and capillaries throughout the body[271]. Oxygen gradients have been artificially created in vitro to demonstrate cell migration in decellularized constructs is higher than with a constant high or low oxygen concentration[272]. Due to oxygen gradients having far reaching effects, a reliable method to measure oxygen concentration has been an important area of research.

One of the most established methods for measuring oxygen has been to use electrodes with diameters of a few microns. Oxygen concentration can be measured at small spatial volumes known by the positioning

of the electrode tip in living tissue and engineering constructs both in vitro and in vivo. However this is tedious and requires mechanical tissue disturbance which increases with resolution both in time and space. Imaging has allowed more data to be collected using paramagnetic resonance, fluorescence or phosphorescent quenching[273] and cellular imaging using reporter constructs[274] and internalized dyes. Iodine-substituted boron dyes function as oxygen sensors by emitting a phosphorescent peak, which varies based on the local oxygen concentration. Comparing this to the fluorescent emission arising from the same material, produces an internally standardized ratiometric oxygen sensor overcoming the complexity of many light based systems requiring a separate standard fluorophore for photobleaching correction.

In this thesis oxygen sensing functionalization of model tissue engineering scaffolds constructed of nanofibers using the electrospinning technique was examined. The properties of scaffolds where the oxygen sensitive dye is blended with a biodegradable polymer are compared to the dye chemically conjugated directly to a biodegradable polymer, removing the need to physically blend with a polymer prior to electrospinning to achieve the ECM mimetic morphology. Oxygen calibration curves as well as *in vitro* and *in vivo* experiments demonstrated the utility of this new nanofiber based oxygen sensor for cell culture, ischemic conditions and as a support for cell transplant.

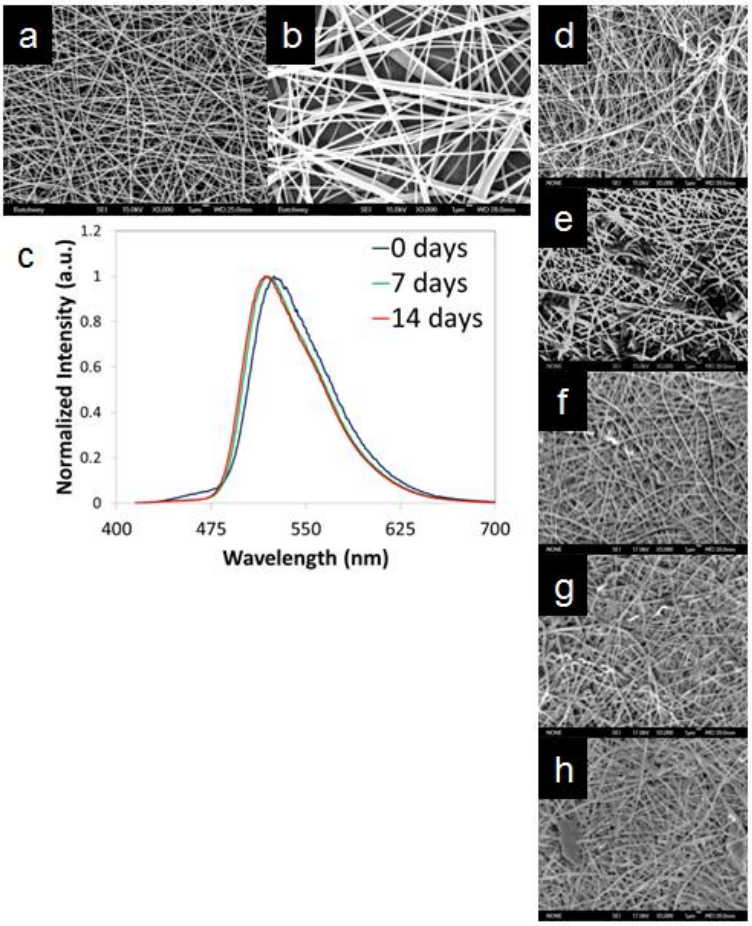

Supplementary Figure 1: Characterization following aqueous degradation

Adding the dye to a solution of PLGA (85:15 LA:GA subunit ratio) does not result in a loss of cylindrical fiber morphology **(b)** compared to the polymer alone **(a)** when the weight of the mixture was kept constant. The normalized phosphorescent peak displayed a blue shift with time in aqueous media **(c)**. The fiber morphology did not change noticeably over a 14 day degradation study as expected since the 85:15 polymer is known to be slower degrading (**d, day 0; e, day 1; f, day 3; g, day 7; h, day 14**).

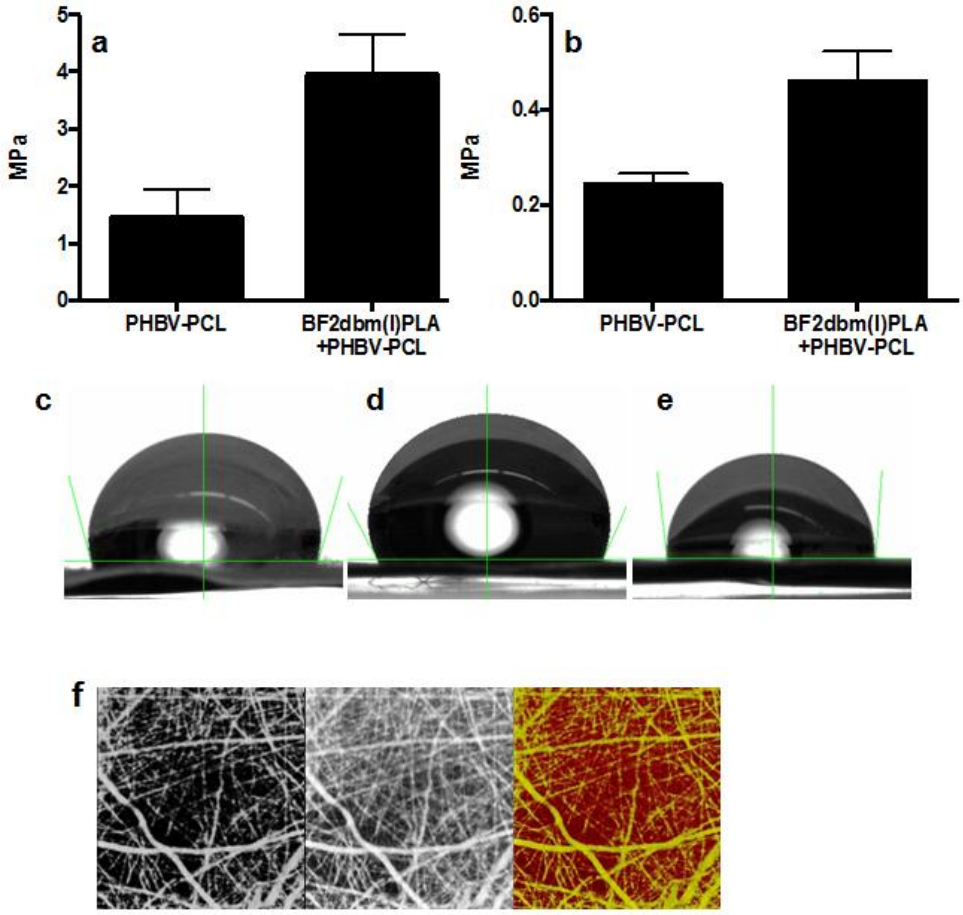

Supplementary Figure 2: Material characterization of dual layer scaffold

(a) Young's Modulus and **(b)** ultimate tensile strength suggest the boron dye layer attaches to the PHBV & PCL layer. (n=3 for each group). The water contact angle was also found to be a composite of the two materials **(c**, Boron Dye PLA Fibers; **d**, PHBV & PCL fibers; **e**, PHBV & PCL Boron Dye dual layer scaffold**)** (n=3 for each group), suggesting that the boron dye nanofibers are incompletely covering the PHBV layer. **(f)** Confocal microscopy show the boron dye layer over the PHBV & PCL layer.

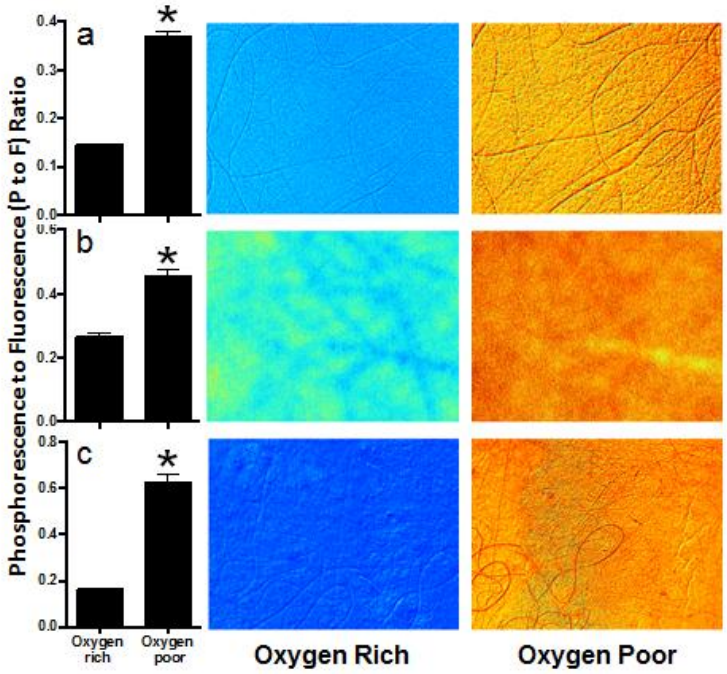

Supplementary Figure 3: Ratiometric imaging shows no quantitative effect by imaging through the PHBV & PCL fibers or in aqueous media

Nanofibers responded with greater phosphorescence in a low oxygen environment when imaged directly **(a)**, imaged through the PHBV/PCL support layer **(b)**, and imaged directly but submerged in phosphate buffered saline **(c)**. *p<0.05, two-tailed independent means t-test.

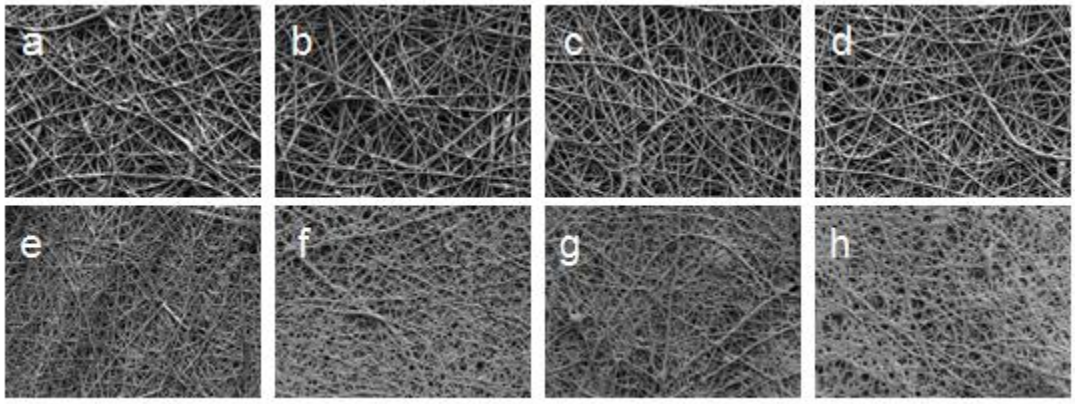

Supplementary Figure 4: The boron dye sensor layer swelled with time in aqueous media

The support layer (PHBV & PCL) nanofibers did not change with time(**a**, day 0; **b**, day 7; **c**, day 14; **d**, day 21). The boron dye layer showed the smaller diameter at time zero (**e**), and the diameters swelled over time in aqueous media (**f**, day 7; **g**, day 14; **h**, day 21).

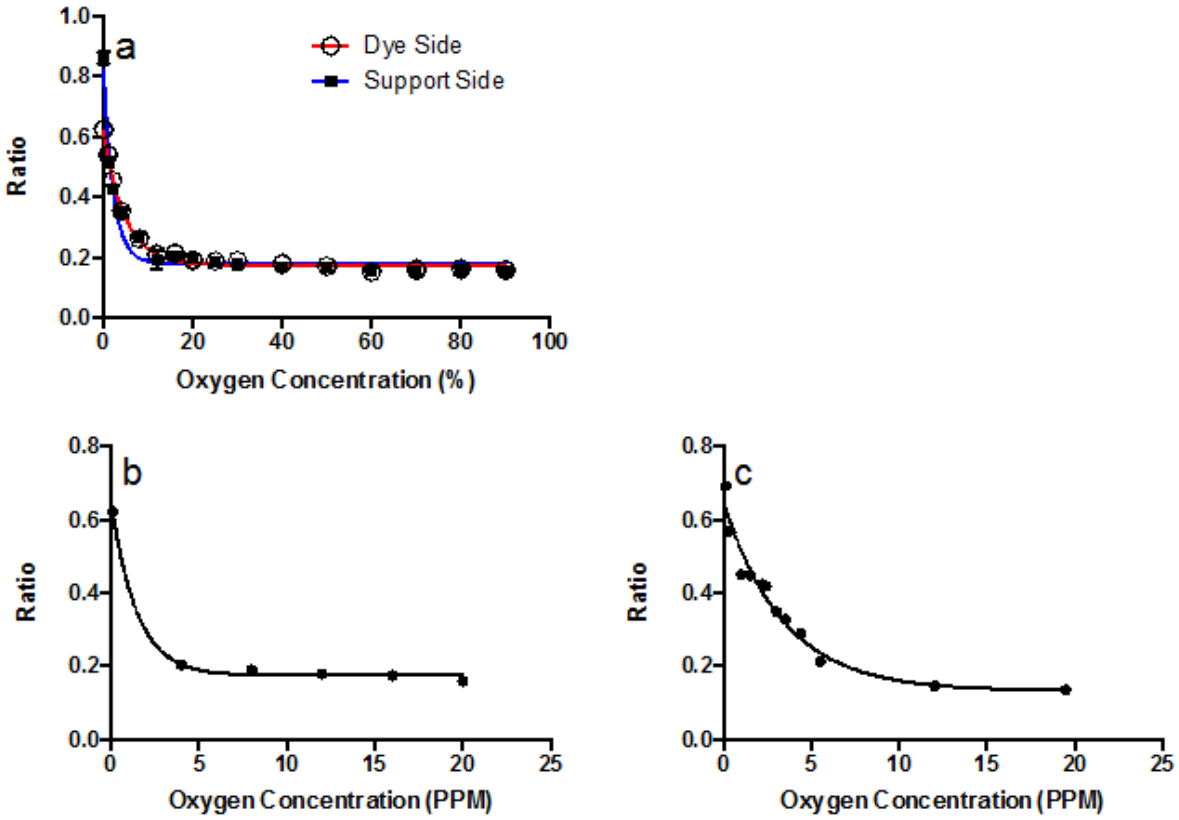

Supplementary Figure 5: Sensor ratio changes quantifiably with change in oxygen concentration

The calibration of the boron dye fibers is not affected by imaging through the support layer **(a)** the presence of aqueous media such as PBS **(b)** or DMEM **(c)** The oxygen concentration is shown in percent for air measurements while in PPM for aqueous measurements.

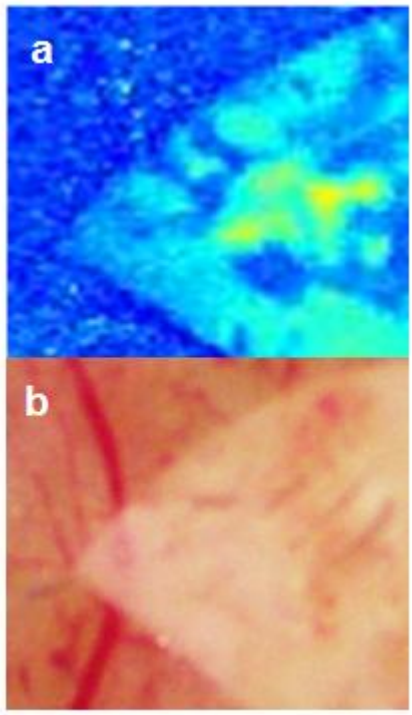

Supplementary Figure 6: An oxygen gradients near blood vessel pair

Nanofibers showed an oxygen gradient with radial distance from an arteriovenous pair of micro vessels. Ratiometric image **(a)** and corresponding brighfield image **(b)**.

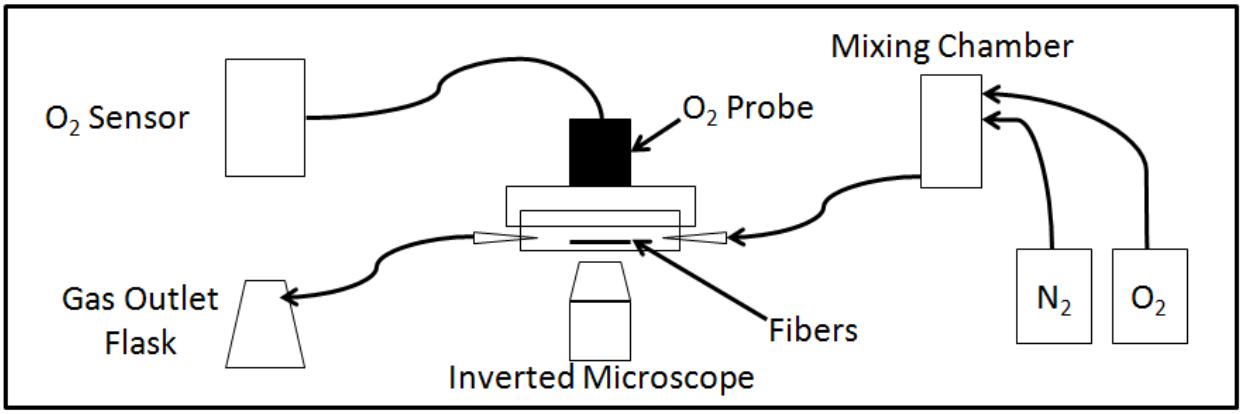

Supplementary Figure 7: Diagram of apparatus for controlling oxygen percentage. Curved arrows indicate the flow of gas through the apparatus.

CHAPTER 3: DEVELOPMENT OF A PRECONDITIONED TISSUE ENGINEERED SITE FOR PANCREATIC ISLET TRANSPLANTATION

INTRODUCTION

Revascularization of transplanted islets has been identified as a barrier to success. While the islets are known to produce significant amounts of angiogenic factors such as Vascular Endothelial Growth Factor (VEGF), this is not enough to overcome the lack of blood vessels in or around the islet. Hypoxia induced islet necrosis, caused by insufficient diffusion limited nutrient delivery, then contributes to graft function decline. One method to address this challenge has been to engineer islets of a sufficiently small size, reducing the need for blood vessel growth. However, culture time and handling of the islets may be drawbacks to this approach.

Local delivery of sphingosine-1-phosphate (S1P) receptor targeted drugs expands microvascular network density surrounding biodegradable polymer implants. S1P is a pleiotropic autocrine and paracrine signaling small molecule that regulates the behavior of endothelial cells (ECs)[275], [276] and smooth muscle cells (SMCs)[277], [278] through its action at 5 G-protein coupled cell surface receptors (S1P1-S1P5). The local release of FTY720, an activator of S1P1 and S1P3 expressed on cells including SMCs and ECs, increases functional length density, arteriolar diameter, and vascular branching[279].

FTY720 has been investigated as an alternative transplant drug, owing in part to its ability to sequester lymphocytes in secondary lymphoid tissues. It possesses qualities such as low renal toxicity and no direct adverse effect on islet health, unlike many immune suppression drugs. Systemic delivery of FTY720 has been shown to be anti-angiogenic[223], [280], [281]. In contrast, local delivery of FTY720 from biodegradable polymer scaffold films stimulates increases in functional length density, arteriolar diameter, and vascular branching.

Based on these effects an investigation of local release of FTY720 for the specific application of islet transplant is investigated below. Nanofibers are chosen as the polymer vehicle and are made using the electrospinning technique. The choice of polymer and the construction of a preconditioned site using the proposed device is validated *in vivo*.

METHODS

Preparation of nanofibers

PLAGA nanofibers are electrospun from polymer solutions of PLAGA (50:50 LA:GA, Lakeshore Biomaterials, Birmingham, AL, USA) solvated in Methylene Chloride (Fisher Scientific, Waltham, MA, USA). FTY720 (Cayman Chemical, Ann Arbor, Michigan) is solvated directly or first dissolved in dimethyl sulfoxide (DMSO, Sigma) and mixed into the polymer solution at a 1:200 or 1:400 ratio by weight (drug : polymer). The polymer solution is 20% (wt by vol) and is provided with a 1mL/hour flow rate by syringe pump (World Precision Instruments, Sarasota, FL, USA) using an 18G blunt tipped needle. A tip to collector distance of 5cm with an applied voltage of 14-16kV was utilized.

PLAGA & PCL nanofibers were made from polycaprolactone (PCL; Sigma, USA) and PLAGA. Briefly, they were combined in a 1:1 (w/w) ratio and then dissolved in 3:1 (v/v) chloroform : methanol. The final concentration of polymer solution was 18% (w/v). The solution was agitated until the polymer dissolved and then loaded into a 3mL rubber-free syringe. Electrospinning was performed at a flow rate of 1.0 mL/hour, an applied voltage of 19 kV, and a working distance of 10 cm. Nanofibers were collected on a stationary aluminum plate and then stored in a desiccator until use. To make drug-loaded nanofibers, FTY720 (Cayman Chemical, Ann Arbor, MI, USA) was dissolved in 3:1 chloroform methanol solution and 1:1 PCL/PLAGA was added at a concentration of 20% (w/v). The final drug:polymer ratio was 1:200 (w/w). Electrospinning was performed at a flow rate of 1.0 mL/hour, an applied voltage of 19 kV, and a working distance of 15 cm in order to form nanofibers of similar morphology to unloaded nanofibers.

Characterization of nanofibers

Characterization of nanofiber diameter and morphology was performed using a JEOL 6400 scanning electron microscope (SEM) with Orion image processing. Samples were coated with gold and then imaged at a working distance of 39-43 mm and an accelerating voltage of 15 kV. Diameter was assessed using ImageJ (NIH, USA).

Mouse Dorsal Skinfold Window Chamber Model

All surgeries were performed according to a protocol approved by the Institutional Animal Care and Use Committee at the University of Virginia. 12 NOD male mice (Jackson Laboratories, Bar Harbor, ME, USA) were used prior to reaching hyperglycemia. Each animal was implanted with both polymer nanofibers and FTY720-loaded nanofibers. Anesthesia was induced with isoflurane gas (2-3%) and the surgical plane was maintained throughout the procedure with a nose cone (1-2%) equipped with a scavenging apparatus. Dorsal skin was attached to a corkboard with 26 gauge needles and the top layer of skin corresponding with the window portion of the chamber (10mm diameter) was removed to expose the cutaneous microcirculation of the panniculus carnosus. Ringers solution was added throughout the process to keep the area hydrated. The top titanium chamber was secured with sutures and the screws were tightened to hold the chamber together. Ringers solution was used to fill the cavity before implanting 6 mm diameter nanofiber scaffolds and applying the glass coverslip. Following surgery animals were given bupronex once every 12 hours for 48 hours.

Light microscopy (Nikon, Melville, NY) images were taken on Days 0, 3, 7, 10, and 14 after surgery with a 4X objective and then combined into a montage for analysis. Light was filtered through a blue filter to excite hemoglobin and the montaged images were cut in half to create the regions near each implant. Thresholding modifications were applied to the montaged images so that the total area of blood vessels for each animal could be measured.

Pocket Fabrication

Pocket fabrication was completed in a sterile fume hood. A rectangular piece of the fibers (2cm wide) was soaked in EtOH and peeled from the aluminum foil. Once fibers were relatively dry, the piece was folded over to form a 1cm wide piece. These folded fibers were heat-sealed at 1cm intervals using a metal plate heated in an oven (125˚ C) or on a hot plate. After cutting through the heat-seals, pockets (~1cm2) are formed; each pocket having one folded side, two heat-sealed sides, and one open side.

To continue to prepare the pockets, salt interspersed pockets were placed in a FTY720 saturated PBS solution and placed on a rocker in a cold room (4degC) for 18-24 hours to dissolve the salt, leaving the fibers more porous.

Glucose Testing

Blood was drawn by tail clip and measured on an Accu-Chek Advantage handheld blood glucose meter (Roche, IN). Glucoses were measured every day following transplant.

Islet Isolation

Pancreatic islets were isolated from C57BL/6 mice (Jackson Laboratories, Bar Harbor, ME) that were sacrificed immediately prior to the procedure. After confirmation of euthanasia, a lateral incision exposed the peritoneal cavity and two lobes of the liver were placed onto sterile gauze over the animal's ribcage. The common bile duct was occluded by tying off using suture at the entrance to the intestine and was cannulated with a 30G needle for injection of 2-3mL of 1.4mg/mL collagenase P (Roche) dissolved in Hank's Balanced Salt Solution (HBSS, Thermo Scientific) supplemented with 10mg/L heat treated bovine serum albumin and 0.35g/L sodium bicarbonate (supplemented HBSS). The pancreas was carefully removed from the animal after distension and placed in 1mL of supplemented HBSS on ice to which 4 mL of enzyme solution was added in individual 15mL centrifuge tubes for each mouse. Incubation in a 37degC water bath (15 minutes was selected with this batch of enzyme) was followed by

vigorous shaking by hand to disrupt tissue structure. Next the tubes were placed immediately on ice and the balance of the 15 mL was filled with supplemented HBSS. Two washes in supplemented HBSS were followed by a filtering through a steel mesh and density separation with Histopaque 1077(Sigma #10771). Two more washes and a wash in fully supplemented culture media (RPMI1640 + 10% FBS, 2% Penicillin Streptomycin + 2.5% 1X HEPES) completed the isolation. The islets were placed onto ice in 50mL tubes containing 10mL of media and transported to another building for the *in vivo* experiment 4 hours after isolation completion.

Islet Implant Loading and Transplant

After islets were cultured overnight, they were hand picked to high purity and counted. A "U" shaped piece of Enduragen decellularized dermis was inserted into the pocket with the "open end" of the insert pointed toward the open end of the pocket. For *in vitro* studies, islets were then loaded into the pocket by drawing them into a 200uL pipet, allowing them to settle to the bottom by gravity and then dispensing them by adjusting the volume specified to advance the volume slowly rather than dispensing the whole liquid volume. The final side was closed via heat sealing, this time using a heated pair of smooth surface hemostats.

For *in vivo* studies, this same procedure was followed for simultaneous islet-implant procedures. For preconditioning studies, the pocket was constructed with the insert and the final end was sealed using the heated hemostats. At the first procedure the animal was anesthetized using isoflurane as described for the dorsal skinfold window chamber. The hair was removed using a depilating agent following shaving with an electronic trimmer and the site was cleaned with iodine and ethanol washes in triplicate. An incision through the skin and then through the IP wall was made on the left flank where access to the left kidney is made. The pocket was inserted into the peritoneal space and a single suture was run though a sealed edge of the pocket to attach it to the inside of the peritoneal wall. Therefore, it contacted the wall on one side and internal organs on the other usually consisting of a combination of the kidney, spleen, and pancreas. The animal was then sutured with separate sutures for the IP wall and the skin closure. At the second

procedure a new incision was made near the previous one to gain access to the implant. Then the pocket was pierced by a needle loaded with the islets for injection.

Glucose Stimulated Insulin Secretion (GSIS) and Viability Staining

Islets after treatment or with the polymers being studied were washed once with low glucose (2.8mM) KRB buffer to remove the culture media and placed in the incubator for an hour. Two washes in low glucose KRB was then performed to start the 2 hour incubation at 37degC in 2mL low glucose. 1mL samples were then collected being careful not to aspirate any cellular material, immediately placed on ice in 1.5 mL centrifuge tubes, and then stored in the freezer until ELISA. The islets were then washed in low glucose twice followed by addition of 2mL of high glucose for the next 2 hour incubation. Again samples were taken and frozen until analysis. The rest of the high glucose was removed and replaced by low glucose KRB to reduce the stress to the islets.

Propidum iodide (PI) was then added (alone for the FTY720 dose response experiment) or with fluorescein diacetate (FDA) for the polymer incubation experiments. Imaging was conducted with UV excitation and a red and green fluorescent filter on an inverted Zeiss microscope with a Zeiss Axiocam color camera mounted. Image analysis for the polymer assays was by visual inspection to estimate percentage viability of individual islets. The FTY720 dose response was based on the PI florescence intensity in the image with a constant exposure of 300ms in ImageJ (NIH, USA).

FTY720 Dose Response

FTY720 was first solvated in 100% ethanol to a concentration of 2 mg/mL. A stock solution was made by mixing 1:1 by volume with diH_20. Then 50 uL of this solution was added to 50mL of culture media to create a 1000ng/mL FTY720 solution. This was diluted appropriately with media for the other concentrations tested to make 2mL final volumes for 6 well plate wells. The islets were then incubated for 19 hours at 37degC. This solution was removed with the first wash as described for GSIS above. Following the GSIS procedure the islets were stained for viability as described at the end of the previous section with PI. A 5X image for each well was used to quantify the fluorescence intensity in ImageJ. The mean florescence intensity was calculated for each well and then averaged for the groups.

ECM Dimensional Stability

Acellular porcine dermis (ENDURAGen) and acellular human cadaveric dermis (AlloDerm) were cut into 1cm x 1cm squares and kept at the supplied thickness of approx. 1mm. Following implantation in distinct subcutaneous pockets in a Sprague-Dawley rat for 4,8 and 12 weeks implants were harvested and fixed in 4%PFA for 48 hours and subsequently kept in 70% EtOH. Extraneous tissue was removed under a stereomicroscope and then images were taken of the implants. The longest two axies were measured in the images and the ratio was taken. Therefore a value near to 1 indicated a square shape, while values further from one indicated shifting toward a rectangular shape.

Ex Vivo Pocket Challenge

Single pockets loaded with islets were implanted in mice for 12 hours or 5 days. The implants were removed intact from the animal and challenged per the GSIS procedure above.

Histology

Explanted tissue was fixed in buffered formalin for 24 hours at room temperature and subsequently kept in 70% ethanol at 4 deg C before embedding in paraffin. Tissue specimens were embedded at the University of Virginia Research Histology Core. Sections of the paraffin blocks were cut at 5 micron thickness. Hematoxylin and Eosin (H&E) stain was also completed at the Research Histology Core.

Ultrasound

Animals were placed supine on a heated stage and sedated with an isoflurane nose cone. Imaging sessions did not last longer than 30 minutes for a given mouse. A Vevo 2100 (VisualSonics, Toronto, Canada) was used with a frequency operating at approximately 30MHz. Ultrasound gel was placed between the animals skin and the probe surface. The probe was mounted while the animal/platform could then be translated under the probe to obtain the images shown.

Statistics

A two way Student's T-test was applied with unequal variance in Microsoft Excel, with a p-value <0.05 considered significant unless otherwise noted.

RESULTS

PLAGA fiber morphology changes with FTY720 loading depends on presence of vehicle

Uniform PLAGA nanofiber morphology was obtained through adjustment of a single solvent (MeCl2, **Appendix Figure 1**). Addition of FTY720 to PLAGA nanofibers resulted in a loss of uniform morphology that had been obtained for PLAGA nanofibers (**Figure 8 A,B**). To ensure uniform mixing of FTY720 with the polymer solution, a solvent of DMSO was applied for the small molecule. The addition of DMSO alone resulted in the formation of beads, while the addition of FTY720 dissolved in the DMSO resulted in reduced bead size and reduced fiber diameter (**Figure 8 C,D**).

Selection of PHBV to replace PLAGA in FTY720 loaded nanofibers

S1P receptor 1,3,4,5 agonist FTY720 was loaded into PLAGA blend nanofibers and cultured with islets isolated from mice to reveal that the viability of mouse islets is restored back to that of islets cultured in media alone (**Figure 8 E**). The viability of human islets was reduced by FTY720 addition to PLAGA fibers (**Figure 9 D**), but in contrast fibers made of PHBV left the viability equivalent to the media only controls. PHBV was selected to replace PLAGA blended with PCL. Consideration of the barriers translatability of PLAGA also supported this choice. This still allowed the ratio of the two polymers in the blend to be changed, the benefits of PCL on fiber morphology to be retained (**Figure 9 A-C**) and the ability to adjust the degradation rate of the non-PCL component remain as both PHBV and PLAGA are co-polymers whose monomer ratio affects the degradation rate.

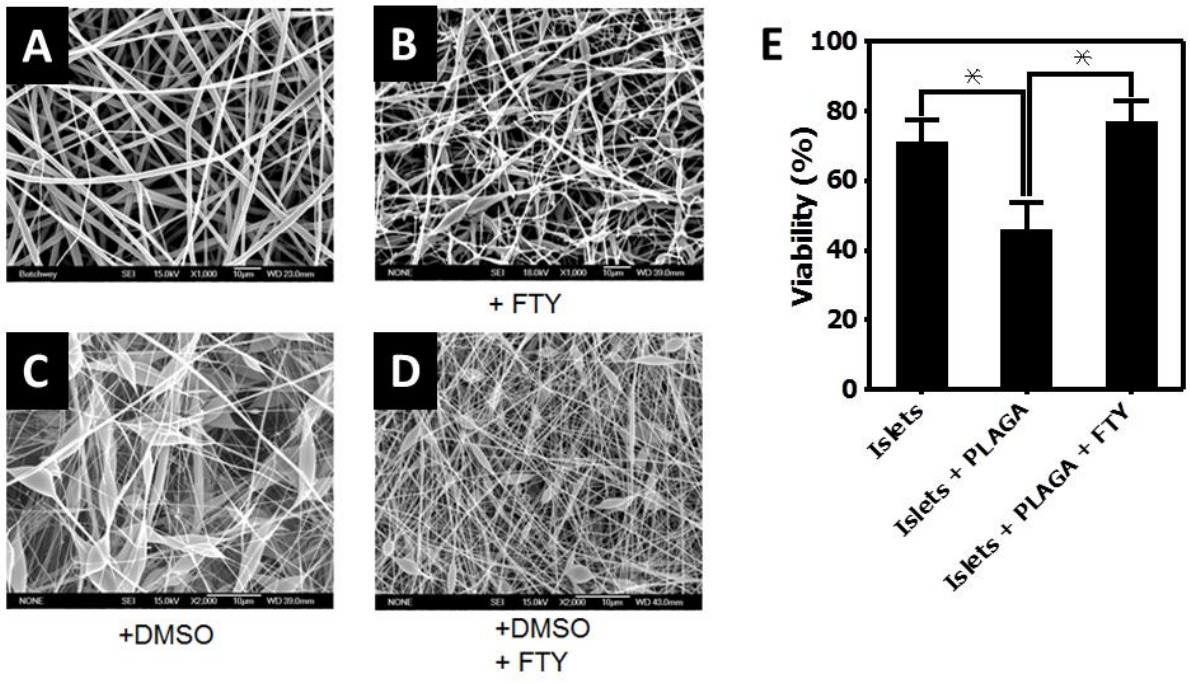

Figure 8: FTY720 loading increases or reduces morphological uniformity and improves mouse islet viability

Optimized PLAGA fibers have a uniform morphology **(A)**, however the addition of FTY720 caused the diameters to become non-uniform as the morphology approached beading as well as forming discontinuities in the fiber mesh **(B)**. When DMSO was used as a FTY720 vehicle beads developed, however the fibers that had a reduced diameter **(D)** compared to the polymer alone fibers **(A)**. Interestingly, when the DMSO vehicle was added without FTY720, the beads were more numerous and larger **(C)**. **(E)** Percentage of viable cells within each islet was quantified by visual inspection of individual islets stained by PI and FDA. *$p<0.05$, Standard error indicated by vertical bars.

Vascularization is Increased by FTY720 Loading in Nanofibers

Knowing from previous studies in the laboratory that locally released FTY720 was proangiogenic, causing increased arteriolar diameter and vessel length density, the extension of this to nanofibers was expected. To test the nanofibers and the truly local effect of the FTY720 release, two nanofiber fabric mats were placed at opposite ends of the dorsal skinfold window chamber imaging area. The volume fraction was examined in proximity to each implant and compared to show that the majority of the time (except for day 3 of 14) the larger blood volume was nearer to the FTY720 implant (**Figure 9 F**).

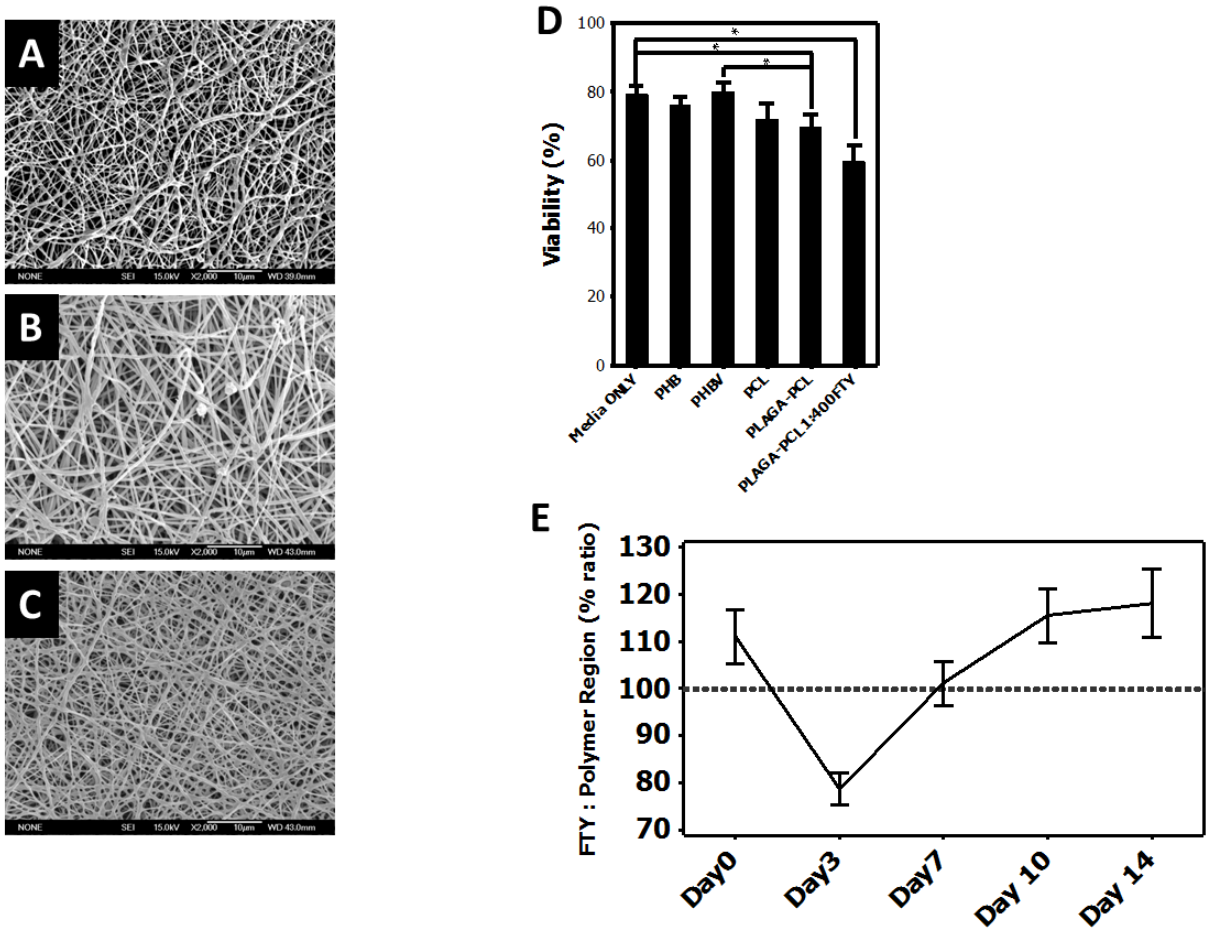

Figure 9: PHBV displayed the greatest human islet viability among polymers tested and vessel volume fraction was highest in the vicinity of FTY720 loaded implants.

The fiber morphology changes with the addition of FTY720 to PLAGA & PCL fibers **(B,C)** were less drastic compared to the vehicle alone **(A)**. The viability of human islets was compared when several polymers were incubated with the islets **(D)**. n=50,50,50,30,50,39 islets visually inspected for Media, PHB, PHBV, PCL, PLAGA & PCL, PLAGA & PCL 1:400 FTY respectively. **(F)** The volume of blood standardized to the area analyzed was found to be highest the majority of days within a 14 day observation period nearer to the FTY720 loaded implants. n=12,10,12,10,10 for Day 0,3,7,10,14 respectively. *$p<0.05$

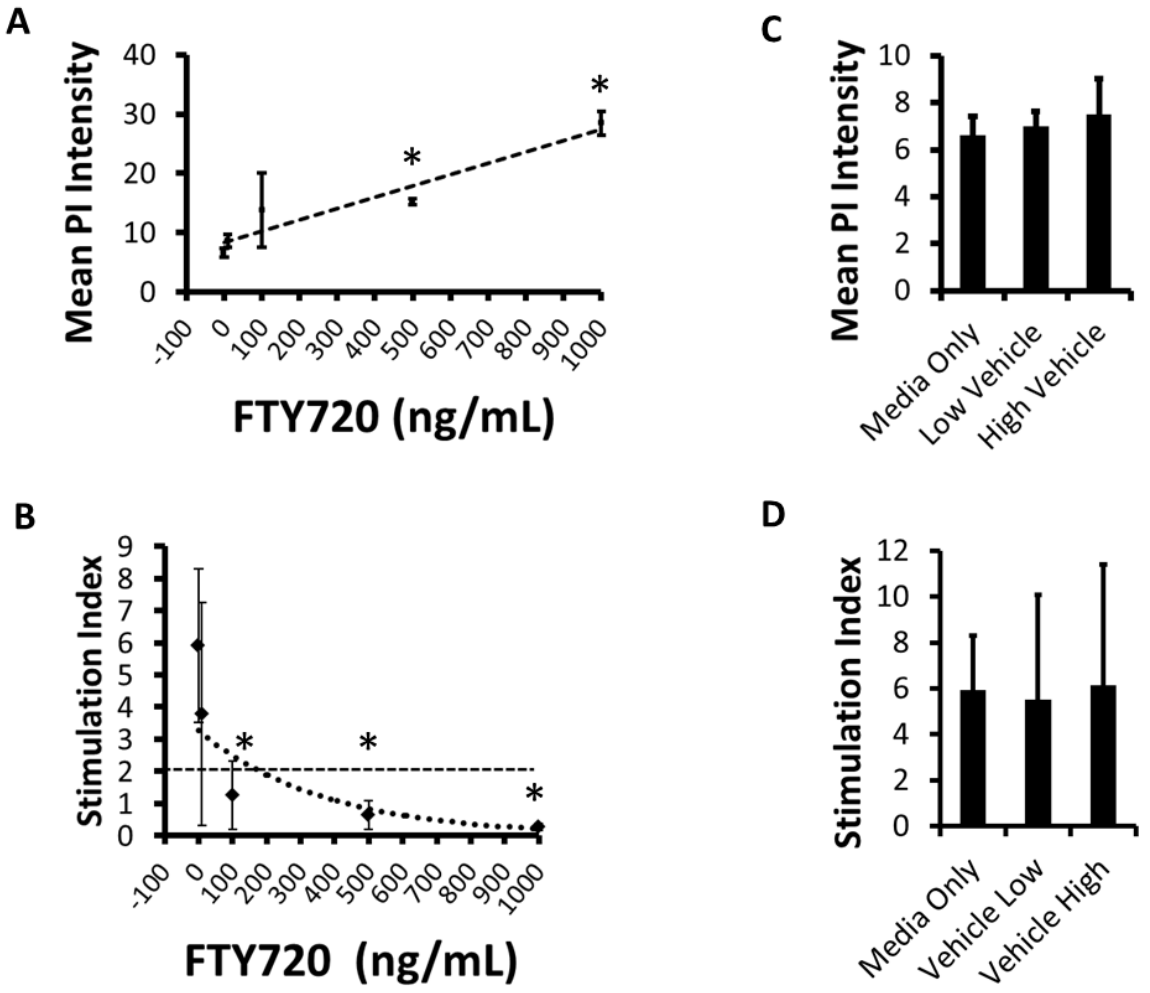

Figure 10: High concentrations of FTY720 cause loss of function and viability of mouse islets

In vitro dose response of mouse islet apoptosis/necrosis **(A)** and stimulation index **(B)** to increasing amounts of FTY720 added to media. Viability **(C)** and stimulation index **(D)** are shown for the ethanol vehicle used for the smallest and largest FTY720 concentrations. n=4,3,2,2,2 wells for 0,10,100,500,1000 ng/mL respectively and 2,3 for 10 and 1000 vehicle respectively. *p<0.05 compared to media only control

FTY720 is toxic to islets in high concentration

If FTY720 is delivered from a scaffold in which islets are placed in close proximity, a locally high concentration of FTY720 would be seen by the islets. Others have found FTY720 to have no detrimental effect on islets, however these investigations were conducted at room temperature[282]. Experiments conducted at 37degC showed mixed results. Providing soluble FTY720 at a known concentration to islets

in culture showed that concentrations of 500ng/mL and above the viability was significantly compromised (**Figure 10 A**), while at doses of 100ng/mL and above islet function was significantly compromised (**Figure 10 B**). The addition of the FTY720 vehicle did not have an effect on either metric (**Figure 10 C,D**).

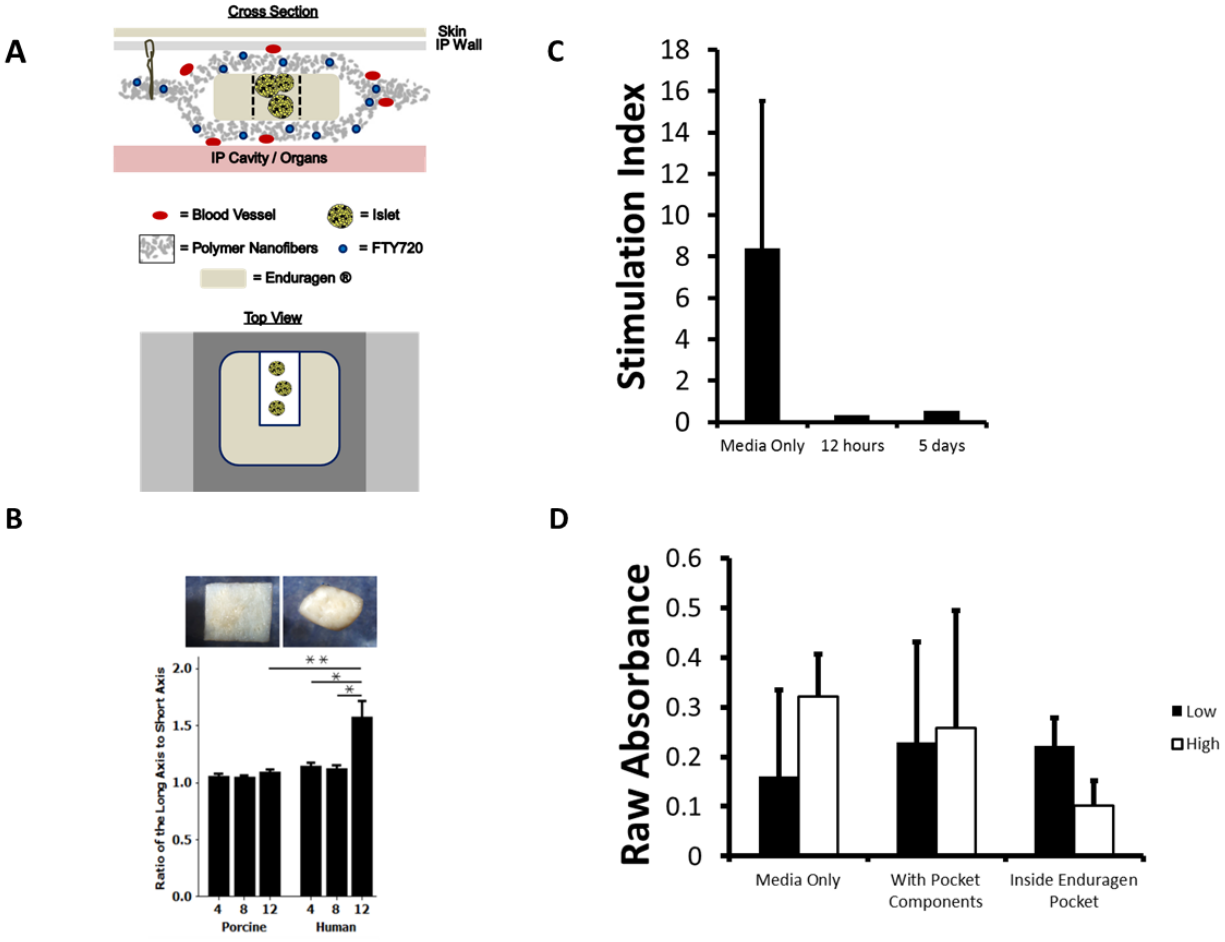

Figure 11: Culture *in vitro* or implantation *in vivo* into pockets decreases islet function

(A) Diagram showing the construction of a pocket with an Enduragen insert to maintain a separation between the nanofiber layers for the islet to occupy. **(B)** Enduragen is dimensionally stable as can be seen by the ratio of the axis lengths. **(C)** *Ex vivo* function of mouse islets is reduced after as short as 12 hours of *in vivo* implantation in a mouse (single experiments, media only shows stimulation of islets at the 12 hour timepoint that were maintained in an incubator in suspension culture, mean of 3 wells). **(D)** In vitro experiments also showed loss of stimulated insulin secretion.

Reduced islet function inside a pocket

Because islets have a three dimensional spheroidal shape, keeping a mechanical separation between the layers of nanofibers is important. Rather than use a synthetic material for this, two decellularized ECM products were considered. The porcine decellularized dermis (Enduragen) was found to be dimensionally stable over the course of 12 weeks subcutaneously in a murine model compared to human decellularized dermis (Alloderm) (**Figure 11 B**). Using this result a macroencapsulation device can be made. As a preliminary assay, islets were loaded into pockets, transplanted, removed and challenged *in vitro*. There was no islet function left in the pocket 5 days or even 12 hours following the transplant (**Figure 11 C**). Islets placed within the pocket and only cultured in vitro also displayed a loss of stimulated insulin secretion (**Figure 11 D**), indicating that the environment inside the device is not hospitable to islets in this form.

Prevascularized conditioned nanofiber pocket for islet transplant

In order to take advantage of the proangiogenic effects of locally released FTY720, and to avoid the detrimental effects of soluble FTY720, a preconditioning method was employed. In this model, the pocket is implanted without any islets, followed by a second procedure where islets are transplanted into the preconditioned nanofiber pocket. When implanted subcutaneously the void that could accept a 28G needle within the pocket was maintained for up to 3 months, as was visualized under ultrasound examination (**Figure 12 A-D**). Syngenic islet transplants into STZ diabetic mice showed that only when the pocket had preconditioned the space prior to the islet transplant did the animals have a return to normoglycemia (**Figure 12 E**).

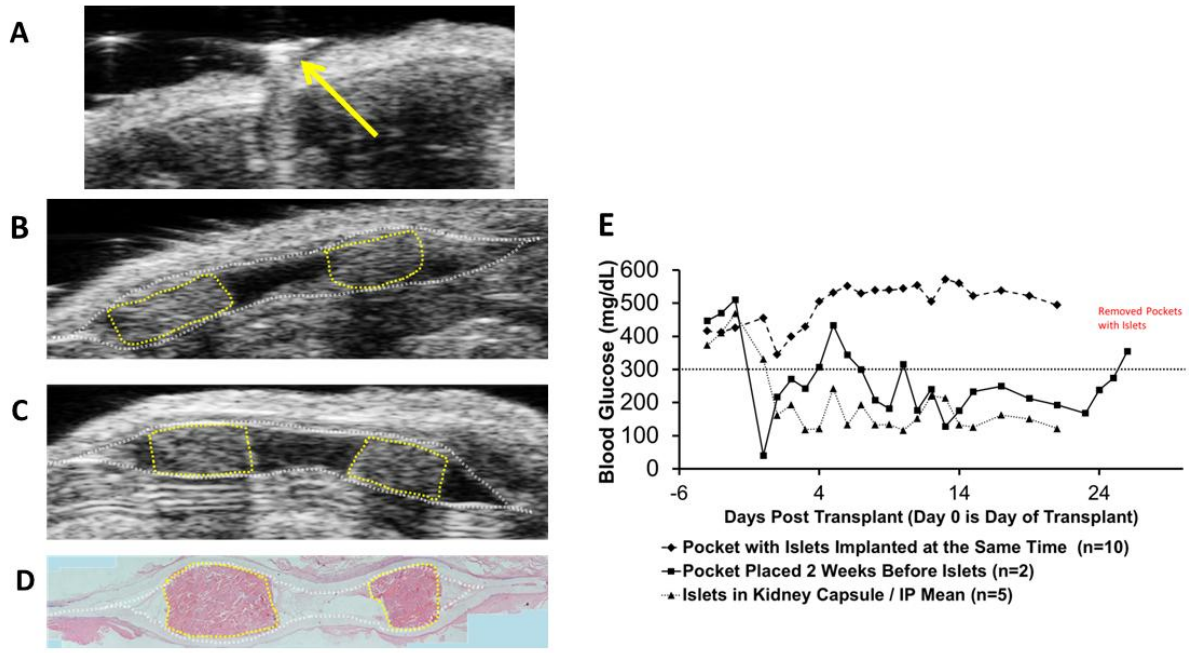

Figure 12: Pre-conditioned site restores glucose control in chemically induced diabetic animals

A subcutaneously placed pocket monitored by ultrasound maintains a void large enough for a 28G needle **(A, arrow)** at 1 month **(B)** and 3 months **(C)** corresponding with H&E **(D)**. **(E)** Islets placed in a preconditioned pocket function better than islets contained in a pocket at the time of device implant compared with freely implanted islets.

DISCUSSION

The immune system clearly plays an important role in the loss of islet mass following islet transplant in Type 1 Diabetes. The immune system attack can be divided into several distinct mechanisms in the case of the portal vein infusion. Within the first few hours after transplant the Immediate Blood Mediated Inflammatory Response (IBMIR) responds to the foreign body. The autoimmune attack that originally caused the disease also is reinvigorated. Depending on the source of islets used, there may be any number of foreign antigens that continue to promote an immune attack. Finally, if the islets have been encapsulated the encapsulation material may elicit a response from the immune system.

Factors in the microenvironment of the islets that promote cell death also play an important role. Cytokines released by the immune system may deactivate survival pathways within the beta cells. In fact, the original loss of beta cell mass that causes Type 1 Diabetes, is related to cell death pathways in the beta cell stimulated by Interleukin-1-beta (IL-1beta), Tumor Necrosis Factor Alpha (TNF alpha), and interferon gamma (IFNgamma)[283]. The effects of local FTY720 delivery on reducing inflammation are clear in a localized environment (**Appendix Figure 3**).

Two weeks is believed to be enough time for a significant amount of the FTY720 to be released and removed from the transplant site in preparation for islets. Although there would be extra cost in doing a two step procedure, many other macroencapsulation devices are being proposed as rechargeable, which would be multiple steps. It remains to be seen if this device would support long term survival of islets, but if it does two procedures at the beginning would be less costly than multiple follow-up procedures over the span of years.

FTY720 is released as the polymer swells and degrades and the local concentration of FTY720 is high surrounding the scaffold. To test the truly local nature of the FTY720 action, two polymer disks, one loaded with FTY720 and one without were placed at opposite ends of the same dorsal skinfold window. It was found that for the majority of a 14 day observation period there was a greater volume of blood

within vessels nearer the FTY720 scaffold. Although this could have been a result of greater inflammation, inflammatory cytokines were already known to be reduced by the local release of FTY720 from polymers in subcutaneous tissue. When two sheets of nanofibers were placed on opposite flanks of a mouse there was a reduced inflammatory macrophage content around the FTY720 releasing fibers as compared to the unloaded ones in each mouse (**Appendix Figure 3**). Therefore it appears that both the proangiogenic and immune modulatory effects have a local component. These experiments would also suggest that the local angiogenic effect may be more related to vessel maturation, than the increases in length density when only one polymer scaffold is implanted.

Considering the predisposition of islets to hypoxic related damage, it would increase the chances of islet survival if the proangiogenic and immunomodulatory effects of local FTY720 release could be harnessed prior to the implantation of islets. Considering the negative correlation of islet health with FTY720 concentration at 37degC, a preconditioning approach would also allow the implant concentration of FTY720 to be reduced before islets are infused. Although the *in vivo* results have been mixed thus far with the preconditioning scheme, this is the only method where the pocket has produced any cured animals that were confirmed to be related to the transplant via removal of the implant.

CONCLUSION

Despite the fact that tissue engineering scaffold volume will greatly effect the appearance of reconstructive surgeries where they are used, little is known about the volume of many implants once they are placed *in vivo*. Furthermore, in the case where cells are within a macroencapsulation device, scaffold contraction could mean mechanical forces that would disrupt the 3 dimensional arrangement of cells. In the case of pancreatic islets the spherical shape of the aggregate of beta cells is known to be more effective than the dispersed beta cells. Chapter 1 of this thesis interrogated 4 implant types for soft tissue reconstruction finding that a cross-linked porcine decellularized dermis (Enduragen) implant was the most dimensionally stable as also shown in Chapter 3.

The human decellularized dermis insert within the implant not only provides a void for the islet infusion to be inserted, but also prevents the nanofibers from closing down on the islets disrupting their spheroidal structure. Encapsulating the islets in a hydrogel or in microcapsules inside the device would be an alternative way to support the 3D structure. Although this would prevent the islets from contacting the ECM mimetic nanofibers one could hypothesize this would be helpful. When cultured, non-tissue culture treated plates are preferred to reduce the attachment of islets, which causes a decrease in their spheroidal shape. One of the benefits of nanofibers is increased cell attachment which in this case might be detrimental to the islets. Therefore, if the islets were otherwise encapsulated, the nanofibers could be used to contact the surrounding tissue, increasing the biocompatibility with the host. It is also unclear why the stimulation index of human islets was found to be greater when in contact with the nanofibers. Differences between human and mouse islets are known and in these experiments differences in duration of culture before the experiment and the health of control islets, measured by stimulation index, were also different. It should also be noted that fibrous mats have been used to encourage the aggregation of individual cells into pseudo islets[284], [285], underscoring the need for further investigation.

Including natural ECM polymers in the capsules or hydrogel has been shown to increase the health of encapsulated islets. In agreement with this result, inclusion of collagen in PCL nanofibers increased the viability of islets in culture in a preliminary experiment (**Appendix Figure 2**). It is plausible that

presentation of cellular ligands overcomes the effect of islet disaggregation that is seen. Inclusion of an accessory cell type other than dermal fibroblasts may greatly improve the results of cell pre-seeding. Bone marrow derived stem cells have been shown to improve islet transplant outcomes when co-transplanted. Adipose derived stem cells are another cell type that are easily harvested from patients and could be used as an autologous cell source. In fact, work using the same FTY720 loaded PLAGA&PCL nanofibers seeded with ADSCs is underway for bone defect healing.

Scaffold oxygenation is required for cell residence. Diffusion of oxygen into the scaffold is likely to be the limiting factor among nutrients needed by cells. Pancreatic islets are highly metabolically active and are predisposed to hypoxic injury after having the normally rich blood supply destroyed during the isolation process from the rest of the pancreas. Chapter 2 of this thesis developed a 2nd generation dual emissive boron dye nanofiber scaffold based on the conjugation of this dye to a low molecular weight polymer. Therefore a longer time of functional readouts after aqueous degradation was found than when the dye was only blended with a polymer. The calibrated fibers could sense oxygen gradients from adhered cell monolayers that were dependent on cell seeding density, indicating that the sensor scaffold could be used *in vitro* to study scaffold oxygenation.

Next the scaffolds were placed onto dorsal subcutaneous tissue for three assays. The reoxygenation of subcutaneous tissue was followed for 48 hours, showing that as the tissue is recovering from the insult the oxygenation is steadily increasing. A fast response to acute ischemia demonstrates that these fibers could be useful in studying models of ischemic conditions, such as stroke, peripheral arterial disease, and myocardial infarction. This technique would be well suited for applications where it is desirable not to induce a sedated state for hypoxia monitoring timepoints, as the boron dye nanofibers only require a color camera image to give a hypoxia map.

It is known that pancreatic islets experience hypoxic conditions post-transplant in several transplantation sites, which differs from the highly oxygenated normal state. Imaging the nanofibers for only 7 minutes after infusion of recently isolated islets demonstrated the capability of these fibers to sense islet transplant

relevant hypoxia. The imaging through the support layer demonstrates that fibers within a construct or macroencapsulation device can be used to probe dissolved oxygen tension.

The physiological response to hypoxia is to stimulate angiogenesis. In Chapter 1, the cell preseeded nanofibers were found to stimulate angiogenesis at 4 weeks quite well and reduce cytotoxic immunity at 12 weeks, however there were costs in terms of the foreign body response to the implant. The small molecule FTY720 can be loaded into the nanofiber membrane for sustained release, making the scaffold shelf ready instead of requiring a cell seeding step. Results demonstrated that with FTY720 loaded in the fibers there was an increase in length density. This result extended to moderately diabetic animals, a significant finding considering that diabetes causes microvascular disregulation.

Further investigation is required to determine the effects of elevated blood glucose on SMC, EC, and progenitor cell functions under FTY720 treatment in diabetic microvascular beds (**Appendix Figure 5**). At least three possibilities regarding the differences seen between moderately diabetic and non-diabetic animals warrant further investigation, including: 1) EC physiology and angiogensis are altered by hyperglycemia[286–288]; 2) circulating progenitor cells are reduced in peripheral blood when exposed to hyperglycemia[289–291]; 3) the effect of recently induced diabetes on microvessel expansion may be related to the elevated blood glucose during the 7 day study or to a recent increase in blood glucose. The later hypothesis has been recently investigated with a model of glycemic variability, where the greater glucose variability significantly impaired angiogenesis following hind-limb ischemia[292]. Thus, it is possible that the duration of time following diabetes induction provided an environment where an increase in blood glucose affected the FTY720 mediated microvessel expansion. It is also interesting to note the disparity in length density at Day 0, which affect differences noted in this study. Results from other studies show a similar low length density in diabetic animals on Day 0 (results not shown), suggesting that the vascularization of the thin subcutaneous muscle imaged in the dorsal skinfold window chamber may be affected by hyperglycemia at baseline.

Length density declined from Day 3 to Day 7 in the non-diabetic animals suggesting that the amount of FTY720 being released from the scaffold may have already passed a peak. Increased surface area for polymer degradation known to happen by hydrolysis of the ester linkages would promote faster degradation of nanofibers, supporting the hypothesis that the fibers would release FTY720 quicker than thin films. As discussed above the moderately diabetic animals continued to increase in length density indicating a differential response to FTY720 release associated with STZ-induced diabetes.

In conclusion, this thesis presents the development of a tissue engineered islet transplantation site with 3 main qualities; implant dimensional stability, hypoxia diagnostic sensors, and a vascularized immunomodulated environment. This is achieved with FTY720 loaded nanofibers combined with low molecular weight polymer conjugated boron dye nanofibers. The supporting findings address major barriers to islet transplant and may impact other cell based tissue engineering applications.

REFERENCES

[1] S. C. Bain, G. V Gill, P. H. Dyer, A. F. Jones, M. Murphy, K. E. Jones, C. Smyth, and A. H. Barnett, "Characteristics of Type 1 diabetes of over 50 years duration (the Golden Years Cohort).," *Diabetic medicine□: a journal of the British Diabetic Association*, vol. 20, no. 10, pp. 808–11, Oct. 2003.

[2] H. A. Keenan, T. Costacou, J. K. Sun, A. Doria, J. Cavellerano, J. Coney, T. J. Orchard, L. P. Aiello, and G. L. King, "Clinical factors associated with resistance to microvascular complications in diabetic patients of extreme disease duration: the 50-year medalist study.," *Diabetes care*, vol. 30, no. 8, pp. 1995–7, Aug. 2007.

[3] J. K. Sun, H. A. Keenan, J. D. Cavallerano, B. F. Asztalos, E. J. Schaefer, D. R. Sell, C. M. Strauch, V. M. Monnier, A. Doria, L. P. Aiello, and G. L. King, "Protection from retinopathy and other complications in patients with type 1 diabetes of extreme duration: the joslin 50-year medalist study.," *Diabetes care*, vol. 34, no. 4, pp. 968–74, Apr. 2011.

[4] H. A. Keenan, J. K. Sun, J. Levine, A. Doria, L. P. Aiello, G. Eisenbarth, S. Bonner-Weir, and G. L. King, "Residual insulin production and pancreatic ß-cell turnover after 50 years of diabetes: Joslin Medalist Study.," *Diabetes*, vol. 59, no. 11, pp. 2846–53, Nov. 2010.

[5] H.-C. Yeh, T. T. Brown, N. Maruthur, P. Ranasinghe, Z. Berger, Y. D. Suh, L. M. Wilson, E. B. Haberl, J. Brick, E. B. Bass, and S. H. Golden, "Comparative effectiveness and safety of methods of insulin delivery and glucose monitoring for diabetes mellitus: a systematic review and meta-analysis.," *Annals of internal medicine*, vol. 157, no. 5, pp. 336–47, Sep. 2012.

[6] A. M. Shapiro, J. R. Lakey, E. A. Ryan, G. S. Korbutt, E. Toth, G. L. Warnock, N. M. Kneteman, and R. V Rajotte, "Islet transplantation in seven patients with type 1 diabetes mellitus using a glucocorticoid-free immunosuppressive regimen.," *The New England journal of medicine*, vol. 343, no. 4, pp. 230–8, Jul. 2000.

[7] A. M. J. Shapiro, C. Ricordi, B. J. Hering, H. Auchincloss, R. Lindblad, R. P. Robertson, A. Secchi, M. D. Brendel, T. Berney, D. C. Brennan, E. Cagliero, R. Alejandro, E. A. Ryan, B. DiMercurio, P. Morel, K. S. Polonsky, J.-A. Reems, R. G. Bretzel, F. Bertuzzi, T. Froud, R. Kandaswamy, D. E. R. Sutherland, G. Eisenbarth, M. Segal, J. Preiksaitis, G. S. Korbutt, F. B. Barton, L. Viviano, V. Seyfert-Margolis, J. Bluestone, and J. R. T. Lakey, "International trial of the Edmonton protocol for islet transplantation.," *The New England journal of medicine*, vol. 355, no. 13, pp. 1318–30, Sep. 2006.

[8] F. B. Barton, M. R. Rickels, R. Alejandro, B. J. Hering, S. Wease, B. Naziruddin, J. Oberholzer, J. S. Odorico, M. R. Garfinkel, M. Levy, F. Pattou, T. Berney, A. Secchi, S. Messinger, P. A. Senior, P. Maffi, A. Posselt, P. G. Stock, D. B. Kaufman, X. Luo, F. Kandeel, E. Cagliero, N. A. Turgeon, P. Witkowski, A. Naji, P. J. O'Connell, C. Greenbaum, Y. C. Kudva, K. L. Brayman, M. J. Aull, C. Larsen, T. W. H. Kay, L. A. Fernandez, M.-C. Vantyghem, M. Bellin, and A. M. J. Shapiro, "Improvement in outcomes of clinical islet transplantation: 1999-2010.," *Diabetes care*, vol. 35, no. 7, pp. 1436–45, Jul. 2012.

[9] A. Bharat, N. Benshoff, B. Olack, S. Ramachandran, N. M. Desai, and T. Mohanakumar, "Novel in vivo murine model to study islet potency: engraftment and function.," *Transplantation*, vol. 79, no. 11, pp. 1627–30, Jun. 2005.

[10] T. Kobayashi, Y. Aomatsu, H. Iwata, T. Kin, H. Kanehiro, M. Hisanaga, S. Ko, M. Nagao, and Y. Nakajima, "Indefinite islet protection from autoimmune destruction in nonobese diabetic mice by agarose microencapsulation without immunosuppression.," *Transplantation*, vol. 75, no. 5, pp. 619–25, Mar. 2003.

[11] T. Kobayashi, Y. Aomatsu, H. Iwata, T. Kin, H. Kanehiro, M. Hisanga, S. Ko, M. Nagao, G. Harb, and Y. Nakajima, "Survival of microencapsulated islets at 400 days posttransplantation in the omental pouch of NOD mice.," *Cell transplantation*, vol. 15, no. 4, pp. 359–65, Jan. 2006.

[12] V. F. Duvivier-Kali, A. Omer, R. J. Parent, J. J. O'Neil, and G. C. Weir, "Complete protection of islets against allorejection and autoimmunity by a simple barium-alginate membrane.," *Diabetes*, vol. 50, no. 8, pp. 1698–705, Aug. 2001.

[13] H. Cui, C. Tucker-Burden, S. M. D. Cauffiel, A. K. Barry, N. N. Iwakoshi, C. J. Weber, and S. A. Safley, "Long-term metabolic control of autoimmune diabetes in spontaneously diabetic nonobese diabetic mice by nonvascularized microencapsulated adult porcine islets.," *Transplantation*, vol. 88, no. 2, pp. 160–9, Jul. 2009.

[14] S. A. Safley, L. M. Kapp, C. Tucker-Burden, B. Hering, J. A. Kapp, and C. J. Weber, "Inhibition of cellular immune responses to encapsulated porcine islet xenografts by simultaneous blockade of two different costimulatory pathways.," *Transplantation*, vol. 79, no. 4, pp. 409–18, Feb. 2005.

[15] M. K. Reimer, S. P. Mokshagundam, K. Wyler, F. Sundler, B. Ahrén, and J. I. Stagner, "Local growth factors are beneficial for the autonomic reinnervation of transplanted islets in rats.," *Pancreas*, vol. 26, no. 4, pp. 392–7, May 2003.

[16] J. Stagner, B. Ahren, F. Sundler, and K. White, "Reconstructing the pancreas: restoration of normoglycemia, exocrine function, and islet innervation by islet transplantation to the pancreas.," *Transplantation proceedings*, vol. 40, no. 2, pp. 452–4, Mar. 2008.

[17] J. H. Brauker, V. E. Carr-Brendel, L. A. Martinson, J. Crudele, W. D. Johnston, and R. C. Johnson, "Neovascularization of synthetic membranes directed by membrane microarchitecture.," *Journal of biomedical materials research*, vol. 29, no. 12, pp. 1517–24, Dec. 1995.

[18] J. Brauker, L. A. Martinson, S. K. Young, and R. C. Johnson, "Local inflammatory response around diffusion chambers containing xenografts. Nonspecific destruction of tissues and decreased local vascularization.," *Transplantation*, vol. 61, no. 12, pp. 1671–7, Jun. 1996.

[19] M. Kumagai-Braesch, S. Jacobson, H. Mori, X. Jia, T. Takahashi, A. Wernerson, M. Flodström-Tullberg, and A. Tibell, "The TheraCyte(TM) Device Protects against Islet Allograft Rejection in Immunized Hosts.," *Cell transplantation*, Oct. 2012.

[20] T. Loudovaris, S. Jacobs, S. Young, D. Maryanov, J. Brauker, and R. C. Johnson, "Correction of diabetic nod mice with insulinomas implanted within Baxter immunoisolation devices.," *Journal of molecular medicine (Berlin, Germany)*, vol. 77, no. 1, pp. 219–22, Jan. 1999.

[21] K. W. Broadhead, R. Biran, and P. A. Tresco, “Hollow fiber membrane diffusive permeability regulates encapsulated cell line biomass, proliferation, and small molecule release.,” *Biomaterials*, vol. 23, no. 24, pp. 4689–99, Dec. 2002.

[22] S. R. Winn, J. P. Hammang, D. F. Emerich, A. Lee, R. D. Palmiter, and E. E. Baetge, “Polymer-encapsulated cells genetically modified to secrete human nerve growth factor promote the survival of axotomized septal cholinergic neurons.,” *Proceedings of the National Academy of Sciences of the United States of America*, vol. 91, no. 6, pp. 2324–8, Mar. 1994.

[23] W. Wang, Y. Gu, Y. Tabata, M. Miyamoto, H. Hori, N. Nagata, M. Touma, A. N. Balamurugan, Y. Kawakami, M. Nozawa, and K. Inoue, “Reversal of diabetes in mice by xenotransplantation of a bioartificial pancreas in a prevascularized subcutaneous site.,” *Transplantation*, vol. 73, no. 1, pp. 122–9, Jan. 2002.

[24] W. Wang, Y. Gu, H. Hori, T. Sakurai, A. Hiura, S. Sumi, Y. Tabata, and K. Inoue, “Subcutaneous transplantation of macroencapsulated porcine pancreatic endocrine cells normalizes hyperglycemia in diabetic mice.,” *Transplantation*, vol. 76, no. 2, pp. 290–6, Jul. 2003.

[25] C. A. Hoesli, M. Luu, and J. M. Piret, “A novel alginate hollow fiber bioreactor process for cellular therapy applications.,” *Biotechnology progress*, vol. 25, no. 6, pp. 1740–51.

[26] T. Maki, C. J. Mullon, B. A. Solomon, and A. P. Monaco, “Novel delivery of pancreatic islet cells to treat insulin-dependent diabetes mellitus.,” *Clinical pharmacokinetics*, vol. 28, no. 6, pp. 471–82, Jun. 1995.

[27] F. Lim and A. M. Sun, “Microencapsulated islets as bioartificial endocrine pancreas.,” *Science (New York, N.Y.)*, vol. 210, no. 4472, pp. 908–10, Nov. 1980.

[28] A. Omer, V. F. Duvivier-Kali, N. Trivedi, K. Wilmot, S. Bonner-Weir, and G. C. Weir, “Survival and maturation of microencapsulated porcine neonatal pancreatic cell clusters transplanted into immunocompetent diabetic mice.,” *Diabetes*, vol. 52, no. 1, pp. 69–75, Jan. 2003.

[29] V. F. Duvivier-Kali, A. Omer, M. D. Lopez-Avalos, J. J. O’Neil, and G. C. Weir, “Survival of microencapsulated adult pig islets in mice in spite of an antibody response.,” *American journal of transplantation : official journal of the American Society of Transplantation and the American Society of Transplant Surgeons*, vol. 4, no. 12, pp. 1991–2000, Dec. 2004.

[30] K. Moore, J. Amos, J. Davis, R. Gourdie, and J. D. Potts, “Characterization of polymeric microcapsules containing a low molecular weight peptide for controlled release.,” *Microscopy and microanalysis : the official journal of Microscopy Society of America, Microbeam Analysis Society, Microscopical Society of Canada*, vol. 19, no. 1, pp. 213–26, Feb. 2013.

[31] S. Shin, J. E. Shin, and Y. J. Yoo, “Attachment of alginate microcapsules onto plasma-treated PDMS sheet for retrieval after transplantation.,” *Biotechnology and applied biochemistry*, May 2013.

[32] R. F. Gibly, X. Zhang, M. L. Graham, B. J. Hering, D. B. Kaufman, W. L. Lowe, and L. D. Shea, “Extrahepatic islet transplantation with microporous polymer scaffolds in syngeneic mouse and allogeneic porcine models.,” *Biomaterials*, vol. 32, no. 36, pp. 9677–84, Dec. 2011.

[33] A. J. Hussey, M. Winardi, J. Wilson, N. Forster, W. A. Morrison, A. J. Penington, K. R. Knight, and S. J. Feeney, "Pancreatic islet transplantation using vascularised chambers containing nerve growth factor ameliorates hyperglycaemia in diabetic mice.," *Cells, tissues, organs*, vol. 191, no. 5, pp. 382–93, Jan. 2010.

[34] E. Pedraza, A.-C. Brady, C. A. Fraker, R. D. Molano, S. Sukert, D. M. Berman, N. S. Kenyon, A. Pileggi, C. Ricordi, and C. L. Stabler, "Macroporous Three Dimensional PDMS Scaffolds for Extrahepatic Islet Transplantation.," *Cell transplantation*, Oct. 2012.

[35] E. Pedraza, A.-C. Brady, C. A. Fraker, and C. L. Stabler, "Synthesis of macroporous poly(dimethylsiloxane) scaffolds for tissue engineering applications.," *Journal of biomaterials science. Polymer edition*, vol. 24, no. 9, pp. 1041–56, Jun. 2013.

[36] J. T. Daoud, M. S. Petropavlovskaia, J. M. Patapas, C. E. Degrandpré, R. W. Diraddo, L. Rosenberg, and M. Tabrizian, "Long-term in vitro human pancreatic islet culture using three-dimensional microfabricated scaffolds.," *Biomaterials*, vol. 32, no. 6, pp. 1536–42, Feb. 2011.

[37] J. M. Dufour, R. V Rajotte, M. Zimmerman, A. Rezania, T. Kin, D. E. Dixon, and G. S. Korbutt, "Development of an ectopic site for islet transplantation, using biodegradable scaffolds.," *Tissue engineering*, vol. 11, no. 9–10, pp. 1323–31.

[38] D. M. Salvay, C. B. Rives, X. Zhang, F. Chen, D. B. Kaufman, W. L. Lowe, and L. D. Shea, "Extracellular matrix protein-coated scaffolds promote the reversal of diabetes after extrahepatic islet transplantation.," *Transplantation*, vol. 85, no. 10, pp. 1456–64, May 2008.

[39] D. M. Berman, J. J. O'Neil, L. C. K. Coffey, P. C. J. Chaffanjon, N. M. Kenyon, P. Ruiz, A. Pileggi, C. Ricordi, and N. S. Kenyon, "Long-term survival of nonhuman primate islets implanted in an omental pouch on a biodegradable scaffold.," *American journal of transplantation : official journal of the American Society of Transplantation and the American Society of Transplant Surgeons*, vol. 9, no. 1, pp. 91–104, Jan. 2009.

[40] J. H. Juang, S. Bonner-Weir, Y. Ogawa, J. P. Vacanti, and G. C. Weir, "Outcome of subcutaneous islet transplantation improved by polymer device.," *Transplantation*, vol. 61, no. 11, pp. 1557–61, Jun. 1996.

[41] J. Kriz, G. Vilk, D. M. Mazzuca, P. M. Toleikis, P. J. Foster, and D. J. G. White, "A novel technique for the transplantation of pancreatic islets within a vascularized device into the greater omentum to achieve insulin independence.," *American journal of surgery*, vol. 203, no. 6, pp. 793–7, Jun. 2012.

[42] R. A. Valdés-González, L. M. Dorantes, G. N. Garibay, E. Bracho-Blanchet, A. J. Mendez, R. Dávila-Pérez, R. B. Elliott, L. Terán, and D. J. G. White, "Xenotransplantation of porcine neonatal islets of Langerhans and Sertoli cells: a 4-year study.," *European journal of endocrinology / European Federation of Endocrine Societies*, vol. 153, no. 3, pp. 419–27, Sep. 2005.

[43] R. Valdes-Gonzalez, A. L. Rodriguez-Ventura, D. J. G. White, E. Bracho-Blanchet, A. Castillo, B. Ramírez-González, M. G. López-Santos, B. H. León-Mancilla, and L. M. Dorantes, "Long-term follow-up of patients with type 1 diabetes transplanted with neonatal pig islets.," *Clinical and experimental immunology*, vol. 162, no. 3, pp. 537–42, Dec. 2010.

[44] A. L. R.-V. Rafael Valdés-González, "Long-Term Survival of Neonatal Porcine Islets Without Sertoli Cells in Rabbits," *Archives of Clinical and Experimental Surgery (ACES)*, vol. 2, no. 2, 2013.

[45] N. A. Forster, A. J. Penington, A. A. Hardikar, J. A. Palmer, A. Hussey, J. Tai, W. A. Morrison, and S. J. Feeney, "A prevascularized tissue engineering chamber supports growth and function of islets and progenitor cells in diabetic mice," *Islets*, vol. 3, no. 5, pp. 271–283, Sep. 2011.

[46] J. I. Lee, R. Nishimura, H. Sakai, N. Sasaki, and T. Kenmochi, "A newly developed immunoisolated bioartificial pancreas with cell sheet engineering.," *Cell transplantation*, vol. 17, no. 1–2, pp. 51–9, Jan. 2008.

[47] J. I. Lee, J. Y. Kim, H. W. Kim, S. J. Bae, D. J. Joo, K. H. Huh, Y. H. Fang, J. H. Jeong, M. S. Kim, and Y. S. Kim, "Long-term viability of transplanted hybrid cellular spheroids within chondrocyte sheets.," *Transplantation proceedings*, vol. 44, no. 4, pp. 1162–5, May 2012.

[48] J. M. Pollok, J. F. Begemann, P. M. Kaufmann, D. Kluth, C. E. Broelsch, J. R. Izbicki, and X. Rogiers, "Long-term insulin-secretory function of islets of Langerhans encapsulated with a layer of confluent chondrocytes for immunoisolation.," *Pediatric surgery international*, vol. 15, no. 3–4, pp. 164–7, Jan. 1999.

[49] H. Aghajani-Lazarjani, E. Vasheghani-Farahani, S. A. Shojaosadati, S. Hashemi-Najafabadi, S. Zahediasl, T. Tiraihi, and F. Atyabi, "The effect of two different polyethylene glycol (PEG) derivatives on the immunological response of PEG grafted pancreatic islets.," *Journal of artificial organs□: the official journal of the Japanese Society for Artificial Organs*, vol. 13, no. 4, pp. 218–24, Dec. 2010.

[50] S. Kizilel, A. Scavone, X. Liu, J.-M. Nothias, D. Ostrega, P. Witkowski, and M. Millis, "Encapsulation of pancreatic islets within nano-thin functional polyethylene glycol coatings for enhanced insulin secretion.," *Tissue engineering. Part A*, vol. 16, no. 7, pp. 2217–28, Jul. 2010.

[51] D. Y. Lee, J. H. Nam, and Y. Byun, "Effect of polyethylene glycol grafted onto islet capsules on prevention of splenocyte and cytokine attacks.," *Journal of biomaterials science. Polymer edition*, vol. 15, no. 6, pp. 753–66, Jan. 2004.

[52] D. Y. Lee, K. Yang, S. Lee, S. Y. Chae, K.-W. Kim, M. K. Lee, D.-J. Han, and Y. Byun, "Optimization of monomethoxy-polyethylene glycol grafting on the pancreatic islet capsules.," *Journal of biomedical materials research*, vol. 62, no. 3, pp. 372–7, Dec. 2002.

[53] Y. Teramura, O. P. Oommen, J. Olerud, J. Hilborn, and B. Nilsson, "Microencapsulation of cells, including islets, within stable ultra-thin membranes of maleimide-conjugated PEG-lipid with multifunctional crosslinkers.," *Biomaterials*, vol. 34, no. 11, pp. 2683–93, Apr. 2013.

[54] J. T. Wilson, W. Cui, and E. L. Chaikof, "Layer-by-layer assembly of a conformal nanothin PEG coating for intraportal islet transplantation.," *Nano letters*, vol. 8, no. 7, pp. 1940–8, Jul. 2008.

[55] J.-H. Jeong, S. W. Hong, S. Hong, S. Yook, Y. Jung, J.-B. Park, C. D. Khue, B.-H. Im, J. Seo, H. Lee, C.-H. Ahn, D. Y. Lee, and Y. Byun, "Surface camouflage of pancreatic islets using 6-arm-PEG-catechol in combined therapy with tacrolimus and anti-CD154 monoclonal antibody for xenotransplantation.," *Biomaterials*, vol. 32, no. 31, pp. 7961–70, Nov. 2011.

[56] T. Bhaiji, Z.-L. Zhi, and J. C. Pickup, “Improving cellular function and immune protection via layer-by-layer nanocoating of pancreatic islet β-cell spheroids cocultured with mesenchymal stem cells.,” *Journal of biomedical materials research. Part A*, vol. 100, no. 6, pp. 1628–36, Jun. 2012.

[57] K. S. Jones, M. V Sefton, and R. M. Gorczynski, “In vivo recognition by the host adaptive immune system of microencapsulated xenogeneic cells.,” *Transplantation*, vol. 78, no. 10, pp. 1454–62, Nov. 2004.

[58] A. N. Balamurugan, Y. Gu, Y. Tabata, M. Miyamoto, W. Cui, H. Hori, A. Satake, N. Nagata, W. Wang, and K. Inoue, “Bioartificial pancreas transplantation at prevascularized intermuscular space: effect of angiogenesis induction on islet survival.,” *Pancreas*, vol. 26, no. 3, pp. 279–85, Apr. 2003.

[59] B. Ludwig, A. Rotem, J. Schmid, G. C. Weir, C. K. Colton, M. D. Brendel, T. Neufeld, N. L. Block, K. Yavriyants, A. Steffen, S. Ludwig, T. Chavakis, A. Reichel, D. Azarov, B. Zimermann, S. Maimon, M. Balyura, T. Rozenshtein, N. Shabtay, P. Vardi, K. Bloch, P. de Vos, A. V Schally, S. R. Bornstein, and U. Barkai, “Improvement of islet function in a bioartificial pancreas by enhanced oxygen supply and growth hormone releasing hormone agonist.,” *Proceedings of the National Academy of Sciences of the United States of America*, vol. 109, no. 13, pp. 5022–7, Mar. 2012.

[60] R. P. Lanza, A. M. Beyer, J. E. Staruk, and W. L. Chick, “Biohybrid artificial pancreas. Long-term function of discordant islet xenografts in streptozotocin diabetic rats.,” *Transplantation*, vol. 56, no. 5, pp. 1067–72, Nov. 1993.

[61] R. P. Lanza, A. M. Beyer, and W. L. Chick, “Xenogenic humoral responses to islets transplanted in biohybrid diffusion chambers.,” *Transplantation*, vol. 57, no. 9, pp. 1371–5, May 1994.

[62] G. F. Klomp, H. Hashiguchi, P. C. Ursell, Y. Takeda, T. Taguchi, and W. H. Dobelle, “Macroporous hydrogel membranes for a hybrid artificial pancreas. II. Biocompatibility.,” *Journal of biomedical materials research*, vol. 17, no. 5, pp. 865–71, Sep. 1983.

[63] J. Bodziony and J. Stanosek, “[Treatment of diabetes by implantation of isolated islands of Langerhans in semipermeable chambers].,” *Zeitschrift für experimentelle Chirurgie, Transplantation, und künstliche Organe : Organ der Sektion Experimentelle Chirurgie der Gesellschaft für Chirurgie der DDR*, vol. 18, no. 4, pp. 215–23, Jan. 1985.

[64] M. Goto, Y. Yoshikawa, K. Matsuo, A. Shirasu, N. Ogawa, H. Takahashi, Y. Saitoh, K. Fujimori, Y. Kurokawa, M. Tamai, and S. Satomi, “Optimization of a prominent oxygen-permeable device for pancreatic islets.,” *Transplantation proceedings*, vol. 40, no. 2, pp. 411–2, Mar. 2008.

[65] E. S. O’Sullivan, A. Vegas, D. G. Anderson, and G. C. Weir, “Islets transplanted in immunoisolation devices: a review of the progress and the challenges that remain.,” *Endocrine reviews*, vol. 32, no. 6, pp. 827–44, Dec. 2011.

[66] E. Lam, R. T. Kilani, Y. Li, E. E. Tredget, and A. Ghahary, “Stratifin-induced matrix metalloproteinase-1 in fibroblast is mediated by c-fos and p38 mitogen-activated protein kinase activation.,” *The Journal of investigative dermatology*, vol. 125, no. 2, pp. 230–8, Aug. 2005.

[67] A. Ghaffari, Y. Li, A. Karami, M. Ghaffari, E. E. Tredget, and A. Ghahary, “Fibroblast extracellular matrix gene expression in response to keratinocyte-releasable stratifin.,” *Journal of cellular biochemistry*, vol. 98, no. 2, pp. 383–93, May 2006.

[68] M. Edward, J. A. Quinn, and W. Sands, “Keratinocytes stimulate fibroblast hyaluronan synthesis through the release of stratifin: a possible role in the suppression of scar tissue formation.,” *Wound repair and regeneration : official publication of the Wound Healing Society [and] the European Tissue Repair Society*, vol. 19, no. 3, pp. 379–86.

[69] F. Folli, V. Guzzi, L. Perego, D. K. Coletta, G. Finzi, C. Placidi, S. La Rosa, C. Capella, C. Socci, D. Lauro, D. Tripathy, C. Jenkinson, R. Paroni, E. Orsenigo, G. Cighetti, L. Gregorini, C. Staudacher, A. Secchi, A. Bachi, M. Brownlee, and P. Fiorina, “Proteomics reveals novel oxidative and glycolytic mechanisms in type 1 diabetic patients’ skin which are normalized by kidney-pancreas transplantation.,” *PloS one*, vol. 5, no. 3, p. e9923, Jan. 2010.

[70] G. E. Lim, M. Piske, and J. D. Johnson, “14-3-3 proteins are essential signalling hubs for beta cell survival.,” *Diabetologia*, vol. 56, no. 4, pp. 825–37, Apr. 2013.

[71] K. Sidthipong, S. Todo, I. Takei, I. Kojima, and K. Umezawa, “Screening of new bioactive metabolites for diabetes therapy.,” *Internal and emergency medicine*, vol. 8 Suppl 1, pp. S57–9, Apr. 2013.

[72] S. Akashi, M. Sho, H. Kashizuka, K. Hamada, N. Ikeda, Y. Kuzumoto, Y. Tsurui, T. Nomi, T. Mizuno, H. Kanehiro, M. Hisanaga, S. Ko, and Y. Nakajima, “A novel small-molecule compound targeting CCR5 and CXCR3 prevents acute and chronic allograft rejection.,” *Transplantation*, vol. 80, no. 3, pp. 378–84, Aug. 2005.

[73] N. Zhang, D. Su, S. Qu, T. Tse, R. Bottino, A. N. Balamurugan, J. Xu, J. S. Bromberg, and H. H. Dong, “Sirolimus is associated with reduced islet engraftment and impaired beta-cell function.,” *Diabetes*, vol. 55, no. 9, pp. 2429–36, Sep. 2006.

[74] R. Nishimura, S. Nishioka, I. Fujisawa, H. Shiku, M. Shimada, S. Sekiguchi, K. Fujimori, A. Ushiyama, T. Matsue, N. Ohuchi, S. Satomi, and M. Goto, “Tacrolimus inhibits the revascularization of isolated pancreatic islets.,” *PloS one*, vol. 8, no. 4, p. e56799, Jan. 2013.

[75] Z. Guo, A. S. Chong, J. Shen, P. Foster, H. N. Sankary, L. McChesney, D. Mital, S. C. Jensik, H. Gebel, and J. W. Williams, “Leflunomide, a potential immunosuppressant for pancreatic islet transplantation.,” *Transplantation proceedings*, vol. 29, no. 1–2, pp. 1296–7.

[76] C. Rastellini, L. Cicalese, R. Leach, M. Braun, J. J. Fung, T. E. Starzl, and A. S. Rao, “Prolonged survival of islet allografts following combined therapy with tacrolimus and leflunomide.,” *Transplantation proceedings*, vol. 31, no. 1–2, pp. 646–7.

[77] L. Wennberg, Z. Song, J. Zhang, W. Bennet, S. Nava, S. Bari, B. Sundberg, O. Korsgren, and C. G. Groth, “Diabetic rats transplanted with adult porcine islets and immunosuppressed with cyclosporine, mycophenolate mofetil, and leflunomide remain normoglycemic for up to 100 days.,” *Transplantation proceedings*, vol. 32, no. 5, p. 1061, Aug. 2000.

[78] L. Wennberg, Z. Song, W. Bennet, J. Zhang, S. Nava, B. Sundberg, S. Bari, C. G. Groth, and O. Korsgren, “Diabetic rats transplanted with adult porcine islets and immunosuppressed with

cyclosporine A, mycophenolate mofetil, and leflunomide remain normoglycemic for up to 100 days.," *Transplantation*, vol. 71, no. 8, pp. 1024–33, Apr. 2001.

[79] H. Amemiya, "Deoxyspergualin: clinical trials in renal graft rejection. Japan Collaborative Transplant Study of Deoxyspergualin.," *Annals of the New York Academy of Sciences*, vol. 685, pp. 196–201, Jun. 1993.

[80] J. Henretta, K. Pittman, T. McFadden, J. Thomas, and F. Thomas, "Deoxyspergualin and rabbit antithymocyte globulin markedly prolong discordant pig pancreatic islet xenografts.," *Transplantation proceedings*, vol. 25, no. 1 Pt 1, pp. 412–3, Feb. 1993.

[81] H. Holcombe, I. Mellman, C. A. Janeway, K. Bottomly, and B. N. Dittel, "The immunosuppressive agent 15-deoxyspergualin functions by inhibiting cell cycle progression and cytokine production following naive T cell activation.," *Journal of immunology (Baltimore, Md.□: 1950)*, vol. 169, no. 9, pp. 4982–9, Nov. 2002.

[82] B. R. Hsu, F. H. Chang, J. H. Juang, Y. Y. Huang, and S. H. Fu, "The rescue effect of 15-deoxyspergualin on intraperitoneal microencapsulated xenoislets.," *Cell transplantation*, vol. 8, no. 3, pp. 307–15.

[83] D. B. Kaufman, P. F. Gores, M. J. Field, A. C. Farney, S. A. Gruber, E. Stephanian, and D. E. Sutherland, "Effect of 15-deoxyspergualin on immediate function and long-term survival of transplanted islets in murine recipients of a marginal islet mass.," *Diabetes*, vol. 43, no. 6, pp. 778–83, Jun. 1994.

[84] T. Llyung, J. Contreras, F. Thomas, K. Pittman, and J. Thomas, "Long-term (10-month) pig islet xenograft tolerance using measured total lymphoid irradiation, splenectomy, short-term rabbit antithymocyte globulin, and deoxyspergualin without long-term immunosuppression.," *Transplantation proceedings*, vol. 31, no. 1–2, pp. 962–3.

[85] K. Pittman, F. Thomas, T. McFadden, C. Haisch, and J. Thomas, "Reduction in primary nonfunction of pancreas islet transplants with antithymocyte globulin agents, deoxyspergualin, and splenectomy.," *Transplantation proceedings*, vol. 25, no. 1 Pt 2, pp. 986–7, Feb. 1993.

[86] F. Thomas, K. Pittman, T. Ljung, and E. Cekada, "Deoxyspergualin is a unique immunosuppressive agent with selective utility in inducing tolerance to pancreas islet xenografts.," *Transplantation proceedings*, vol. 27, no. 1, pp. 417–9, Feb. 1995.

[87] Y. Song, E. Margolles-Clark, C. A. Fraker, J. D. Weaver, C. Ricordi, A. Pileggi, C. L. Stabler, and P. Buchwald, "Feasibility of localized immunosuppression: 3. Preliminary evaluation of organosilicone constructs designed for sustained drug release in a cell transplant environment using dexamethasone.," *Die Pharmazie*, vol. 67, no. 5, pp. 394–9, May 2012.

[88] N. Bocca, A. Pileggi, R. D. Molano, S. Marzorati, W. Wu, N. Bodor, C. Ricordi, and P. Buchwald, "Soft corticosteroids for local immunosuppression: exploring the possibility for the use of loteprednol etabonate for islet transplantation.," *Die Pharmazie*, vol. 63, no. 3, pp. 226–32, Mar. 2008.

[89] P. Buchwald, N. Bocca, S. Marzorati, G. Hochhaus, N. Bodor, C. Stabler, N. S. Kenyon, L. Inverardi, R. D. Molano, C. Ricordi, and A. Pileggi, "Feasibility of localized immunosuppression:

1. Exploratory studies with glucocorticoids in a biohybrid device designed for cell transplantation.," *Die Pharmazie*, vol. 65, no. 6, pp. 421–8, Jun. 2010.

[90] B. P. Cummings, A. A. Bremer, T. J. Kieffer, D. D'Alessio, and P. J. Havel, "Investigation of the mechanisms contributing to the compensatory increase in insulin secretion during dexamethasone-induced insulin resistance in rhesus macaques.," *The Journal of endocrinology*, vol. 216, no. 2, pp. 207–15, Jan. 2013.

[91] A. Rafacho, L. Marroquí, S. R. Taboga, J. L. F. Abrantes, L. R. Silveira, A. C. Boschero, E. M. Carneiro, J. R. Bosqueiro, A. Nadal, and I. Quesada, "Glucocorticoids in vivo induce both insulin hypersecretion and enhanced glucose sensitivity of stimulus-secretion coupling in isolated rat islets.," *Endocrinology*, vol. 151, no. 1, pp. 85–95, Jan. 2010.

[92] L. P. Roma, K. L. A. Souza, E. M. Carneiro, A. C. Boschero, and J. R. Bosqueiro, "Pancreatic islets from dexamethasone-treated rats show alterations in global gene expression and mitochondrial pathways.," *General physiology and biophysics*, vol. 31, no. 1, pp. 65–76, Mar. 2012.

[93] A. Ngo, D. E. R. Sutherland, G. J. Beilman, and M. D. Bellin, "Deterioration of glycemic control after corticosteroid administration in islet autotransplant recipients: a cautionary tale.," *Acta diabetologica*, Aug. 2011.

[94] S. Gremlich, R. Roduit, and B. Thorens, "Dexamethasone induces posttranslational degradation of GLUT2 and inhibition of insulin secretion in isolated pancreatic beta cells. Comparison with the effects of fatty acids.," *The Journal of biological chemistry*, vol. 272, no. 6, pp. 3216–22, Feb. 1997.

[95] I. K. Jeong, S. H. Oh, B. J. Kim, J. H. Chung, Y. K. Min, M. S. Lee, M. K. Lee, and K. W. Kim, "The effects of dexamethasone on insulin release and biosynthesis are dependent on the dose and duration of treatment.," *Diabetes research and clinical practice*, vol. 51, no. 3, pp. 163–71, Mar. 2001.

[96] A. Rafacho, S. Quallio, D. L. Ribeiro, S. R. Taboga, F. M. M. Paula, A. C. Boschero, and J. R. Bosqueiro, "The adaptive compensations in endocrine pancreas from glucocorticoid-treated rats are reversible after the interruption of treatment.," *Acta physiologica (Oxford, England)*, vol. 200, no. 3, pp. 223–35, Nov. 2010.

[97] J. M. Dufour, B. Dass, K. R. Halley, G. S. Korbutt, D. E. Dixon, and R. V Rajotte, "Sertoli cell line lacks the immunoprotective properties associated with primary Sertoli cells.," *Cell transplantation*, vol. 17, no. 5, pp. 525–34, Jan. 2008.

[98] U. N. Das, "Lipoxins, resolvins, and protectins in the prevention and treatment of diabetic macular edema and retinopathy.," *Nutrition (Burbank, Los Angeles County, Calif.)*, vol. 29, no. 1, pp. 1–7, Jan. 2013.

[99] Z. Yang, M. Chen, J. D. Ellett, L. B. Fialkow, J. D. Carter, and J. L. Nadler, "The novel anti-inflammatory agent lisofylline prevents autoimmune diabetic recurrence after islet transplantation.," *Transplantation*, vol. 77, no. 1, pp. 55–60, Jan. 2004.

[100] P. Chhabra, K. Wang, Q. Zeng, M. Jecmenica, L. Langman, J. Linden, R. J. Ketchum, and K. L. Brayman, "Adenosine A(2A) agonist administration improves islet transplant outcome: Evidence for the role of innate immunity in islet graft rejection.," *Cell transplantation*, vol. 19, no. 5, pp. 597–612, Jan. 2010.

[101] T. Nitta, T. Itoh, N. Matsuoka, T. Mera, D. Kojima, M. Nakano, Y. Yamashita, and Y. Yasunami, "Prevention of early loss of transplanted islets in the liver of mice by adenosine.," *Transplantation*, vol. 88, no. 1, pp. 49–56, Jul. 2009.

[102] S. Schneider and H. H. Klein, "Inosine improves islet xenograft survival in immunocompetent diabetic mice.," *European journal of medical research*, vol. 10, no. 7, pp. 283–6, Jul. 2005.

[103] V. Cantaluppi, L. Biancone, F. Figliolini, S. Beltramo, D. Medica, M. C. Deregibus, F. Galimi, R. Romagnoli, M. Salizzoni, C. Tetta, G. P. Segoloni, and G. Camussi, "Microvesicles derived from endothelial progenitor cells enhance neoangiogenesis of human pancreatic islets.," *Cell transplantation*, vol. 21, no. 6, pp. 1305–20, Jan. 2012.

[104] J. Henriksnäs, J. Lau, G. Zang, P.-O. Berggren, M. Köhler, and P.-O. Carlsson, "Markedly decreased blood perfusion of pancreatic islets transplanted intraportally into the liver: disruption of islet integrity necessary for islet revascularization.," *Diabetes*, vol. 61, no. 3, pp. 665–73, Mar. 2012.

[105] J. Olerud, M. Johansson, J. Lawler, N. Welsh, and P.-O. Carlsson, "Improved vascular engraftment and graft function after inhibition of the angiostatic factor thrombospondin-1 in mouse pancreatic islets.," *Diabetes*, vol. 57, no. 7, pp. 1870–7, Jul. 2008.

[106] N. Zhang, S. Qu, J. Xu, J. S. Bromberg, and H. H. Dong, "Inhibition of angiogenesis is associated with reduced islet engraftment in diabetic recipient mice.," *Transplantation proceedings*, vol. 37, no. 10, pp. 4452–7, Dec. 2005.

[107] A. E. Elcin and Y. M. Elcin, "Localized angiogenesis induced by human vascular endothelial growth factor-activated PLGA sponge.," *Tissue engineering*, vol. 12, no. 4, pp. 959–68, Apr. 2006.

[108] D. Lindhorst, F. Tavassol, C. von See, P. Schumann, M. W. Laschke, Y. Harder, K.-H. Bormann, H. Essig, H. Kokemüller, A. Kampmann, A. Voss, R. Mülhaupt, M. D. Menger, N.-C. Gellrich, and M. Rücker, "Effects of VEGF loading on scaffold-confined vascularization.," *Journal of biomedical materials research. Part A*, vol. 95, no. 3, pp. 783–92, Dec. 2010.

[109] S. Singh, B. M. Wu, and J. C. Y. Dunn, "Delivery of VEGF using collagen-coated polycaprolactone scaffolds stimulates angiogenesis.," *Journal of biomedical materials research. Part A*, vol. 100, no. 3, pp. 720–7, Mar. 2012.

[110] R. B. Vernon, A. Preisinger, M. D. Gooden, L. A. D'Amico, B. B. Yue, P. L. Bollyky, C. S. Kuhr, T. R. Hefty, G. T. Nepom, and J. A. Gebe, "Reversal of diabetes in mice with a bioengineered islet implant incorporating a type I collagen hydrogel and sustained release of vascular endothelial growth factor.," *Cell transplantation*, vol. 21, no. 10, pp. 2099–110, Jan. 2012.

[111] E. A. Phelps, D. M. Headen, W. R. Taylor, P. M. Thulé, and A. J. García, "Vasculogenic bio-synthetic hydrogel for enhancement of pancreatic islet engraftment and function in type 1 diabetes.," *Biomaterials*, vol. 34, no. 19, pp. 4602–11, Jun. 2013.

[112] A. Golocheikine, V. Tiriveedhi, N. Angaswamy, N. Benshoff, R. Sabarinathan, and T. Mohanakumar, "Cooperative signaling for angiogenesis and neovascularization by VEGF and HGF following islet transplantation.," *Transplantation*, vol. 90, no. 7, pp. 725–31, Oct. 2010.

[113] S. Sigrist, A. Mechine-Neuville, K. Mandes, V. Calenda, S. Braun, G. Legeay, J. P. Bellocq, M. Pinget, and L. Kessler, "Influence of VEGF on the viability of encapsulated pancreatic rat islets after transplantation in diabetic mice.," *Cell transplantation*, vol. 12, no. 6, pp. 627–35, Jan. 2003.

[114] S. Kang, H. S. Park, A. Jo, S. H. Hong, H. N. Lee, Y. Y. Lee, J. S. Park, H. S. Jung, S. S. Chung, and K. S. Park, "Endothelial progenitor cell cotransplantation enhances islet engraftment by rapid revascularization.," *Diabetes*, vol. 61, no. 4, pp. 866–76, Apr. 2012.

[115] Y. Cheng, Y.-F. Liu, J.-L. Zhang, T.-M. Li, and N. Zhao, "Elevation of vascular endothelial growth factor production and its effect on revascularization and function of graft islets in diabetic rats.," *World journal of gastroenterology : WJG*, vol. 13, no. 20, pp. 2862–6, May 2007.

[116] N. Zhang, A. Richter, J. Suriawinata, S. Harbaran, J. Altomonte, L. Cong, H. Zhang, K. Song, M. Meseck, J. Bromberg, and H. Dong, "Elevated vascular endothelial growth factor production in islets improves islet graft vascularization.," *Diabetes*, vol. 53, no. 4, pp. 963–70, Apr. 2004.

[117] D. Su, N. Zhang, J. He, S. Qu, S. Slusher, R. Bottino, S. Bertera, J. Bromberg, and H. H. Dong, "Angiopoietin-1 production in islets improves islet engraftment and protects islets from cytokine-induced apoptosis.," *Diabetes*, vol. 56, no. 9, pp. 2274–83, Sep. 2007.

[118] N. Yin, N. Zhang, J. Xu, Q. Shi, Y. Ding, and J. S. Bromberg, "Targeting lymphangiogenesis after islet transplantation prolongs islet allograft survival.," *Transplantation*, vol. 92, no. 1, pp. 25–30, Jul. 2011.

[119] T. Dietrich, F. Bock, D. Yuen, D. Hos, B. O. Bachmann, G. Zahn, S. Wiegand, L. Chen, and C. Cursiefen, "Cutting edge: lymphatic vessels, not blood vessels, primarily mediate immune rejections after transplantation.," *Journal of immunology (Baltimore, Md. : 1950)*, vol. 184, no. 2, pp. 535–9, Jan. 2010.

[120] N. Yin, N. Zhang, G. Lal, J. Xu, M. Yan, Y. Ding, and J. S. Bromberg, "Lymphangiogenesis is required for pancreatic islet inflammation and diabetes.," *PloS one*, vol. 6, no. 11, p. e28023, Jan. 2011.

[121] M. Ferdaoussi, S. Abdelli, J.-Y. Yang, M. Cornu, G. Niederhauser, D. Favre, C. Widmann, R. Regazzi, B. Thorens, G. Waeber, and A. Abderrahmani, "Exendin-4 protects beta-cells from interleukin-1 beta-induced apoptosis by interfering with the c-Jun NH2-terminal kinase pathway.," *Diabetes*, vol. 57, no. 5, pp. 1205–15, May 2008.

[122] J.-H. Kang, S.-Y. Chang, H.-J. Jang, D.-B. Kim, G. R. Ryu, S. H. Ko, I.-K. Jeong, Y.-H. Jo, and M.-J. Kim, "Exendin-4 inhibits interleukin-1beta-induced iNOS expression at the protein level, but not at the transcriptional and posttranscriptional levels, in RINm5F beta-cells.," *The Journal of endocrinology*, vol. 202, no. 1, pp. 65–75, Jul. 2009.

[123] J.-H. Jeong, S. Yook, Y. Jung, B.-H. Im, M. Lee, C.-H. Ahn, D. Y. Lee, and Y. Byun, "Functional enhancement of beta cells in transplanted pancreatic islets by secretion signal peptide-linked exendin-4 gene transduction.," *Journal of controlled release : official journal of the Controlled Release Society*, vol. 159, no. 3, pp. 368–75, May 2012.

[124] J.-H. Juang, C.-H. Kuo, C.-H. Wu, and C. Juang, "Exendin-4 treatment expands graft beta-cell mass in diabetic mice transplanted with a marginal number of fresh islets.," *Cell transplantation*, vol. 17, no. 6, pp. 641–7, Jan. 2008.

[125] A. Sharma, A. Sörenby, A. Wernerson, S. Efendic, M. Kumagai-Braesch, and A. Tibell, "Exendin-4 treatment improves metabolic control after rat islet transplantation to athymic mice with streptozotocin-induced diabetes.," *Diabetologia*, vol. 49, no. 6, pp. 1247–53, Jun. 2006.

[126] A. King, J. Lock, G. Xu, S. Bonner-Weir, and G. C. Weir, "Islet transplantation outcomes in mice are better with fresh islets and exendin-4 treatment.," *Diabetologia*, vol. 48, no. 10, pp. 2074–9, Oct. 2005.

[127] S. Duncanson and A. Sambanis, "Dual factor delivery of CXCL12 and Exendin-4 for improved survival and function of encapsulated beta cells under hypoxic conditions.," *Biotechnology and bioengineering*, Feb. 2013.

[128] H. A. Arafat, A. K. Katakam, G. Chipitsyna, Q. Gong, A. R. Vancha, J. Gabbeta, and D. C. Dafoe, "Osteopontin protects the islets and beta-cells from interleukin-1 beta-mediated cytotoxicity through negative feedback regulation of nitric oxide.," *Endocrinology*, vol. 148, no. 2, pp. 575–84, Feb. 2007.

[129] E.-K. Kim, K.-B. Kwon, M.-Y. Song, M.-J. Han, J.-H. Lee, Y.-R. Lee, J.-H. Lee, D.-G. Ryu, B.-H. Park, and J.-W. Park, "Flavonoids protect against cytokine-induced pancreatic beta-cell damage through suppression of nuclear factor kappaB activation.," *Pancreas*, vol. 35, no. 4, pp. e1–9, Nov. 2007.

[130] E.-K. Kim, K.-B. Kwon, M.-Y. Song, S.-W. Seo, S.-J. Park, S.-O. Ka, L. Na, K.-A. Kim, D.-G. Ryu, H.-S. So, R. Park, J.-W. Park, and B.-H. Park, "Genistein protects pancreatic beta cells against cytokine-mediated toxicity.," *Molecular and cellular endocrinology*, vol. 278, no. 1–2, pp. 18–28, Nov. 2007.

[131] E. K. Kim, K. B. Kwon, J. H. Lee, B. H. Park, J. W. Park, H. K. Lee, E. C. Jhee, and J. Y. Yang, "Inhibition of cytokine-mediated nitric oxide synthase expression in rat insulinoma cells by scoparone.," *Biological & pharmaceutical bulletin*, vol. 30, no. 2, pp. 242–6, Feb. 2007.

[132] J. A. Emamaullee, L. Stanton, C. Schur, and A. M. J. Shapiro, "Caspase inhibitor therapy enhances marginal mass islet graft survival and preserves long-term function in islet transplantation.," *Diabetes*, vol. 56, no. 5, pp. 1289–98, May 2007.

[133] J. A. Emamaullee, J. Davis, R. Pawlick, C. Toso, S. Merani, S.-X. Cai, B. Tseng, and A. M. J. Shapiro, "The caspase selective inhibitor EP1013 augments human islet graft function and longevity in marginal mass islet transplantation in mice.," *Diabetes*, vol. 57, no. 6, pp. 1556–66, Jun. 2008.

[134] J. D. Rivas-Carrillo, A. Soto-Gutierrez, N. Navarro-Alvarez, H. Noguchi, T. Okitsu, Y. Chen, T. Yuasa, K. Tanaka, M. Narushima, A. Miki, H. Misawa, Y. Tabata, H.-S. Jun, S. Matsumoto, I. J. Fox, N. Tanaka, and N. Kobayashi, "Cell-permeable pentapeptide V5 inhibits apoptosis and enhances insulin secretion, allowing experimental single-donor islet transplantation in mice.," *Diabetes*, vol. 56, no. 5, pp. 1259–67, May 2007.

[135] A. Plesner, P. Liston, R. Tan, R. G. Korneluk, and C. B. Verchere, "The X-linked inhibitor of apoptosis protein enhances survival of murine islet allografts.," *Diabetes*, vol. 54, no. 9, pp. 2533–40, Sep. 2005.

[136] J. L. Contreras, G. Bilbao, C. A. Smyth, X. L. Jiang, D. E. Eckhoff, S. M. Jenkins, F. T. Thomas, D. T. Curiel, and J. M. Thomas, "Cytoprotection of pancreatic islets before and soon after transplantation by gene transfer of the anti-apoptotic Bcl-2 gene.," *Transplantation*, vol. 71, no. 8, pp. 1015–23, Apr. 2001.

[137] W. Wang, Y. Gu, M. Miyamoto, H. Hori, N. Nagata, A. N. Balamurugan, M. Touma, T. Sakurai, and K. Inoue, "Effect of basic fibroblast growth factor on insulin secretion from microencapsulated pancreatic islets: an in vitro study.," *Cell transplantation*, vol. 10, no. 4–5, pp. 465–71, Jan. 2001.

[138] J.-H. Juang, B. R.-S. Hsu, and C.-H. Kuo, "Effects of insulin sensitizers on islet transplantation.," *Transplantation proceedings*, vol. 37, no. 8, pp. 3476–8, Oct. 2005.

[139] B. R.-S. Hsu, S.-H. Fu, K.-W. Ku, T.-Y. Yang, J.-H. Juang, and S.-T. Chen, "Enhancing islet engraftment with rosiglitazone.," *Transplantation proceedings*, vol. 37, no. 1, pp. 245–7.

[140] D. R. Laybutt, Y. C. Hawkins, J. Lock, J. Lebet, A. Sharma, S. Bonner-Weir, and G. C. Weir, "Influence of diabetes on the loss of beta cell differentiation after islet transplantation in rats.," *Diabetologia*, vol. 50, no. 10, pp. 2117–25, Oct. 2007.

[141] J. C. Ferrer-Garcia, J. F. Merino-Torres, G. Pérez Bermejo, C. Herrera-Vela, J. L. Ponce-Marco, and F. Piñon-Selles, "Insulin-induced normoglycemia reduces islet number needed to achieve normoglycemia after allogeneic islet transplantation in diabetic mice.," *Cell transplantation*, vol. 12, no. 8, pp. 849–57, Jan. 2003.

[142] M. Biarnés, M. Montolio, V. Nacher, M. Raurell, J. Soler, and E. Montanya, "Beta-cell death and mass in syngeneically transplanted islets exposed to short- and long-term hyperglycemia.," *Diabetes*, vol. 51, no. 1, pp. 66–72, Jan. 2002.

[143] J. H. Juang, S. Bonner-Weir, Y. J. Wu, and G. C. Weir, "Beneficial influence of glycemic control upon the growth and function of transplanted islets.," *Diabetes*, vol. 43, no. 11, pp. 1334–9, Nov. 1994.

[144] O. Korsgren, L. Jansson, S. Sandler, and A. Andersson, "Hyperglycemia-induced B cell toxicity. The fate of pancreatic islets transplanted into diabetic mice is dependent on their genetic background.," *The Journal of clinical investigation*, vol. 86, no. 6, pp. 2161–8, Dec. 1990.

[145] O. Korsgren, L. Jansson, and A. Andersson, "Effects of hyperglycemia on function of isolated mouse pancreatic islets transplanted under kidney capsule.," *Diabetes*, vol. 38, no. 4, pp. 510–5, Apr. 1989.

[146] M. Nakano, Y. Yasunami, T. Maki, S. Kodama, Y. Ikehara, T. Nakamura, M. Tanaka, and S. Ikeda, “Hepatocyte growth factor is essential for amelioration of hyperglycemia in streptozotocin-induced diabetic mice receiving a marginal mass of intrahepatic islet grafts.,” *Transplantation*, vol. 69, no. 2, pp. 214–21, Jan. 2000.

[147] E. S. Yolcu, H. Zhao, L. Bandura-Morgan, C. Lacelle, K. B. Woodward, N. Askenasy, and H. Shirwan, “Pancreatic islets engineered with SA-FasL protein establish robust localized tolerance by inducing regulatory T cells in mice.,” *Journal of immunology (Baltimore, Md.□: 1950)*, vol. 187, no. 11, pp. 5901–9, Dec. 2011.

[148] J. T. Wilson, C. A. Haller, Z. Qu, W. Cui, M. K. Urlam, and E. L. Chaikof, “Biomolecular surface engineering of pancreatic islets with thrombomodulin.,” *Acta biomaterialia*, vol. 6, no. 6, pp. 1895–903, Jun. 2010.

[149] W. Cui, J. T. Wilson, J. Wen, J. Angsana, Z. Qu, C. A. Haller, and E. L. Chaikof, “Thrombomodulin improves early outcomes after intraportal islet transplantation.,” *American journal of transplantation□: official journal of the American Society of Transplantation and the American Society of Transplant Surgeons*, vol. 9, no. 6, pp. 1308–16, Jun. 2009.

[150] S. Cabric, J. Sanchez, U. Johansson, R. Larsson, B. Nilsson, O. Korsgren, and P. U. Magnusson, “Anchoring of vascular endothelial growth factor to surface-immobilized heparin on pancreatic islets: implications for stimulating islet angiogenesis.,” *Tissue engineering. Part A*, vol. 16, no. 3, pp. 961–70, Mar. 2010.

[151] H. Chen, Y. Teramura, and H. Iwata, “Co-immobilization of urokinase and thrombomodulin on islet surfaces by poly(ethylene glycol)-conjugated phospholipid.,” *Journal of controlled release□: official journal of the Controlled Release Society*, vol. 150, no. 2, pp. 229–34, Mar. 2011.

[152] N. M. Luan, Y. Teramura, and H. Iwata, “Immobilization of soluble complement receptor 1 on islets.,” *Biomaterials*, vol. 32, no. 20, pp. 4539–45, Jul. 2011.

[153] N. M. Luan, Y. Teramura, and H. Iwata, “Layer-by-layer co-immobilization of soluble complement receptor 1 and heparin on islets.,” *Biomaterials*, vol. 32, no. 27, pp. 6487–92, Sep. 2011.

[154] C.-C. Lin and K. S. Anseth, “Glucagon-like peptide-1 functionalized PEG hydrogels promote survival and function of encapsulated pancreatic beta-cells.,” *Biomacromolecules*, vol. 10, no. 9, pp. 2460–7, Sep. 2009.

[155] N. M. Luan, Y. Teramura, and H. Iwata, “Immobilization of the soluble domain of human complement receptor 1 on agarose-encapsulated islets for the prevention of complement activation.,” *Biomaterials*, vol. 31, no. 34, pp. 8847–53, Dec. 2010.

[156] N. M. Luan and H. Iwata, “Inhibition of instant blood-mediated inflammatory responses by co-immobilization of sCR1 and heparin on islets.,” *Biomaterials*, vol. 34, no. 21, pp. 5019–24, Jul. 2013.

[157] J. I. Stagner, R. S. Seelan, and R. N. Parthasarathy, “Maintenance of aerobic metabolism increases immunoisolated islet survival.,” *Islets*, vol. 3, no. 3, pp. 89–92.

[158] Y. Sato, H. Endo, H. Okuyama, T. Takeda, H. Iwahashi, A. Imagawa, K. Yamagata, I. Shimomura, and M. Inoue, "Cellular hypoxia of pancreatic beta-cells due to high levels of oxygen consumption for insulin secretion in vitro.," *The Journal of biological chemistry*, vol. 286, no. 14, pp. 12524–32, Apr. 2011.

[159] J. Svensson, J. Lau, M. Sandberg, and P.-O. Carlsson, "High vascular density and oxygenation of pancreatic islets transplanted in clusters into striated muscle.," *Cell transplantation*, vol. 20, no. 5, pp. 783–8, Jan. 2011.

[160] J. Lau, J. Henriksnäs, J. Svensson, and P.-O. Carlsson, "Oxygenation of islets and its role in transplantation.," *Current opinion in organ transplantation*, vol. 14, no. 6, pp. 688–93, Dec. 2009.

[161] R. Olsson, A. Maxhuni, and P.-O. Carlsson, "Revascularization of transplanted pancreatic islets following culture with stimulators of angiogenesis.," *Transplantation*, vol. 82, no. 3, pp. 340–7, Aug. 2006.

[162] S. J. Hughes, S. E. Davies, S. H. Powis, and M. Press, "Hyperoxia improves the survival of intraportally transplanted syngeneic pancreatic islets.," *Transplantation*, vol. 75, no. 12, pp. 1954–9, Jun. 2003.

[163] J.-H. Juang, B. R.-S. Hsu, C.-H. Kuo, and S. W.-N. Uengt, "Beneficial effects of hyperbaric oxygen therapy on islet transplantation.," *Cell transplantation*, vol. 11, no. 2, pp. 95–101, Jan. 2002.

[164] F. Goh, R. Long, N. Simpson, and A. Sambanis, "Dual perfluorocarbon method to noninvasively monitor dissolved oxygen concentration in tissue engineered constructs in vitro and in vivo.," *Biotechnology progress*, vol. 27, no. 4, pp. 1115–25, Jul. 2011.

[165] F. Goh and A. Sambanis, "In vivo noninvasive monitoring of dissolved oxygen concentration within an implanted tissue-engineered pancreatic construct.," *Tissue engineering. Part C, Methods*, vol. 17, no. 9, pp. 887–94, Sep. 2011.

[166] K. K. Papas, R. C. Long, A. Sambanis, and I. Constantinidis, "Development of a bioartificial pancreas: II. Effects of oxygen on long-term entrapped betaTC3 cell cultures.," *Biotechnology and bioengineering*, vol. 66, no. 4, pp. 231–7, Jan. 1999.

[167] V. Nadithe and Y. H. Bae, "Hemoglobin conjugates with antioxidant enzymes (hemoglobin-superoxide dismutase-catalase) via poly(ethylene glycol) crosslinker for protection of pancreatic beta RINm5F cells in hypoxia.," *Tissue engineering. Part A*, vol. 17, no. 19–20, pp. 2453–62, Oct. 2011.

[168] V. Nadithe, D. Mishra, and Y. H. Bae, "Poly(ethylene glycol) cross-linked hemoglobin with antioxidant enzymes protects pancreatic islets from hypoxic and free radical stress and extends islet functionality.," *Biotechnology and bioengineering*, vol. 109, no. 9, pp. 2392–401, Sep. 2012.

[169] S. Y. Chae, Y. Y. Kim, S. W. Kim, and Y. H. Bae, "Prolonged glucose normalization of streptozotocin-induced diabetic mice by transplantation of rat islets coencapsulated with crosslinked hemoglobin.," *Transplantation*, vol. 78, no. 3, pp. 392–7, Aug. 2004.

[170] E. Pedraza, M. M. Coronel, C. A. Fraker, C. Ricordi, and C. L. Stabler, "Preventing hypoxia-induced cell death in beta cells and islets via hydrolytically activated, oxygen-generating biomaterials.," *Proceedings of the National Academy of Sciences of the United States of America*, vol. 109, no. 11, pp. 4245–50, Mar. 2012.

[171] S. H. Oh, C. L. Ward, A. Atala, J. J. Yoo, and B. S. Harrison, "Oxygen generating scaffolds for enhancing engineered tissue survival.," *Biomaterials*, vol. 30, no. 5, pp. 757–62, Feb. 2009.

[172] F. Goh, J. D. Gross, N. E. Simpson, and A. Sambanis, "Limited beneficial effects of perfluorocarbon emulsions on encapsulated cells in culture: experimental and modeling studies.," *Journal of biotechnology*, vol. 150, no. 2, pp. 232–9, Oct. 2010.

[173] B. Ludwig, B. Zimerman, A. Steffen, K. Yavriants, D. Azarov, A. Reichel, P. Vardi, T. German, N. Shabtay, A. Rotem, Y. Evron, T. Neufeld, S. Mimon, S. Ludwig, M. D. Brendel, S. R. Bornstein, and U. Barkai, "A novel device for islet transplantation providing immune protection and oxygen supply.," *Hormone and metabolic research = Hormon- und Stoffwechselforschung = Hormones et métabolisme*, vol. 42, no. 13, pp. 918–22, Dec. 2010.

[174] M. Padmasekar, N. Lingwal, B. Samikannu, C. Chen, H. Sauer, and T. Linn, "Exendin-4 protects hypoxic islets from oxidative stress and improves islet transplantation outcome.," *Endocrinology*, vol. 154, no. 4, pp. 1424–33, Apr. 2013.

[175] A. Nataraju, D. Saini, S. Ramachandran, N. Benshoff, W. Liu, W. Chapman, and T. Mohanakumar, "Oleanolic Acid, a plant triterpenoid, significantly improves survival and function of islet allograft.," *Transplantation*, vol. 88, no. 8, pp. 987–94, Oct. 2009.

[176] C. Moriscot, S. Candel, V. Sauret, J. Kerr-Conte, M. J. Richard, M. C. Favrot, and P. Y. Benhamou, "MnTMPyP, a metalloporphyrin-based superoxide dismutase/catalase mimetic, protects INS-1 cells and human pancreatic islets from an in vitro oxidative challenge.," *Diabetes & metabolism*, vol. 33, no. 1, pp. 44–53, Feb. 2007.

[177] L. Park, D. Min, H. Kim, J. Park, S. Choi, and Y. Park, "The combination of metallothionein and superoxide dismutase protects pancreatic β cells from oxidative damage.," *Diabetes/metabolism research and reviews*, vol. 27, no. 8, pp. 802–8, Nov. 2011.

[178] T. B. Mysore, T. A. Shinkel, J. Collins, E. J. Salvaris, N. Fisicaro, L. J. Murray-Segal, L. E. A. Johnson, D. A. Lepore, S. N. Walters, R. Stokes, A. P. Chandra, P. J. O'Connell, A. J. F. d'Apice, and P. J. Cowan, "Overexpression of glutathione peroxidase with two isoforms of superoxide dismutase protects mouse islets from oxidative injury and improves islet graft function.," *Diabetes*, vol. 54, no. 7, pp. 2109–16, Jul. 2005.

[179] X. Li, H. Chen, and P. N. Epstein, "Metallothionein protects islets from hypoxia and extends islet graft survival by scavenging most kinds of reactive oxygen species.," *The Journal of biological chemistry*, vol. 279, no. 1, pp. 765–71, Jan. 2004.

[180] S. Bertera, M. L. Crawford, A. M. Alexander, G. D. Papworth, S. C. Watkins, P. D. Robbins, and M. Trucco, "Gene transfer of manganese superoxide dismutase extends islet graft function in a mouse model of autoimmune diabetes.," *Diabetes*, vol. 52, no. 2, pp. 387–93, Feb. 2003.

[181] A. Jain, A. Jain, A. Gulbake, S. Shilpi, P. Hurkat, and S. K. Jain, "Peptide and protein delivery using new drug delivery systems.," *Critical reviews in therapeutic drug carrier systems*, vol. 30, no. 4, pp. 293–329, Jan. 2013.

[182] B. L. Montalvo-Ortiz, B. Sosa, and K. Griebenow, "Improved enzyme activity and stability in polymer microspheres by encapsulation of protein nanospheres.," *AAPS PharmSciTech*, vol. 13, no. 2, pp. 632–6, Jun. 2012.

[183] Y. Liu, H. Wang, K. Kamei, M. Yan, K.-J. Chen, Q. Yuan, L. Shi, Y. Lu, and H.-R. Tseng, "Delivery of intact transcription factor by using self-assembled supramolecular nanoparticles.," *Angewandte Chemie (International ed. in English)*, vol. 50, no. 13, pp. 3058–62, Mar. 2011.

[184] Z. S. Haidar, R. C. Hamdy, and M. Tabrizian, "Protein release kinetics for core-shell hybrid nanoparticles based on the layer-by-layer assembly of alginate and chitosan on liposomes.," *Biomaterials*, vol. 29, no. 9, pp. 1207–15, Mar. 2008.

[185] S. Benchabane, M. Subirade, and G. W. Vandenberg, "Production of BSA-loaded alginate microcapsules: influence of spray dryer parameters on the microcapsule characteristics and BSA release.," *Journal of microencapsulation*, vol. 24, no. 6, pp. 565–76, Sep. 2007.

[186] G. W. Vandenberg and J. De La Noüe, "Evaluation of protein release from chitosan-alginate microcapsules produced using external or internal gelation.," *Journal of microencapsulation*, vol. 18, no. 4, pp. 433–41.

[187] I. J. Castellanos, K. G. Carrasquillo, J. D. López, M. Alvarez, and K. Griebenow, "Encapsulation of bovine serum albumin in poly(lactide-co-glycolide) microspheres by the solid-in-oil-in-water technique.," *The Journal of pharmacy and pharmacology*, vol. 53, no. 2, pp. 167–78, Feb. 2001.

[188] P. F. Minimol, W. Paul, and C. P. Sharma, "PEGylated starch acetate nanoparticles and its potential use for oral insulin delivery.," *Carbohydrate polymers*, vol. 95, no. 1, pp. 1–8, Jun. 2013.

[189] M. Ganeshkumar, T. Ponrasu, M. Sathishkumar, and L. Suguna, "Preparation of amphiphilic hollow carbon nanosphere loaded insulin for oral delivery.," *Colloids and surfaces. B, Biointerfaces*, vol. 103, pp. 238–43, Mar. 2013.

[190] E. Déat-Lainé, V. Hoffart, G. Garrait, J.-F. Jarrige, J.-M. Cardot, M. Subirade, and E. Beyssac, "Efficacy of mucoadhesive hydrogel microparticles of whey protein and alginate for oral insulin delivery.," *Pharmaceutical research*, vol. 30, no. 3, pp. 721–34, Mar. 2013.

[191] C. Manoharan and J. Singh, "Evaluation of poly (1, 6-bis-(p-carboxyphenoxy) hexane-co-sebacic acid microspheres for controlled basal insulin delivery.," *Pharmaceutical research*, vol. 30, no. 3, pp. 627–40, Mar. 2013.

[192] D. M. Lavin, L. Zhang, S. Furtado, R. A. Hopkins, and E. Mathiowitz, "Effects of protein molecular weight on the intrinsic material properties and release kinetics of wet spun polymeric microfiber delivery systems.," *Acta biomaterialia*, vol. 9, no. 1, pp. 4569–78, Jan. 2013.

[193] P. Fonte, F. Andrade, F. Araújo, C. Andrade, J. das Neves, and B. Sarmento, "Chitosan-coated solid lipid nanoparticles for insulin delivery.," *Methods in enzymology*, vol. 508, pp. 295–314, Jan. 2012.

[194] K. Bowey, B. E. Swift, L. E. Flynn, and R. J. Neufeld, "Characterization of biologically active insulin-loaded alginate microparticles prepared by spray drying.," *Drug development and industrial pharmacy*, vol. 39, no. 3, pp. 457–65, Mar. 2013.

[195] A. M. Davalli, Y. Ogawa, L. Scaglia, Y. J. Wu, J. Hollister, S. Bonner-Weir, and G. C. Weir, "Function, mass, and replication of porcine and rat islets transplanted into diabetic nude mice.," *Diabetes*, vol. 44, no. 1, pp. 104–11, Jan. 1995.

[196] A. M. Davalli, L. Scaglia, D. H. Zangen, J. Hollister, S. Bonner-Weir, and G. C. Weir, "Vulnerability of islets in the immediate posttransplantation period. Dynamic changes in structure and function.," *Diabetes*, vol. 45, no. 9, pp. 1161–7, Sep. 1996.

[197] G. Miao, R. P. Ostrowski, J. Mace, J. Hough, A. Hopper, R. Peverini, R. Chinnock, J. Zhang, and E. Hathout, "Dynamic production of hypoxia-inducible factor-1alpha in early transplanted islets.," *American journal of transplantation : official journal of the American Society of Transplantation and the American Society of Transplant Surgeons*, vol. 6, no. 11, pp. 2636–43, Nov. 2006.

[198] C. Toso, V. Serre-Beinier, J. Emamaullee, S. Merani, M. Armanet, A. Wojtusciszyn, D. Bosco, T. Calandra, T. Roger, P. Morel, A. M. J. Shapiro, and T. Berney, "The role of macrophage migration inhibitory factor in mouse islet transplantation.," *Transplantation*, vol. 86, no. 10, pp. 1361–9, Nov. 2008.

[199] M. F. Crutchlow, M. Yu, Y.-S. Bae, S. Deng, and D. A. Stoffers, "Exendin-4 does not promote Beta-cell proliferation or survival during the early post-islet transplant period in mice.," *Transplantation proceedings*, vol. 40, no. 5, pp. 1650–7, Jun. 2008.

[200] N. H. Davies, C. Schmidt, D. Bezuidenhout, and P. Zilla, "Sustaining neovascularization of a scaffold through staged release of vascular endothelial growth factor-A and platelet-derived growth factor-BB.," *Tissue engineering. Part A*, vol. 18, no. 1–2, pp. 26–34, Jan. 2012.

[201] I. Freeman and S. Cohen, "The influence of the sequential delivery of angiogenic factors from affinity-binding alginate scaffolds on vascularization.," *Biomaterials*, vol. 30, no. 11, pp. 2122–31, Apr. 2009.

[202] H. Yang, H. Iwata, H. Shimizu, T. Takagi, T. Tsuji, and F. Ito, "Comparative studies of in vitro and in vivo function of three different shaped bioartificial pancreases made of agarose hydrogel.," *Biomaterials*, vol. 15, no. 2, pp. 113–20, Jan. 1994.

[203] B. Kulseng, G. Skjåk-Braek, L. Ryan, A. Andersson, A. King, A. Faxvaag, and T. Espevik, "Transplantation of alginate microcapsules: generation of antibodies against alginates and encapsulated porcine islet-like cell clusters.," *Transplantation*, vol. 67, no. 7, pp. 978–84, Apr. 1999.

[204] A. King, J. Lau, A. Nordin, S. Sandler, and A. Andersson, "The effect of capsule composition in the reversal of hyperglycemia in diabetic mice transplanted with microencapsulated allogeneic islets.," *Diabetes technology & therapeutics*, vol. 5, no. 4, pp. 653–63, Jan. 2003.

[205] M. Manish, A. Rahi, M. Kaur, R. Bhatnagar, and S. Singh, “A Single-Dose PLGA Encapsulated Protective Antigen Domain 4 Nanoformulation Protects Mice against Bacillus anthracis Spore Challenge.,” *PloS one*, vol. 8, no. 4, p. e61885, Jan. 2013.

[206] J. Park and J. E. Babensee, “Differential functional effects of biomaterials on dendritic cell maturation.,” *Acta biomaterialia*, vol. 8, no. 10, pp. 3606–17, Oct. 2012.

[207] T. T. Dang, A. V Thai, J. Cohen, J. E. Slosberg, K. Siniakowicz, J. C. Doloff, M. Ma, J. Hollister-Lock, K. M. Tang, Z. Gu, H. Cheng, G. C. Weir, R. Langer, and D. G. Anderson, “Enhanced function of immuno-isolated islets in diabetes therapy by co-encapsulation with an anti-inflammatory drug.,” *Biomaterials*, vol. 34, no. 23, pp. 5792–801, Jul. 2013.

[208] J. W. Lee, Y. J. Park, S. J. Lee, S. K. Lee, and K. Y. Lee, “The effect of spacer arm length of an adhesion ligand coupled to an alginate gel on the control of fibroblast phenotype.,” *Biomaterials*, vol. 31, no. 21, pp. 5545–51, Jul. 2010.

[209] T. W. Link, D. R. Arifin, C. M. Long, P. Walczak, N. Muja, A. Arepally, and J. W. M. Bulte, “Use of Magnetocapsules for In Vivo Visualization and Enhanced Survival of Xenogeneic HepG2 Cell Transplants.,” *Cell medicine*, vol. 4, no. 2, pp. 77–84, Feb. 2012.

[210] P. Wang and A. Moore, “Theranostic magnetic resonance imaging of type 1 diabetes and pancreatic islet transplantation.,” *Quantitative imaging in medicine and surgery*, vol. 2, no. 3, pp. 151–62, Sep. 2012.

[211] N. Sakata, M. Goto, Y. Gumpei, M. Mizuma, F. Motoi, S. Satomi, and M. Unno, “Intraoperative ultrasound examination is useful for monitoring transplanted islets: a case report.,” *Islets*, vol. 4, no. 5, pp. 339–42.

[212] P. Wang, Z. Medarova, and A. Moore, “Molecular imaging: a promising tool to monitor islet transplantation.,” *Journal of transplantation*, vol. 2011, p. 202915, Jan. 2011.

[213] B. P. Barnett, J. Ruiz-Cabello, P. Hota, R. Ouwerkerk, M. J. Shamblott, C. Lauzon, P. Walczak, W. D. Gilson, V. P. Chacko, D. L. Kraitchman, A. Arepally, and J. W. M. Bulte, “Use of perfluorocarbon nanoparticles for non-invasive multimodal cell tracking of human pancreatic islets.,” *Contrast media & molecular imaging*, vol. 6, no. 4, pp. 251–9.

[214] D. R. Arifin, C. M. Long, A. A. Gilad, C. Alric, S. Roux, O. Tillement, T. W. Link, A. Arepally, and J. W. M. Bulte, “Trimodal gadolinium-gold microcapsules containing pancreatic islet cells restore normoglycemia in diabetic mice and can be tracked by using US, CT, and positive-contrast MR imaging.,” *Radiology*, vol. 260, no. 3, pp. 790–8, Sep. 2011.

[215] L. A. Crowe, F. Ris, S. Nielles-Vallespin, P. Speier, S. Masson, M. Armanet, P. Morel, C. Toso, D. Bosco, T. Berney, and J.-P. Vallee, “A novel method for quantitative monitoring of transplanted islets of langerhans by positive contrast magnetic resonance imaging.,” *American journal of transplantation : official journal of the American Society of Transplantation and the American Society of Transplant Surgeons*, vol. 11, no. 6, pp. 1158–68, Jun. 2011.

[216] N. Lee, H. Kim, S. H. Choi, M. Park, D. Kim, H.-C. Kim, Y. Choi, S. Lin, B. H. Kim, H. S. Jung, H. Kim, K. S. Park, W. K. Moon, and T. Hyeon, “Magnetosome-like ferrimagnetic iron oxide nanocubes for highly sensitive MRI of single cells and transplanted pancreatic islets.,”

Proceedings of the National Academy of Sciences of the United States of America, vol. 108, no. 7, pp. 2662–7, Feb. 2011.

[217] Z. Medarova and A. Moore, "MRI as a tool to monitor islet transplantation.," *Nature reviews. Endocrinology*, vol. 5, no. 8, pp. 444–52, Aug. 2009.

[218] Z. Medarova, P. Vallabhajosyula, A. Tena, N. Evgenov, P. Pantazopoulos, V. Tchipashvili, G. Weir, D. Sachs, and A. Moore, "In vivo imaging of autologous islet grafts in the liver and under the kidney capsule in non-human primates.," *Transplantation*, vol. 87, no. 11, pp. 1659–66, Jun. 2009.

[219] B. P. Barnett, A. Arepally, P. V Karmarkar, D. Qian, W. D. Gilson, P. Walczak, V. Howland, L. Lawler, C. Lauzon, M. Stuber, D. L. Kraitchman, and J. W. M. Bulte, "Magnetic resonance-guided, real-time targeted delivery and imaging of magnetocapsules immunoprotecting pancreatic islet cells.," *Nature medicine*, vol. 13, no. 8, pp. 986–91, Aug. 2007.

[220] N. V Evgenov, Z. Medarova, G. Dai, S. Bonner-Weir, and A. Moore, "In vivo imaging of islet transplantation.," *Nature medicine*, vol. 12, no. 1, pp. 144–8, Jan. 2006.

[221] G. Miao, J. Mace, M. Kirby, A. Hopper, R. Peverini, R. Chinnock, J. Shapiro, and E. Hathout, "In vitro and in vivo improvement of islet survival following treatment with nerve growth factor.," *Transplantation*, vol. 81, no. 4, pp. 519–24, Feb. 2006.

[222] J. G. Graham, X. Zhang, A. Goodman, K. Pothoven, J. Houlihan, S. Wang, R. M. Gower, X. Luo, and L. D. Shea, "PLG Scaffold Delivered Antigen-Specific Regulatory T Cells Induce Systemic Tolerance in Autoimmune Diabetes.," *Tissue engineering. Part A*, vol. 19, no. 11–12, pp. 1465–75, Jun. 2013.

[223] G. Schmid, M. Guba, I. Ischenko, A. Papyan, M. Joka, S. Schrepfer, C. J. Bruns, K.-W. Jauch, C. Heeschen, and C. Graeb, "The immunosuppressant FTY720 inhibits tumor angiogenesis via the sphingosine 1-phosphate receptor 1.," *Journal of cellular biochemistry*, vol. 101, no. 1, pp. 259–70, May 2007.

[224] N. Yan, X. Zhang, Q. Cai, X. Yang, X. Zhou, B. Wang, and X. Deng, "The Effects of Lactidyl/Glycolidyl Ratio and Molecular Weight of Poly(d,l-Lactide-co-Glycolide) on the Tetracycline Entrapment and Release Kinetics of Drug-Loaded Nanofibers.," *Journal of biomaterials science. Polymer edition*, May 2011.

[225] V. Holan, M. Chudickova, P. Trosan, E. Svobodova, M. Krulova, S. Kubinova, E. Sykova, J. Sirc, J. Michalek, M. Juklickova, M. Munzarova, and A. Zajicova, "Cyclosporine A-loaded and stem cell-seeded electrospun nanofibers for cell-based therapy and local immunosuppression.," *Journal of controlled release□: official journal of the Controlled Release Society*, vol. 156, no. 3, pp. 406–12, Dec. 2011.

[226] M. E. Padin-Iruegas, Y. Misao, M. E. Davis, V. F. M. Segers, G. Esposito, T. Tokunou, K. Urbanek, T. Hosoda, M. Rota, P. Anversa, A. Leri, R. T. Lee, and J. Kajstura, "Cardiac progenitor cells and biotinylated insulin-like growth factor-1 nanofibers improve endogenous and exogenous myocardial regeneration after infarction.," *Circulation*, vol. 120, no. 10, pp. 876–87, Sep. 2009.

[227] S. G. Kumbar, L. S. Nair, S. Bhattacharyya, and C. T. Laurencin, "Polymeric nanofibers as novel carriers for the delivery of therapeutic molecules.," *Journal of nanoscience and nanotechnology*, vol. 6, no. 9–10, pp. 2591–607.

[228] F. Du, H. Wang, W. Zhao, D. Li, D. Kong, J. Yang, and Y. Zhang, "Gradient nanofibrous chitosan/poly ε -caprolactone scaffolds as extracellular microenvironments for vascular tissue engineering.," *Biomaterials*, vol. 33, no. 3, pp. 762–70, Jan. 2012.

[229] J. Venugopal and S. Ramakrishna, "Biocompatible nanofiber matrices for the engineering of a dermal substitute for skin regeneration.," *Tissue engineering*, vol. 11, no. 5–6, pp. 847–54.

[230] I. Shabani, V. Haddadi-Asl, M. Soleimani, E. Seyedjafari, F. Babaeijandaghi, and N. Ahmadbeigi, "Enhanced infiltration and biomineralization of stem cells on collagen-grafted three-dimensional nanofibers.," *Tissue engineering. Part A*, vol. 17, no. 9–10, pp. 1209–18, May 2011.

[231] S. I. Jeong, A.-Y. Lee, Y. M. Lee, and H. Shin, "Electrospun gelatin/poly(L-lactide-co-epsilon-caprolactone) nanofibers for mechanically functional tissue-engineering scaffolds.," *Journal of biomaterials science. Polymer edition*, vol. 19, no. 3, pp. 339–57, Jan. 2008.

[232] R. A. Neal, S. S. Tholpady, P. L. Foley, N. Swami, R. C. Ogle, and E. A. Botchwey, "Alignment and composition of laminin-polycaprolactone nanofiber blends enhance peripheral nerve regeneration.," *Journal of biomedical materials research. Part A*, Nov. 2011.

[233] Z. Huang, R. H. Daniels, R.-J. Enzerink, V. Hardev, V. Sahi, and S. B. Goodman, "Effect of nanofiber-coated surfaces on the proliferation and differentiation of osteoprogenitors in vitro.," *Tissue engineering. Part A*, vol. 14, no. 11, pp. 1853–9, Dec. 2008.

[234] J. Shen, X. Fu, L. Ou, M. Zhang, Y. Guan, K. Wang, Y. Che, D. Kong, G. Steinhof, W. Li, Y. Yu, and N. Ma, "Construction of ureteral grafts by seeding urothelial cells and bone marrow mesenchymal stem cells into polycaprolactone-lecithin electrospun fibers.," *The International journal of artificial organs*, vol. 33, no. 3, pp. 161–70, Mar. 2010.

[235] J. Jia, Y.-Y. Duan, J. Yu, and J.-W. Lu, "Preparation and immobilization of soluble eggshell membrane protein on the electrospun nanofibers to enhance cell adhesion and growth.," *Journal of biomedical materials research. Part A*, vol. 86, no. 2, pp. 364–73, Aug. 2008.

[236] J. R. Venugopal, Y. Zhang, and S. Ramakrishna, "In vitro culture of human dermal fibroblasts on electrospun polycaprolactone collagen nanofibrous membrane.," *Artificial organs*, vol. 30, no. 6, pp. 440–6, Jun. 2006.

[237] J. T. Seil and T. J. Webster, "Spray deposition of live cells throughout the electrospinning process produces nanofibrous three-dimensional tissue scaffolds.," *International journal of nanomedicine*, vol. 6, pp. 1095–9, Jan. 2011.

[238] Z. C. C. Chen, A. K. Ekaputra, K. Gauthaman, P. G. Adaikan, H. Yu, and D. W. Hutmacher, "In vitro and in vivo analysis of co-electrospun scaffolds made of medical grade poly(epsilon-caprolactone) and porcine collagen.," *Journal of biomaterials science. Polymer edition*, vol. 19, no. 5, pp. 693–707, Jan. 2008.

[239] S. Ghanaati, R. E. Unger, M. J. Webber, M. Barbeck, C. Orth, J. A. Kirkpatrick, P. Booms, A. Motta, C. Migliaresi, R. A. Sader, and C. J. Kirkpatrick, "Scaffold vascularization in vivo driven by primary human osteoblasts in concert with host inflammatory cells.," *Biomaterials*, vol. 32, no. 32, pp. 8150–60, Nov. 2011.

[240] M. Skotak, J. Ragusa, D. Gonzalez, and A. Subramanian, "Improved cellular infiltration into nanofibrous electrospun cross-linked gelatin scaffolds templated with micrometer-sized polyethylene glycol fibers.," *Biomedical materials (Bristol, England)*, vol. 6, no. 5, p. 055012, Oct. 2011.

[241] A. O. Gee, B. M. Baker, A. M. Silverstein, G. Montero, J. L. Esterhai, and R. L. Mauck, "Fabrication and evaluation of biomimetic-synthetic nanofibrous composites for soft tissue regeneration.," *Cell and tissue research*, vol. 347, no. 3, pp. 803–13, Mar. 2012.

[242] S. A. Maher, R. L. Mauck, L. Rackwitz, and R. S. Tuan, "A nanofibrous cell-seeded hydrogel promotes integration in a cartilage gap model.," *Journal of tissue engineering and regenerative medicine*, vol. 4, no. 1, pp. 25–9, Jan. 2010.

[243] X. Xin, M. Hussain, and J. J. Mao, "Continuing differentiation of human mesenchymal stem cells and induced chondrogenic and osteogenic lineages in electrospun PLGA nanofiber scaffold.," *Biomaterials*, vol. 28, no. 2, pp. 316–25, Jan. 2007.

[244] X. M. Mo, C. Y. Xu, M. Kotaki, and S. Ramakrishna, "Electrospun P(LLA-CL) nanofiber: a biomimetic extracellular matrix for smooth muscle cell and endothelial cell proliferation.," *Biomaterials*, vol. 25, no. 10, pp. 1883–90, May 2004.

[245] H. Yoshimoto, Y. M. Shin, H. Terai, and J. P. Vacanti, "A biodegradable nanofiber scaffold by electrospinning and its potential for bone tissue engineering.," *Biomaterials*, vol. 24, no. 12, pp. 2077–82, May 2003.

[246] M. Dvir-Ginzberg, I. Gamlieli-Bonshtein, R. Agbaria, and S. Cohen, "Liver tissue engineering within alginate scaffolds: effects of cell-seeding density on hepatocyte viability, morphology, and function.," *Tissue engineering*, vol. 9, no. 4, pp. 757–66, Aug. 2003.

[247] J. Kisiday, M. Jin, B. Kurz, H. Hung, C. Semino, S. Zhang, and A. J. Grodzinsky, "Self-assembling peptide hydrogel fosters chondrocyte extracellular matrix production and cell division: implications for cartilage tissue repair.," *Proceedings of the National Academy of Sciences of the United States of America*, vol. 99, no. 15, pp. 9996–10001, Jul. 2002.

[248] W. Rumsey, J. Vanderkooi, and D. Wilson, "Imaging of phosphorescence: a novel method for measuring oxygen distribution in perfused tissue," *Science*, vol. 241, no. 4873, pp. 1649–1651, Sep. 1988.

[249] Y.-J. Ren, S. Zhang, R. Mi, Q. Liu, X. Zeng, M. Rao, A. Hoke, and H.-Q. Mao, "Enhanced differentiation of human neural crest stem cells towards the Schwann cell lineage by aligned electrospun fiber matrix.," *Acta biomaterialia*, vol. 9, no. 8, pp. 7727–36, Apr. 2013.

[250] S. Lee, M. K. Leach, S. A. Redmond, S. Y. C. Chong, S. H. Mellon, S. J. Tuck, Z.-Q. Feng, J. M. Corey, and J. R. Chan, "A culture system to study oligodendrocyte myelination processes using engineered nanofibers.," *Nature methods*, vol. 9, no. 9, pp. 917–22, Sep. 2012.

[251] C.-W. Hsiao, M.-Y. Bai, Y. Chang, M.-F. Chung, T.-Y. Lee, C.-T. Wu, B. Maiti, Z.-X. Liao, R.-K. Li, and H.-W. Sung, "Electrical coupling of isolated cardiomyocyte clusters grown on aligned conductive nanofibrous meshes for their synchronized beating.," *Biomaterials*, vol. 34, no. 4, pp. 1063–72, Jan. 2013.

[252] M. Yeo, H. Lee, and G. Kim, "Three-dimensional hierarchical composite scaffolds consisting of polycaprolactone, β-tricalcium phosphate, and collagen nanofibers: fabrication, physical properties, and in vitro cell activity for bone tissue regeneration.," *Biomacromolecules*, vol. 12, no. 2, pp. 502–10, Feb. 2011.

[253] M. T. McClendon and S. I. Stupp, "Tubular hydrogels of circumferentially aligned nanofibers to encapsulate and orient vascular cells.," *Biomaterials*, vol. 33, no. 23, pp. 5713–22, Aug. 2012.

[254] J. Mosinger, K. Lang, L. Plístil, S. Jesenská, J. Hostomský, Z. Zelinger, and P. Kubát, "Fluorescent polyurethane nanofabrics: a source of singlet oxygen and oxygen sensing.," *Langmuir□: the ACS journal of surfaces and colloids*, vol. 26, no. 12, pp. 10050–6, Jun. 2010.

[255] L. Songzhu, D. Xiangting, W. Jinxian, L. Guixia, Y. Wenshen, and J. Ruokun, "Fabrication of Eu(III) complex doped nanofibrous membranes and their oxygen-sensing properties.," *Spectrochimica acta. Part A, Molecular and biomolecular spectroscopy*, vol. 77, no. 4, pp. 885–9, Nov. 2010.

[256] C. Wen, G. Tao, X. Xu, X. Feng, and R. Luo, "A phosphorescent copper(I) complex: synthesis, characterization, photophysical property, and oxygen-sensing behavior.," *Spectrochimica acta. Part A, Molecular and biomolecular spectroscopy*, vol. 79, no. 5, pp. 1345–51, Sep. 2011.

[257] H. Zhang, B. Lei, H. Dong, and Y. Liu, "Oxygen sensing properties of Cu(I) complex/polystyrene composite nanofibers prepared by electrospinning.," *Journal of nanoscience and nanotechnology*, vol. 11, no. 11, pp. 9840–5, Nov. 2011.

[258] H. Hong, L. Zhu, A. Wang, and H. Lu, "Re(I) complex doped nanofibers for oxygen optical sensing.," *Spectrochimica acta. Part A, Molecular and biomolecular spectroscopy*, vol. 98, pp. 466–73, Dec. 2012.

[259] R. Xue, P. Behera, M. S. Viapiano, and J. J. Lannutti, "Rapid response oxygen-sensing nanofibers.," *Materials science & engineering. C, Materials for biological applications*, vol. 33, no. 6, pp. 3450–7, Aug. 2013.

[260] R. A. Murray, G. Zhang, D. Harmata, R. A. Neal, E. A. Botchwey, and C. L. Fraser, "Fabrication and Degradation of Nanofibers Based on Luminescent Boron Dye-PLGA Blends," in *Biomaterials*, vol. 1054, American Chemical Society, 2010, pp. 2–33.

[261] G. Zhang, G. M. Palmer, M. W. Dewhirst, and C. L. Fraser, "A dual-emissive-materials design concept enables tumour hypoxia imaging.," *Nature materials*, vol. 8, no. 9, pp. 747–51, Sep. 2009.

[262] C. E. Forristal, D. R. Christensen, F. E. Chinnery, R. Petruzzelli, K. L. Parry, T. Sanchez-Elsner, and F. D. Houghton, "Environmental oxygen tension regulates the energy metabolism and self-renewal of human embryonic stem cells.," *PloS one*, vol. 8, no. 5, p. e62507, Jan. 2013.

[263] W. L. Grayson, F. Zhao, R. Izadpanah, B. Bunnell, and T. Ma, “Effects of hypoxia on human mesenchymal stem cell expansion and plasticity in 3D constructs.,” *Journal of cellular physiology*, vol. 207, no. 2, pp. 331–9, May 2006.

[264] C. Bath, S. Yang, D. Muttuvelu, T. Fink, J. Emmersen, H. Vorum, J. Hjortdal, and V. Zachar, “Hypoxia is a key regulator of limbal epithelial stem cell growth and differentiation.,” *Stem cell research*, vol. 10, no. 3, pp. 349–60, May 2013.

[265] S. R. L. Stacpoole, D. J. Webber, B. Bilican, A. Compston, S. Chandran, and R. J. M. Franklin, “Neural precursor cells cultured at physiologically relevant oxygen tensions have a survival advantage following transplantation.,” *Stem cells translational medicine*, vol. 2, no. 6, pp. 464–72, Jun. 2013.

[266] A. C. Kendall, J. L. Whatmore, L. W. Harries, P. G. Winyard, G. R. Smerdon, and P. Eggleton, “Changes in inflammatory gene expression induced by hyperbaric oxygen treatment in human endothelial cells under chronic wound conditions.,” *Experimental cell research*, vol. 318, no. 3, pp. 207–16, Feb. 2012.

[267] O. Cuvillier, I. Ader, P. Bouquerel, L. Brizuela, C. Gstalder, and B. Malavaud, “Hypoxia, therapeutic resistance, and sphingosine 1-phosphate.,” *Advances in cancer research*, vol. 117, pp. 117–41, Jan. 2013.

[268] M. Gonsalves, A. L. Barker, J. V Macpherson, P. R. Unwin, D. O’Hare, and C. P. Winlove, “Scanning electrochemical microscopy as a local probe of oxygen permeability in cartilage.,” *Biophysical journal*, vol. 78, no. 3, pp. 1578–88, Mar. 2000.

[269] C. Androjna, J. E. Gatica, J. M. Belovich, and K. A. Derwin, “Oxygen diffusion through natural extracellular matrices: implications for estimating ‘critical thickness’ values in tendon tissue engineering.,” *Tissue engineering. Part A*, vol. 14, no. 4, pp. 559–69, Apr. 2008.

[270] J. E. Valentin, D. O. Freytes, J. M. Grasman, C. Pesyna, J. Freund, T. W. Gilbert, and S. F. Badylak, “Oxygen diffusivity of biologic and synthetic scaffold materials for tissue engineering.,” *Journal of biomedical materials research. Part A*, vol. 91, no. 4, pp. 1010–7, Dec. 2009.

[271] B. R. Duling and R. M. Berne, “Longitudinal gradients in periarteriolar oxygen tension. A possible mechanism for the participation of oxygen in local regulation of blood flow.,” *Circulation research*, vol. 27, no. 5, pp. 669–78, Nov. 1970.

[272] M. Moore, R. Moore, and P. S. McFetridge, “Directed Oxygen Gradients Initiate a Robust Early Remodeling Response in Engineered Vascular Grafts.,” *Tissue engineering. Part A*, May 2013.

[273] Y. Liu and S. Wang, “3D inverted opal hydrogel scaffolds with oxygen sensing capability.,” *Colloids and surfaces. B, Biointerfaces*, vol. 58, no. 1, pp. 8–13, Jul. 2007.

[274] J. Liu, J. Hilderink, T. A. M. Groothuis, C. Otto, C. A. van Blitterswijk, and J. de Boer, “Monitoring nutrient transport in tissue-engineered grafts.,” *Journal of tissue engineering and regenerative medicine*, Jan. 2013.

[275] M. J. Kluk and T. Hla, “Role of the sphingosine 1-phosphate receptor EDG-1 in vascular smooth muscle cell proliferation and migration ,” *Circulation research*, vol. 89, no. 6, pp. 496–502, Sep. 2001.

[276] K. Lockman, J. S. Hinson, M. D. Medlin, D. Morris, J. M. Taylor, and C. P. Mack, “Sphingosine 1-phosphate stimulates smooth muscle cell differentiation and proliferation by activating separate serum response factor co-factors ,” *The Journal of biological chemistry*, vol. 279, no. 41, pp. 42422–42430, Oct. 2004.

[277] X. Peng, P. M. Hassoun, S. Sammani, B. J. McVerry, M. J. Burne, H. Rabb, D. Pearse, R. M. Tuder, and J. G. Garcia, “Protective effects of sphingosine 1-phosphate in murine endotoxin-induced inflammatory lung injury ,” *American journal of respiratory and critical care medicine*, vol. 169, no. 11, pp. 1245–1251, Jun. 2004.

[278] A. H. Zisch, M. P. Lutolf, M. Ehrbar, G. P. Raeber, S. C. Rizzi, N. Davies, H. Schmokel, D. Bezuidenhout, V. Djonov, P. Zilla, and J. A. Hubbell, “Cell-demanded release of VEGF from synthetic, biointeractive cell ingrowth matrices for vascularized tissue growth ,” *The FASEB journal□: official publication of the Federation of American Societies for Experimental Biology*, vol. 17, no. 15, pp. 2260–2262, Dec. 2003.

[279] L. S. Sefcik, C. E. Aronin, A. O. Awojoodu, S. J. Shin, F. Mac Gabhann, T. L. MacDonald, B. R. Wamhoff, K. R. Lynch, S. M. Peirce, and E. A. Botchwey, “Selective activation of sphingosine 1-phosphate receptors 1 and 3 promotes local microvascular network growth ,” *Tissue engineering.Part A*, vol. 17, no. 5–6, pp. 617–629, Mar. 2011.

[280] K. LaMontagne, A. Littlewood-Evans, C. Schnell, T. O’Reilly, L. Wyder, T. Sanchez, B. Probst, J. Butler, A. Wood, G. Liau, E. Billy, A. Theuer, T. Hla, and J. Wood, “Antagonism of sphingosine-1-phosphate receptors by FTY720 inhibits angiogenesis and tumor vascularization ,” *Cancer research*, vol. 66, no. 1, pp. 221–231, Jan. 2006.

[281] G. Schmid, M. Guba, A. Papyan, I. Ischenko, M. Bruckel, C. J. Bruns, K. W. Jauch, and C. Graeb, “FTY720 inhibits tumor growth and angiogenesis ,” *Transplantation proceedings*, vol. 37, no. 1, pp. 110–111, 2005.

[282] W. Truong, J. A. Emamaullee, S. Merani, C. C. Anderson, and A. M. James Shapiro, “Human islet function is not impaired by the sphingosine-1-phosphate receptor modulator FTY720 ,” *American journal of transplantation□: official journal of the American Society of Transplantation and the American Society of Transplant Surgeons*, vol. 7, no. 8, pp. 2031–2038, Aug. 2007.

[283] C. Gysemans, H. Callewaert, L. Overbergh, and C. Mathieu, “Cytokine signalling in the beta-cell: a dual role for IFNgamma ,” *Biochemical Society transactions*, vol. 36, no. Pt 3, pp. 328–333, Jun. 2008.

[284] S. Kodama, K. Kojima, S. Furuta, M. Chambers, A. C. Paz, and C. A. Vacanti, “Engineering functional islets from cultured cells ,” *Tissue engineering.Part A*, vol. 15, no. 11, pp. 3321–3329, Nov. 2009.

[285] C. Song, Y. D. Huang, Z. Wei, Y. Hou, W. J. Xie, R. P. Huang, Y. M. Song, H. G. Lv, and C. F. Song, “Polyglycolic Acid-islet grafts improve blood glucose and insulin concentrations in rats with induced diabetes.,” *Transplantation proceedings*, vol. 41, no. 5, pp. 1789–93, Jun. 2009.

[286] W. Bakker, E. C. Eringa, P. Sipkema, and V. W. van Hinsbergh, “Endothelial dysfunction and diabetes: roles of hyperglycemia, impaired insulin signaling and obesity ,” *Cell and tissue research*, vol. 335, no. 1, pp. 165–189, Jan. 2009.

[287] N. J. Leeper and J. P. Cooke, “MicroRNA and mechanisms of impaired angiogenesis in diabetes mellitus ,” *Circulation*, vol. 123, no. 3, pp. 236–238, Jan. 2011.

[288] A. Sharma, A. K. Singh, J. Warren, R. L. Thangapazham, and R. K. Maheshwari, “Differential regulation of angiogenic genes in diabetic wound healing ,” *The Journal of investigative dermatology*, vol. 126, no. 10, pp. 2323–2331, Oct. 2006.

[289] Z. J. Liu and O. C. Velazquez, “Hyperoxia, endothelial progenitor cell mobilization, and diabetic wound healing ,” *Antioxidants & redox signaling*, vol. 10, no. 11, pp. 1869–1882, Nov. 2008.

[290] E. R. Mohler 3rd, Y. Shi, J. Moore, A. Bantly, D. Hamamdzic, M. Yoder, D. J. Rader, M. Putt, L. Zhang, M. Parmacek, and R. L. Wilensky, “Diabetes reduces bone marrow and circulating porcine endothelial progenitor cells, an effect ameliorated by atorvastatin and independent of cholesterol ,” *Cytometry.Part A□: the journal of the International Society for Analytical Cytology*, vol. 75, no. 1, pp. 75–82, Jan. 2009.

[291] T. Kusuyama, T. Omura, D. Nishiya, S. Enomoto, R. Matsumoto, K. Takeuchi, J. Yoshikawa, and M. Yoshiyama, “Effects of treatment for diabetes mellitus on circulating vascular progenitor cells ,” *Journal of pharmacological sciences*, vol. 102, no. 1, pp. 96–102, Sep. 2006.

[292] B. F., P. D., S. G., Z. F., D. C. R., R. P., L. S., A. V., S. E., M. T., G. G., and F. A., “Glycemic Variability Affects Ischemia-Induced Angiogenesis In Diabetic Mice,” *Clin Sci (Lond).*, 2011. .

[293] M. E. Seaman, S. M. Peirce, and K. Kelly, “Rapid Analysis of Vessel Elements (RAVE): A Tool for Studying Physiologic, Pathologic and Tumor Angiogenesis ,” *PloS one*, vol. 6, no. 6, p. e20807, 2011.

APPENDIX

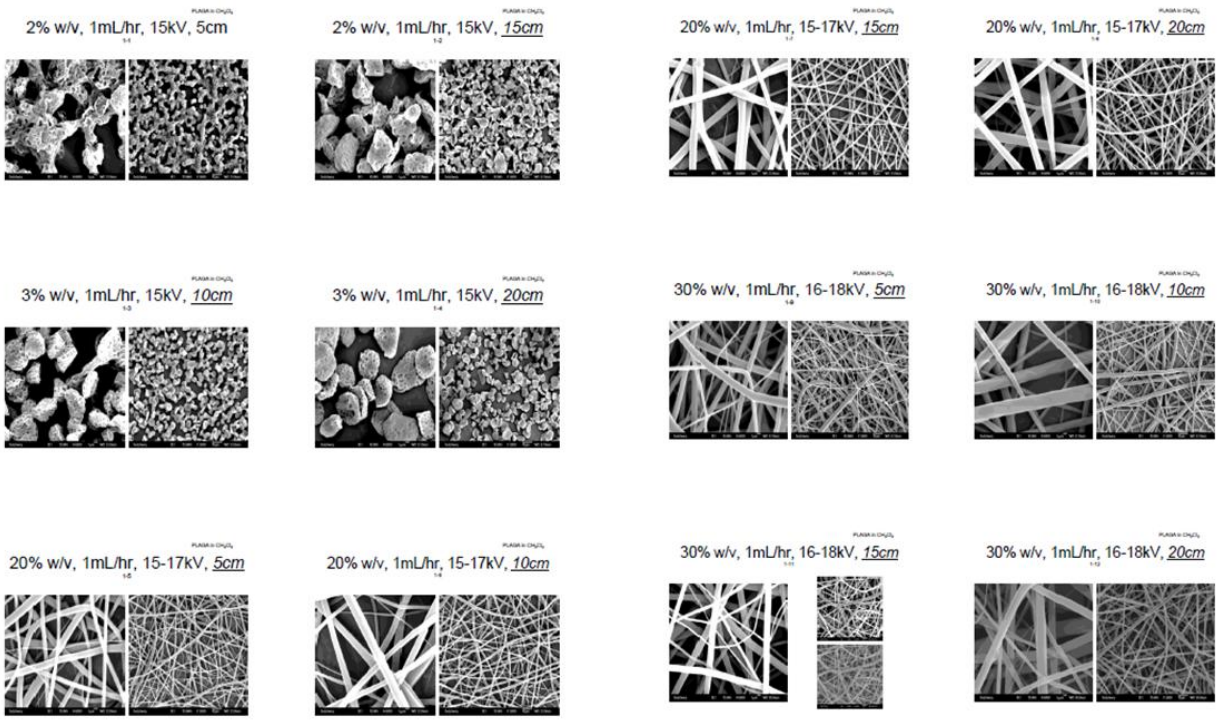

Appendix Figure 1: PLAGA electrospinning optimization

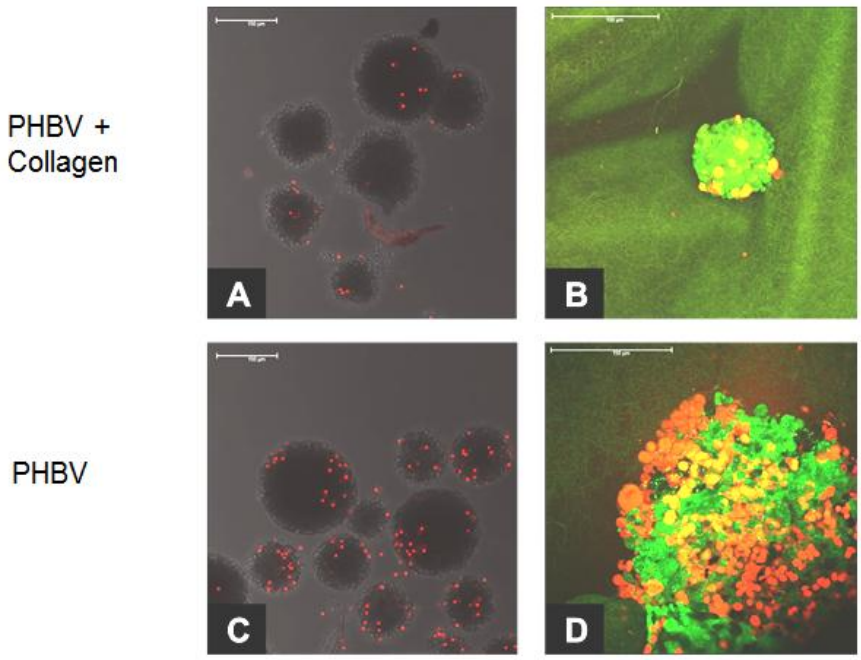

Appendix Figure 2: Confocal Imaging of Propidium Iodide stained pancreatic islets showing decreased cell death when collagen is included in PHBV fibers A,C BALB/C islets. B,D GFP rat islets

Methods:

Islets were isolated as described elsewhere from BALB/C mice and from eGFP rats. After incubation with the polymer nanofibers indicated on the left, the islets were stained with PI and examined under confocal microscopy (Lecia) at the W. M. Keck Center for Cellular Imaging at UVA.

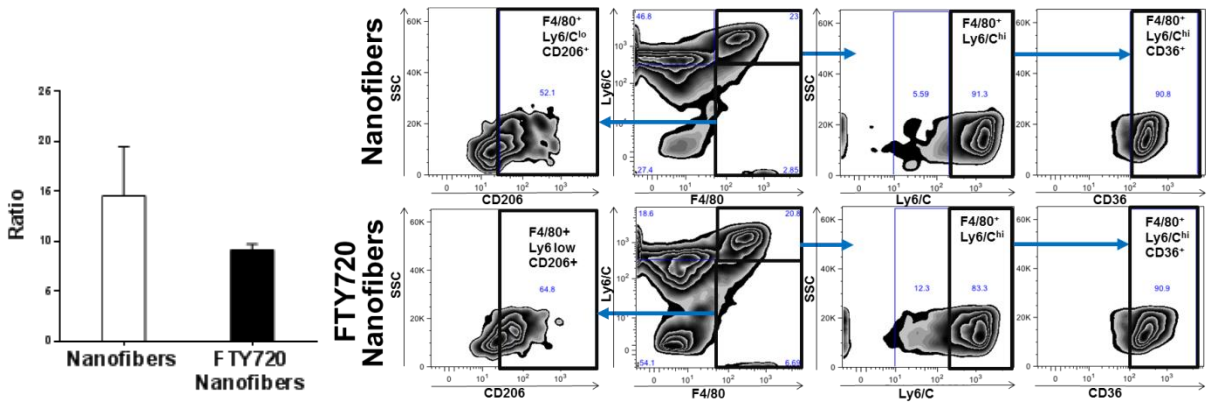

Appendix Figure 3: Inflammatory Cell Ratio is Decreased with FTY720 Nanofibers

Macrophage cell phenotype is an important metric for understanding the inflammatory environment and assessing its potential to support regeneration. Proportions of F4/80lo and F4/80hi expression were nearly equivalent around the two implant types. Within the F4/80lo population, there was a greater expression of Ly6C on cells surrounding the nanofibers implant, possibly indicating important differences in cell types other than macrophages. This same trend occurred in the F4/80hi population, although to a lesser extent. In order to observe changes in the phenotype of macrophage populations, the F4/80hi population was further analyzed (right). The expression of CD36 (thrombospondin receptor) and CD206 (mannose receptor) was examined within this F4/80hi population. No difference was found in the Ly6chi CD36+ cell population, however the Ly6clo CD206+ population of cells was larger surrounding the FTY720-loaded nanofiber implants. The decreased ratio of Ly6chi CD36+ cells to Ly6clo CD206+ cells surrounding the FTY720-loaded implants indicates a decrease in the proportion of macrophages displaying an inflammatory phenotype (left).

Methods:

Nanofibers were made from polycaprolactone (PCL; Sigma, USA) and poly(lactic-*co*-glycolic acid) (PLAGA, Lakeshore Biomaterials, Birmingham, AL). Briefly, they were combined in a 1:1 (w/w) ratio and then dissolved in 3:1 (v/v) chloroform methanol. The final concentration of polymer solution was 18% (w/v). The solution was agitated until the polymer dissolved and then loaded into a 3mL rubber-free syringe. Electrospinning was performed at a flow rate of 1.0 mL/hour, an applied voltage of 19 kV, and a working distance of 10 cm. Nanofibers were collected on a stationary aluminum plate and then stored in a desiccator until use. To make drug-loaded nanofibers, FTY720 (Cayman Chemical, Ann Arbor, MI,

USA) was dissolved in 3:1 chloroform methanol solution and 1:1 PCL/PLAGA was added at a concentration of 20% (w/v). The final drug:polymer ratio was 1:200 (w/w). Electrospinning was performed at a flow rate of 1.0 mL/hour, an applied voltage of 19 kV, and a working distance of 15 cm in order to form nanofibers of similar morphology to unloaded nanofibers. Both unloaded and FTY720-loaded nanofibers were cut into disks with a 6mm biopsy punch for backpacks or into square mats for subcutaneous implant.

Four BALB/C mice were prepared and anesthetized as described for dorsal skinfold window chambers. Two incisions were made near the scapulae on the dorsal of the mice. Each mouse received an unloaded nanofibers implant and a FTY720-loaded nanofibers implant. Implants were inserted into distinct subcutaneous pockets extending away from the spine of the mouse. Both incisions were sutured and mice were given a dose of Bupronex (0.03cc) subcutaneously upon waking. After 12 hours of free access to food and water, the mice were sacrificed using CO2 affixation and the dorsal tissue was harvested. The tissue was cut into 2-3 mm size pieces, and then digested with CollagenaseP (1mg/mL) to create a single cell suspension.

This prepared cell suspension was stained with the following monoclonal antibodies - APC/Cy7 anti-mouse CD4 (Biolegend, San Diego, CA), PE anti-mouse F4/80 Antibody (Biolegend, San Diego, CA), APC anti-mouse CD36 (Biolegend, San Diego, CA), Anti-Mouse Ly-6C PerCP-Cy5.5 (ebioscience, San Diego, CA), CD206 Antibody – Biotin (Serotec, Raleigh, NC), and streptavidin Pacific Orange™ conjugate (Invitrogen Life Technologies, USA). Following staining, cells were fixed in 2% paraformaldehyde at 4°C for 30 min. Cells were then stored in 10% fetal bovine serum (Invitrogen Life Technologies, USA) (FBS) until flow cytometry was performed according to standard procedures and analyzed on a Beckman-Coulter CyAn ADP LX (Brea, California, USA) at the UVA Flow Cytometery Core.

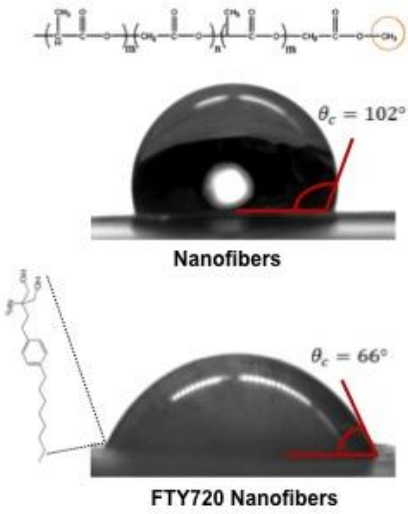

Appendix Figure 4: Glycerin Contact Angle is Decreased by Addition of FTY720 to PHBV& PCL Nanofibers

Changes in surface chemistry were assessed by measuring the contact angle in glycerin droplet experiments. Nanofibers containing FTY720 have reduced hydrophobicity, as demonstrated by the smaller contact angle between nanofibers and glycerin droplet.

Methods:

Contact angle measurements were made by placing a drop of glycerin on the nanofiber surface mounted on the stage of a goniometer (Rame-Hart Standard Contact Angle Goniometer, Model 200; Rame-Hart Instrument Co., Succasunna, NJ). DROPimage Standard software was used to measure the contact angle between the nanofibers and the liquid. At least 3 images were quantified and averaged.

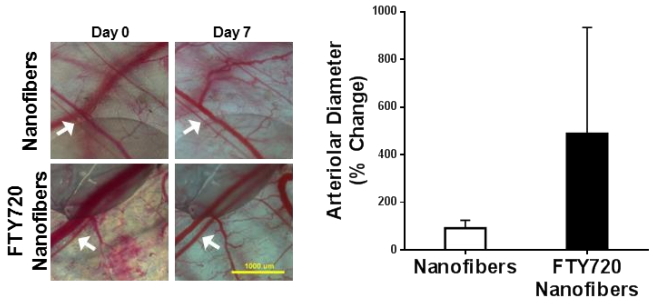

Appendix Figure 5: FTY720 increases arteriolar diameter when released from polymer nanofibers

Intravital images of dorsal skinfold window chamber microvasculature showing the arteriolar diameter increase (left, scale 1000um). The arteriolar diameter of blood vessels surrounding the implants of animals receiving FTY720 loaded implants was increased (right).

See main materials and methods section for dorsal skinfold window chamber.

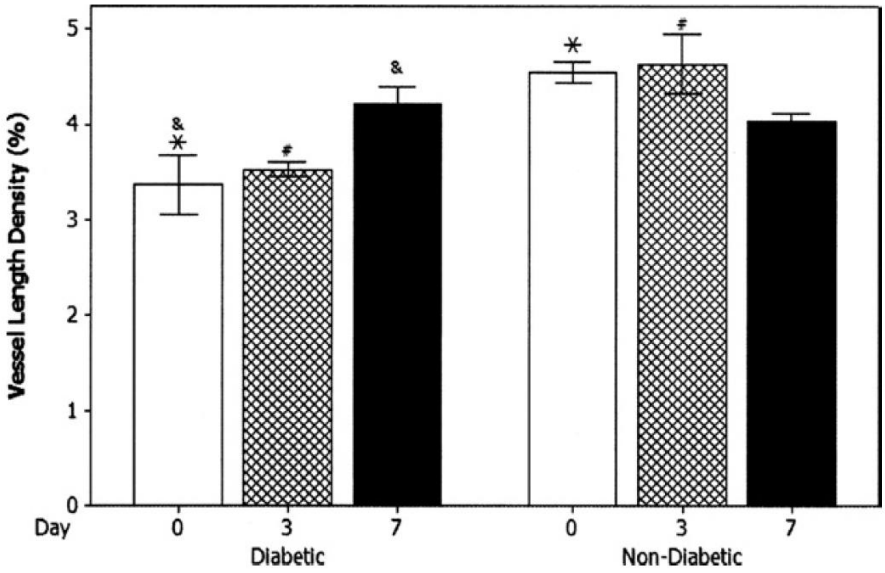

Appendix Figure 6: Vessel length density is steadily increased by FTY720 loaded nanofibers in diabetic animals over 7 days

Vessel length densities over the 7 day observation period for recently induced moderately diabetic and non-diabetic animals. Each bar displays mean of 3 animals with one standard deviation from the mean indicated. All symbols: $p<0.05$. (***Bowers DT et al. Transplant Proc. 2011 Nov;43(9):3285-7. doi: 10.1016/j.transproceed.2011.09.008.***)

Methods:

Nanofiber Mat Fabrication

Nanofibers are electrospun from polymer solutions of PLAGA (50:50 LA:GA, Lakeshore Biomaterials, Birmingham, AL, USA) with and without FTY720 (Cayman Chemical, Ann Arbor, Michigan) which is solvated in Methylene Chloride (Fisher Scientific, Waltham, MA, USA). The polymer solution is 20% (wt by vol) and is provided with a 1mL/hour flow rate by syringe pump (World Precision Instruments, Sarasota, FL, USA) using an 18G blunt tipped needle. A tip to collector distance of 10cm with an applied voltage of 14-16kV was utilized.

Animal Studies

Diabetes was induced in C57bl6/j male mice (Jackson Laboratories, Bar Harbor, ME, USA) by IP injection of STZ (Sigma, St. Louis, MO, USA) to induce moderate diabetes (mean BG: 244mg/dL verses 156 mg/dL non-diabetic animals). Blood glucose measurements were made with an Accu-Chek Advantage handheld meter (Roche, Indianapolis, IN, USA) by tail clip. Dorsal skinfold window chambers were implanted using the previously published technique. 4mm diameter polymer disks were implanted immediately after the dorsal skinfold window chamber surgery and prior to Day 0 images. Light microscopy images were also taken on days 3 and 7 following surgery with a 4X objective, which are then combined into a montage for analysis.

Vessel Analysis

An automated image analysis software (Rapid Analysis of Vessel Elements, RAVE) written for MATLAB was used to process images to quantify length density and vessel volume fraction[293]. Length density is quantified as the total length of all vessels divided by total pixel area. Volume fraction is quantified as a percentage of the image area that is covered by blood vessels as determined by a threshold to distinguish blood vessel from surrounding tissue, and is therefore a weighted average of blood vessel diameter changes.

Statistical Techniques

Student's t-test was used to compare experimental groups where significance was noted with $p<0.05$.

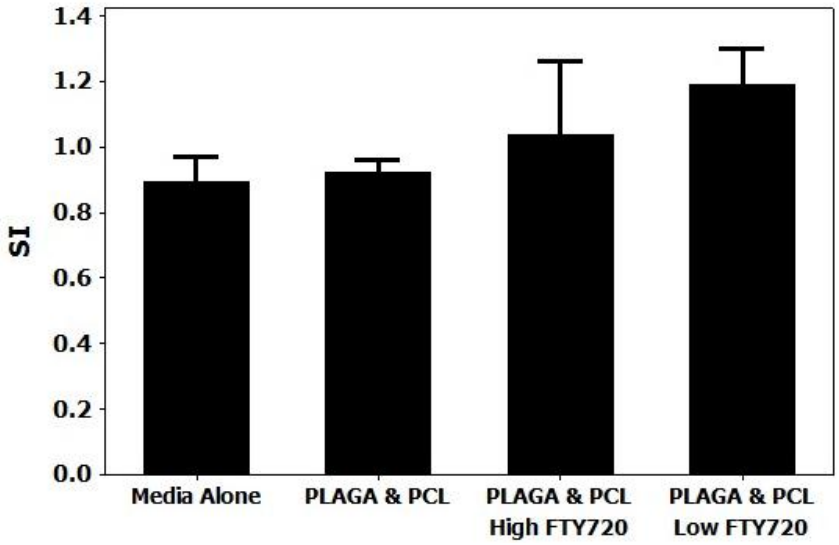

Appendix Figure 7: The stimulation index of cultured non-functional human islets was restored to semi-functional by low dose FTY720 release from PLAGA and PCL nanofibers

Human islets similarly cultured with nanofibers loaded and unloaded with FTY720 showed an increase in function that seemed to be dependent on the dose of FTY720 in the nanofibers.

Methods:

Human islets of were obtained 3 days after the isolation. The islets were hand counted to distribute 50 IEQs into wells of 6 well plates in supplemented CMRL 1066. The islets were then loaded into nanofiber pockets or cultured with the nanofiber sections that would make up a pocket in the well, but not necessarily contacting the islets. The non-contact groups would allow for the effect of any degradation products to be determined. The islets were cultured under these conditions for 24 hours in an incubator. Then they were challenged by the glucose stimulated insulin secretion protocol, with the polymer nanofibers remaining in the wells. During the islet centering for washes the fibers that were not formed into islet containing pockets were moved to the side of the well (stay on the side by the fluid surface tension) as they prevented complete islet centering. The insulin secretion samples in KRB buffer were frozen at -20C until the insulin ELISA was performed.

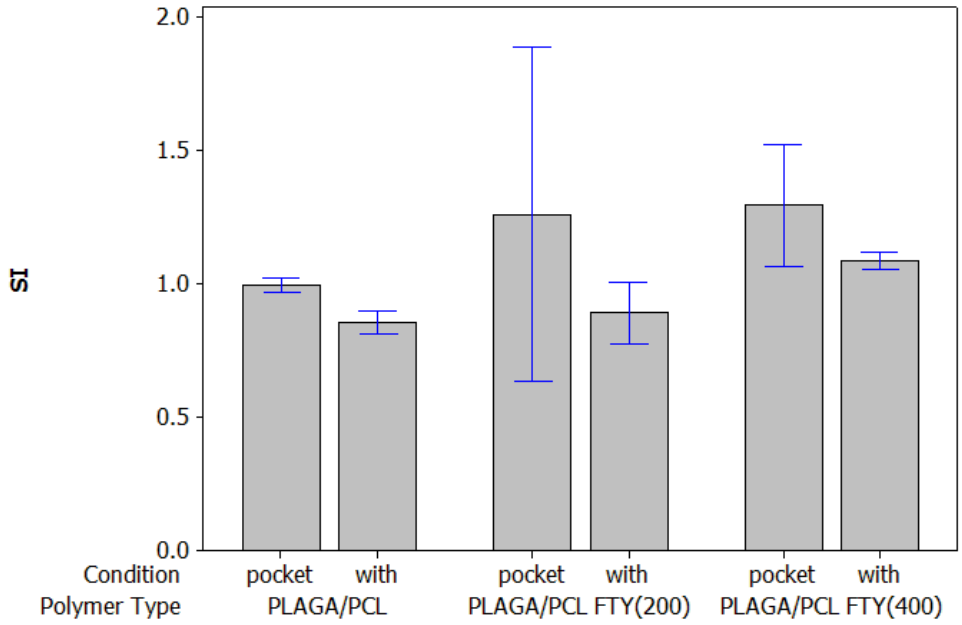

Appendix Figure 8: Function of Human Islets is Improved by Contact with Nanofibers on Two Sides as a Result of Being inside the pocket, as compared to culture with Nanofibers

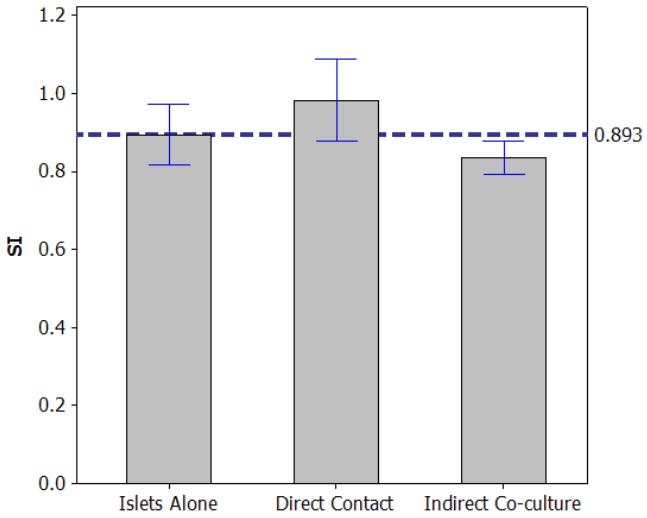

Appendix Figure 9: The Stimulation Index of Cultured Human Islets is Improved by the Contact with Nanofiber Morphology when all the Nanofiber Polymer Types are Averaged